Physical Techniques for the Study of Solid Electrolytes

R. G. LINFORD* and S. HACKWOOD[†]

School of Chemistry, Leicester Polytechnic, Leicester, LE1 9BH, United Kingdom

Contents

Roger Linford is the Reader in Chemistry at Leicester Polytechnic. He received his M.A. and D.Phil. degrees at Oxford, studying low-temperature calorimetry with L. A. K. Staveley. Following 2 years with Emeritus Professor Joel Hildebrand at Berkeley investigating gas solubilities, he returned to the U.K. in 1970 to join Berkeley Nuclear Laboratories. There he led a multidisciplinary team and introduced uhv tribological techniques, Auger electron spectroscopy, Monte Carlo interfacial simulations, and solid-surface thermodynamics into the study of metal-to-metal adhesion. Since taking up his present post in 1973, his major interest is in solid electrolyte interfacial properties. He leads an international program in this field in collaboration with Rutgers University and the Technological University of Denmark under NATO auspices.

Susan Hackwood completed her Ph.D. in 1979 at Leicester Polytechnic, where she undertook a program of research on room temperature solid electrolytes for solid-state battery systems, under the direction of Roger Linford. In 1980 she took a postdoctoral position at Bell Laboratories, Holmdel, NJ, where she is currently a member of the technical staff in the device physics group. She is now working on electrochromic ion insertion and other materials for use in passive display devices.

[†]Present address: Bell Laboratories, Holmdel, NJ 07733.

I. Introduction

A. Nature and Uses

Solid electrolytes have ionic conductivities comparable to those of liquid electrolytes and molten salts.
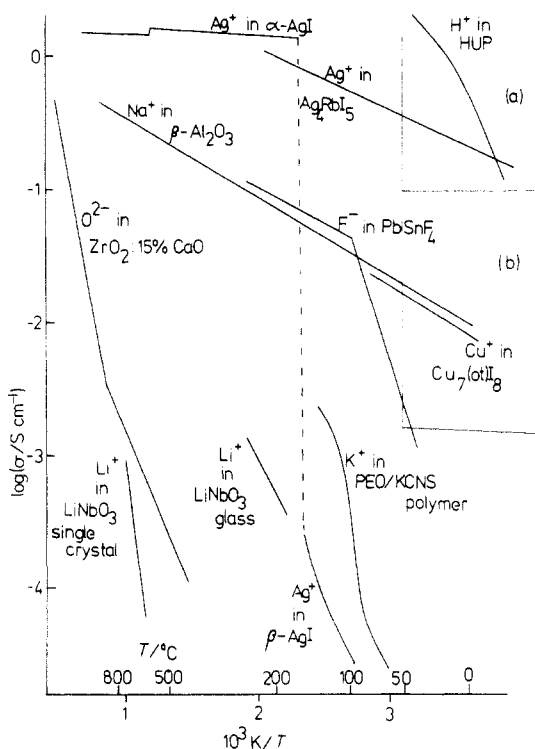
Figure 1. Logarithm of conductivity against reciprocal of temperature for a range of solid electrolytes. The enclosed sections in the top right of the figure represent (a) the area of interest for room temperature high current density applications and (b) that for room temperature low current density applications. (ot) 4-methyl-1,4-oxathianium, (PEO) poly(ethylene oxide), (HUP) hydrogen uranyl phosphate.

The wide diversity of their chemical nature and structural form can be seen from Tables I–IX. In most cases, they exhibit high ionic (electrolytic) conductivity only within a well-defined temperature range, the beginning and end of which are often, but not necessarily, marked by some type of phase change. For example, at room temperature β-AgI is an ionic conductor rather than a solid electrolyte, but at the $\beta \rightarrow \alpha$ transition at 146 °C, the conductivity rises by several orders of magnitude, as shown in Figure 1. The α phase is a solid electrolyte; at the $\alpha \rightarrow$ liquid transition at 555 °C, the conductivity actually *falls* slightly. With CaF_2 there is a similar increase in conductivity on going from the ionic conductor to the solid electrolyte; this takes place over several hundred degrees and is accompanied by a very broad peak in the heat capacity.

Unlike liquid electrolytes, solid materials often show significant electronic conductivity due to the passage of electrons and/or holes. For many purposes, as when oxide films and other materials are used as electrodes, it is advantageous for the material to be a *mixed conductor* with high electrolytic *and* electronic conductivity. In batteries, on the other hand, the use of a mixed conductor as the electrolyte, would cause internal short circuiting and consequent self-discharge. Instead it is necessary to use a *solid electrolyte* exhibiting high electrolytic *but* very low electronic conductivity. Solid electrolytes are to be contrasted with *ionic conductors* in which the electrolytic conductivity, although measurable, is too low for practical applications. The present widespread interest in solid and mixed electrolytes is demonstrated by the large number of books[1-7] and reviews[8-25] that have recently been published.

Solid electrolytes are sometimes called *fast ion conductors* or superionic conductors (a term disliked by some[26] because it incorrectly implies a conduction mechanism akin to superconductivity and defended by others[27] as meaning "supermobile"). It can be useful to retain the term *superionic conductor* to embrace both "mixed conductors" and "solid electrolytes" in order to emphasize their high ionic conductivity. Sometimes it is said that solid electrolytes are characterized by liquid-like sublattices. This is unlikely to be correct for fluorites, e.g., CaF_2, $SrCl_2$, and doped oxides, e.g., $ZrO_2{:}10\%$ Y_2O_3, in which the hopping of defects successfully accounts for the high ionic conductivity (section ID). It is true in a limited sense for some solid electrolytes such as α-AgI and α-CuI which show considerable positional disorder so that the mobile ions are shared over many possible sites. The probability of finding them between sites, however, is small, and so their positions are well-defined. In a liquid, on the other hand, there are no sites and the order is purely short range. The entropy change at the $\beta \rightarrow \alpha$ transition is approximately equal to that of the $\alpha \rightarrow$ liquid transition for AgI, however, and is half the entropy of melting of the alkali halides, thus supporting the argument that one sublattice "melts" at the β–α transition.[28]

The use of solid electrolytes is well established. Following early reports[29,30] of ionic conductivities in solids, Nernst developed a high-temperature cell[31] using a mixed oxide solid electrolyte in 1899. Today, superionic conductors are used for many different applications[32] such as membranes in ion-selective electrodes,[33] capacitors,[34,35] gas sensors,[36,37] electrochromic display devices,[38,39] high-temperature heating elements,[40] intercalation electrodes,[41] power stores, and power sources.[42,43] They are ideal for replacing liquid or paste electrolytes in conventional "dry-cell" batteries[44] and fuel cells.[45] The present energy situation has encouraged close scrutiny of all types of electrochemical power sources (which can be thought of as passive transducers for obtaining electrical energy from chemical reactions in a way not theoretically limited to the Carnot efficiency); solid electrolyte systems are particularly exciting because they are inherently robust, compact, and spill-proof.

B. The Study of Solid Electrolytes

Solid electrolytes interest scientists from many disciplines such as structural and inorganic chemistry, electrochemistry, materials science, physics, crystallography, and computer simulation. Specialists infuse the subject with the concepts and language of their parent discipline, and naturally they concentrate on the study of solid electrolyte materials that best reveal behavior susceptible to their branch of investigation. Thus, structural chemists and theoreticians are greatly interested in the one-dimensional conductor hollandite, $(K, Rb, Cs, or Tl)_{2x}Mg_xTl_{16-x}O_{32}$, although the magnitude of its conductivity is too low to excite the battery technologist. On the other hand, practical battery systems based on AgI or CuI modified by the addition of organic iodides can work efficiently at room temperature, but these solid electrolytes strain the ingenuity of the crystallographer and are rather complex for most types of experimental or theoretical attack. The mode of study chosen for investigating solid elec-

trolytes therefore depends on the motivation.

It is perfectly sensible for the battery technologist to screen new materials to see *whether* they are useful solid electrolytes and *how well* they perform relative to competing materials without considering in detail the structural and compositional features that lead to their particular properties. It is of wider interest to see if the range of usefulness of a given electrolyte can be *extended* by modification of its composition, structure, or form, i.e., single crystal, polycrystal, compacted or sintered powder, glass, thin film, etc. Physical scientists within the solid electrolyte field want to know why a given material has solid electrolyte properties. The interests of the scientist and technologist merge in the desire to develop *general design criteria* that can be used to predict new solid electrolytes suitable for particular requirements.

Each parent discipline imposes its own characteristics on the nature of the questions asked about the solid electrolytes and the approaches used to try to answer them. A battery technologist may choose to study discharge curves, shelf life, mechanical integrity, internal corrosion, and similar parameters of solid electrolytes used within battery systems. These quantities do not have the same fundamental significance as, say, relaxation times derived from NMR line-width measurements or the electronic conductivity of an isolated sample of solid electrolyte. They do pertain, however, to the properties of the electrolyte in the "real" system, and as such they have a role to play in solid electrolyte studies. By contrast, so do precise measurements on isolated samples of electrolyte, which are in effect "model" systems. For example, it may be easier to study a solid electrolyte in its single-crystal form, but if it happens normally to be used as a compacted powder or sinter, then the single crystal is but a model of the real system. Most studies are compromises in which fidelity to the real system is balanced against the ease of measuring informative parameters.

Some properties are studied on isolated samples of solid electrolyte material, whereas others can only be measured when the electrolyte forms part of some wider system such as a test cell. It is helpful to identify four study regimes: (i) isolated, in which the test environment does not modify the behavior of the electrolyte sample, e.g., crystal structure determination; (ii) perturbed, where the test environment affects the material, e.g., electron spectroscopy involving ultra-high-vacuum conditions; (iii) conducting, when test electrodes, which introduce their own additional parameters, are attached to the electrolytes; (iv) applied, in which an electrolyte that forms part of a working device is investigated in situ.

It is useful to bring many techniques to bear on a solid electrolyte if a reliable idea of its behavior, and the cause of that behavior, is to be obtained. A single technique, performed by a specialist, will produce results the interpretation of which could be colored by the concepts prevalent in his field. For example, an electrochemist accustomed to liquid electrolyte systems could underestimate the difference between grain and particle boundary effects in solid electrolyte impedance spectra because such effects do not arise in his parent field. A crystallographer could overemphasize the importance of single-crystal structural data in elucidating

ionic mobility on compacted powder systems. These apparent pitfalls are minimized by comparing the results from many different approaches. Also, some techniques are less sensitive than others to certain features of solid electrolyte behavior. Thus EXAFS studies and diffuse X-ray scattering give a better insight into mobile ion–host lattice interactions than do the X-ray diffraction Bragg peaks used for structural determinations. The detection of a conducting–nonconducting transition would apparently be best performed by studying conductivity as a function of temperature. Poor contact and similar problems may mean that complementary but indirect probes such as variable-temperature X-ray diffraction or differential scanning calorimetry are also useful.

C. Review Purpose and Arrangement

This is not intended to be an overview of existing solid electrolytes nor a means of keeping specialists abreast of the latest developments in their particular field. Instead it is planned so as to give chemists working in other areas an insight into the diversity of techniques used to investigate solid electrolyte behavior and perhaps, more importantly, to identify why a given technique is being used, what information it is capable of giving, and what its limitations are.

The potential scope is enormous, and certain restrictions have been made. Physical techniques are included, but analytical chemical studies and theoretical investigations are not (although computer simulation is treated as being an experimental study of a very well defined, albeit unrealistically idealized, model system). Battery applications are emphasized at the expense of fuel cells and devices. The majority of examples are taken from room-temperature solid electrolytes suitable for low current density applications such as heart pacemaker power cells rather than from oxides, fluorites, glasses, etc., although this is in no way to denigrate the technological and scientific importance of these latter materials. Transport mechanisms, structural properties, and the individual features of particular electrolytes are not considered in any detail, as these would obscure the essential purpose of highlighting the characteristics of the techniques themselves. Before proceeding to an individual treatment of each technique, the dependence of conductivity on composition, temperature, and pressure is considered.

The division of techniques into different classes is rather arbitary and is only one of many such classifications that could be made. It has two advantages to compensate for its undoubted shortcomings. It proceeds from techniques directly pertinent to the electrochemical behavior of the electrolytes to matters such as phase transitions which have a less direct bearing on working device properties; interfacial behavior is treated separately. It also permits techniques that are used for more than one purpose to be easily compared with complementary approaches.

D. Classification and Criteria

Solid electrolytes may be classified in innumerable ways. One which is helpful to the theoretican in that it highlights some of the features that are felt to lead to high ionic conductivity is to subdivide them into three classes:[46] (i) those susceptible to treatment by

defect-hopping models, such as fluorites, doped oxides, and most proton and lithium conductors. In these, small amounts of dopant materials produce a very large effect on the conductivity—they are characterized by high charge, strong interactive forces, high compressibility, low dielectric constant, and low polarizability, and potential energy surface calculations produce deep localized wells; (ii) *liquid-like sublattice* materials such as most Ag^+ and Cu^+ electrolytes—here dopants have only a small effect on the α-phase conductivity and the calculated energy surfaces are rather flat; (iii) intermediate or uncertain, including most of the *layer or tunnel structures* such as β-Al_2O_3.

It is possible to create a high vacancy concentration in defect-type solid electrolytes both by compositional doping as discussed in section IIA and by utilizing a mismatch between stoichiometry and lattice structure.[47] Thus, 25% of anion vacancies can be introduced in a fluorite structure, M_4X_8, by studying δ-Bi_2O_3 rather than CaF_2 or $SrCl_2$. The latter two classes are characterized[48] by possessing a high degree of positional disorder in the mobile ion sublattice to accompany high ionic mobility. This contrasts with materials of the first class such as Li_3N, which[49,50] are superionic but ordered.

In liquid-like sublattice materials, the ions jump between symmetrically and energetically equivalent sites, preferably directly through shared faces. This accounts for the superiority of body centered cubic over face centered cubic materials, as the tetrahedral sites share faces in the former case whereas motion must proceed alternately via the higher energy octahedral sites in the latter. For layer and tunnel structures, the ionic radius must fit the geometry of the conducting path, being neither so small that it gets trapped inside channels or pits in the lattice nor so large that it becomes wedged in the main channels. This explains the minimum found[51] for Na^+ for the enthalpy of motion of ions in β-alumina.

Superionic conductors are widely diverse in form and include inorganic, organic, alloy, ceramic, and glass compounds, and even certain solid elements such as bromine and iodine.[52]

Solid electrolyte materials have the following characteristics: (i) high electrolytic conductivity, (ii) low electronic conductivity, (iii) mechanical integrity, (iv) good mechanical adhesion to suitable electrode materials with which they are chemically and electrochemically compatible, (v) stability, even in the presence of an electric field, (vi) chemical compatibility with reaction products, (vii) a low activation energy of motion, and (viii) a facile conduction pathway across intergranular and interparticle boundaries.

II. Conductivity Dependence

The purpose of this section is to provide a more complete understanding of the nature of the materials studied by the techniques covered in this review and to explain the purpose of studying the composition, temperature, and pressure dependence of solid electrolyte conductivity.

It is insufficient to specify a solid electrolyte by empirical formula alone; the superionic region is a particular part of the temperature, pressure, composition phase diagram in which an appropriate structure occurs at a temperature sufficient to provide the thermal energy to surmount the barriers to ionic motion.

To illustrate this, a few examples will now be considered.

A. Composition

The room temperature ionic conductivity of pure AgI is low; only the high-temperature α phase is superionic, because at lower temperatures the combination of a suitable structure and sufficient thermal energy is not present. A very wide range of inorganic and organic dopants can be added to AgI, however, to produce room temperature solid electrolytes.[32] Indeed the compound Ag_4RbI_5, the first significant room temperature solid electrolyte to be discovered,[53,54] could be considered as a highly doped form of AgI. The addition of about 15 mol % of a variety of ionic organic substances such as tetraalkylammonium[55-57] and sulfonium[58-62] iodides to AgI also produces room temperature solid electrolytes, and similar results are obtained[63-66] with CuI. To elucidate the composition-induced structural changes responsible for the enhancement of ionic conductivity, several structural studies,[67-76] which have been reviewed elsewhere,[16,77] have been carried out, and many examples will be cited later of the application of a wide variety of techniques to room temperature AgI-related solid electrolytes.

Similar composition modified conductivity can be obtained for defect solid electrolytes as well as for the highly mobile sublattice materials such as AgI. Although the ionic conductor LiI with no added dopants is used commercially as a thin film electrolyte,[32] its conductivity can be considerably enhanced[78] by the addition of KSCN. At high temperatures, all defect materials have strongly composition-dependent conductivities at low concentrations but, even at room temperature, the conductivities of solid solutions of heavily doped fluorites are enhanced by several orders of magnitude over the pure material.[79,80]

B. Temperature

Solid electrolytes usually exist within a limited range of temperature below which they are ionic conductors and above which they are molten. At the low-temperature end, there may be a $\beta \rightarrow \alpha$ phase transition accompanied by a spectacular and sudden increase in conductivity, as in the case of AgI. Alternatively, the change from ionic conductor to solid electrolyte may be marked by an increase in conductivity of several orders of magnitude that takes place over a temperature region spanning several hundred degrees; such behavior is shown by certain anion conductors including PbF_2. Within the solid electrolyte region, the conductivity increases as the temperature rises until, at the melting point, the molten salt conductivity is attained.

It is customary to describe the temperature dependence of a physical property, X, in terms of an Arrhenius relationship:

$$X = X_0 \exp(-E/RT)$$

X_0 is the preexponential factor and E is the activation energy. If this holds, then the Arrhenius plot of $\ln X$ against $1/T$ will be a straight line of slope $-E/R$ and intercept X_0. Many physical phenomena give linear Arrhenius plots and can be explained in terms of the concepts involved in the model, namely that transitions

from a given energy state are governed both by temperature-independent parameters, subsumed into X_0, and by a Boltzmann factor describing the temperature-dependent probability of surmounting an energy barrier, E. In orthodox use, E is an enthalpy or an internal energy rather than a free energy, so that the preexponential factor contains not only such terms as the frequency of jump attempts, w, and the jump distances, λ, but also entropy terms of the form $\exp(S/R)$. It has been pointed out[81] that the Arrhenius model not only obscures the role of entropy but also imposes a particular view about the mechanism by which a given transport process proceeds. Although it is customary to quote activation energies for ionic conductivity in solid electrolytes, and thus implicitly to accept the Arrhenius model as a suitable description of the process, it may be conceptually restrictive only to visualize ionic motion as taking place by a series of hops between sites of well-defined energies. Despite these reservations, it is usual to construct Arrhenius plots for the temperature dependence of conductivity. Following the normal format[82] for diffusion

$$D = D_0 \exp(-\Delta H/RT)$$

where $D_0 = (\lambda^2 nw/N) \exp(S/R)$, n is the number of mobile species, and N is the number of sites and using the Nernst–Einstein equation (section IVD) give

$$\sigma T = \sigma_0 \exp(-\Delta H/RT)$$

where $\sigma_0 = (\lambda^2 n^2 wF^2/NR) \exp(S/R)$. Hence the activation energy can be obtained from a plot of $\ln (\sigma T)$ against $1/T$. Since $\ln T$ does not vary much over a small temperature range, a simpler expression can be used:[83]

$$\ln \sigma = \ln \sigma_0 - \ln T - E_a/RT = \ln \sigma^0 - E_a/RT$$

The slope and intercept of the $\ln \sigma$ against $1/T$ plot are less well defined than for the $\ln (\sigma T)$ line, but E_a can be loosely equated to ΔH. For many ionic conductors, the $\ln (\sigma T)$ vs. $1/T$ plot is nonlinear and can be divided into two straight-line portions, each characterized by an activation energy.[84] The interpretation of these in terms of intrinsic and extrinsic behavior is discussed later (section IVD). For solid electrolytes, the Arrhenius plot is normally linear, and the preexponential factor and the activation energy are usually small,[11,12] the latter typically[17] being about 0.2 eV (15–20 kJ mol^{-1}).

Experimentally, the construction of an Arrhenius plot for a solid electrolyte merely requires the determination of conductivity as a function of temperature, either directly or from temperature-dependent impedance plots.[85,86] Accurate temperature measurement requires a well-located temperature probe, however, and maintenance of good electrical contact with test electrodes can be a problem as compression springs tend to relax and embedded test electrodes can deform under thermal strain. Some electrolytes tend to become unstable at elevated temperatures;[58,66,77,87,88] this restricts the range over which the temperature dependence can be investigated.

For certain mixed conductors in which electronic conductivity is appreciable over part of the temperature range, it is very desirable to measure σ from quite low temperatures. In a study of AuI carried out[89] from −160 to 100 °C, it was found that electronic conductivity (ΔH = 0.075 eV) dominated below 0 °C, but that ionic conductivity (ΔH = 0.88 eV) became increasingly important as the decomposition temperature of 100 °C was approached. The temperature dependence of the emf of mixed conductors has also been studied; from measurements[90] on Li-doped AgGaS$_2$, the temperature dependence of the transport number was obtained.

Many doped materials, such as the Tysonite-type fluoride conductors based on CeF$_3$, give an activation energy that depends on the nature of the dopant only below a characteristic temperature, above which it assumes a constant value.[91]

Activation energies from conductivity measurements can be compared with those found from the temperature dependence of othe parameters. Relationships to diffusion parameters are considered later (section IVD); the heat of transport obtained from thermoelectric measurements (section IVB) has also been compared with E_a for Ag$^+$ conductors. It was concluded[92] that, since in AgI–inorganic iodide systems the activation energies were almost equal whereas in AgI–organic iodides they were not, not all the Ag$^+$ ions in the latter materials were free to take part in the conduction process.

Recent examples of temperature dependent conductivity measurements include studies of Ag,[55,83,87,88,92-98] Cu,[64,83,99-102] Li,[103] oxide,[12,24] and fluoride[104-108] conductors.

C. Pressure

Electrolytic conductivity is often reduced at very high pressures because the material undergoes a phase transformation to a nonconducting structure. In compacted powder solid electrolytes, there is an additional effect, which is now considered.

If a solid electrolyte sample is compressed between test electrodes, the measured conductivity initially rises as the applied pressure is increased, until a steady value is reached. The pressure dependence of the conductivity strongly depends on electrolyte form; compacted powder materials show the most marked effect, followed by sinters and polycrystals, with single crystal and vitreous materials being the least affected.

This is in no way surprising as the bulk impedance of solid electrolytes is so low that poor interfacial contact can easily contribute an impedance as large as that of the electrolyte itself. The combined effects of varying compaction pressures and differing electrode–electrolyte contact resistances are predominantly responsible for the variation of 250% in the room temperature conductivity of Ag$_4$RbI$_5$ reported by different workers.[109,110] The contact resistance can be evaluated by measuring σ as a function of test electrode separation distance for electrolyte compacted to the same pressure; extrapolation to zero separation yields the contact term.[109] Its magnitude can be minimized by using easily deformable test electrodes such as Wood's metal.

Electrolyte–test electrode contact is a problem for all electrolytes regardless of their form, although sputtered or vapor-deposited electrodes will maximize the contact area, even if mismatch-induced stress cannot be eliminated. Forms without intraelectrolyte boundaries should in principle show an eventual diminution of σ with increasing pressure as lattice contraction restricts

the mobile ion pathways. For compacted powders and related materials, it might be expected that the bulk conductivity value would be approached as the applied pressure becomes sufficient to eliminate interparticle voids, thus producing the bulk density. In fact, for $Ag_{13}(Me_4N$ or $Et_4N)_2I_{15}$, a plateau in σ is reached at a pressure 25% lower than that required to produce the bulk density.[109] This confirms that the problem is not simply one of interparticle contact area; the interfacial contact region will undoubtably be distorted compared with the bulk, and ionic transport across it will be hindered. The nature and relative magnitudes of the pressure-dependent terms relevant to conductivity across electrolyte boundaries are at present under active consideration.

The dependance of σ on pressure has been studied in detail by Shahi and his colleagues, especially for silver systems.[14,109,111,112]

The capacitance is also affected by pressure and impedance studies at varying pressures have been carried out.[97,112-115] Impedance plots for powdered and sintered materials have also been compared and grain boundary behavior has been considered.[113]

III. Electrochemical Properties—Direct Measurements

Electrochemical methods are primarily concerned with voltage–charge–time relationships, for example, the current that passes in response to an applied voltage, the voltage set up in a galvanic cell as a result of chemical reaction, or capacitive effects caused by charge separation. The galvanic cell voltage will vary according to whether current is allowed to pass or not. If the only probe that is fitted to a cell is a voltage measuring device of virtually infinite resistance (i.e., infinite load), then the cell should behave in a thermodynamically reversible way (see section IVC) and produce its maximum voltage, *the open circuit voltage or ocv*. If the predicted cell reaction is correct and electronic conductivity is absent, the ocv is equal to the emf of the cell reaction; the former is a technological, and the latter a scientific, parameter. When a finite resistance is connected to the cell so that current passes, equilibrium conditions no longer apply and the voltage drops.

The measurement of electrochemical parameters involves making electrical contact with the cell system and consequently creating electrode–electrolyte interfaces which can themselves affect the parameters under study. Different types of electrode are used for these studies. Conductivity measurements require *test* electrodes which are inert; they are not a source or sink for the conducting species and rapidly become polarized. No charge-transfer reactions take place at the interface under the voltage conditions employed for the test. For many studies, *working* electrodes are used, at which interfacial charge-transfer reactions occur. Electrons are removed from the transferred species at a working *anode* whereas reduction occurs at the working *cathode*.

In the case of a galvanic cell, e.g., a primary battery, the anode is by convention negative and the cathode positive since if a wire is connected between the electrodes, electrons pass along it from anode to cathode. For an electrolytic cell, which is one where voltage is applied from an external source (e.g., a secondary

battery under recharge), the charge-transfer reactions proceed in the opposite direction but the sign on the electrode remains the same. Thus the positive electrode of an electrolytic cell is the anode.

In solution electrochemistry, a three-electrode arrangement can be used. Here the voltage is measured between working and *reference* electrode, under zero-current conditions, whereas a circuit involving charge-transfer is completed between working and *counter* electrodes. This arrangement enables detailed studies of the charge-transfer process at the working electrode–electrolyte interface to be carried out. In solid-state three-electrode systems there are additional problems at the electrode–electrolyte interface. With liquid electrolytes, the area of contact is effectively the area of the electrode itself, whereas solid–solid contact takes place only across asperites in the case of compacted powder and similar systems.[116,117] Structural features of the electrode such as surface slopes, etch–pit dislocations, etc., perturb both liquid and solid systems, but lattice distortion in the interfacial region is more pronounced in the solid state. Initial compositional inhomogeneities are present in the interfacial region of both liquid and solid systems because of surface segregation. These may be smoothed out in liquid systems by convection or diffusion. Although for both liquids and solids the limiting step for the redox reaction at the electrolyte interface may be either charge transfer or diffusion, liquid diffusion is more rapid. Also, convection cannot occur at solid interface.

Electrokinetics of the charge-transfer process are more easily studied in liquids than in solids because bad contact, which introduces uncontrollable parameters, is more likely in the latter case. Also, for solid-state systems with wire test electrodes the area of contact is lower and the current density at or near the charge-transfer interface is greater than estimated. Many of these aspects affect the measurements described in section IIIA.

For solid electrolytes, just as for liquids, the reaction at the working electrode interface may be reversible or irreversible. A *reversible* reaction is in equilibrium and is thermodynamically controlled and the electrode kinetics are rapid compared to diffusion. An *irreversible* reaction is not in equilibrium and the rate constant for reactant transport to the interface greatly exceeds that for the charge-transfer step.[118] A test electrode is irreversible in the sense that it blocks a given back reaction (and indeed the forward reaction as well).

The test electrode is an example of an *ideally polarized electrode*, which is one in which charge transfer cannot occur. The word polarized is used in connection with electrolytic cells involving a working electrode and a test electrode, called a *blocking* electrode because it does not act as a supplier of the conducting species (although it can be a sink; Ag can be made to plate on carbon, for example). An example is the Wagner polarization cell (section IIIB1); when a voltage is applied, ionic current soon ceases to flow because ions cannot be provided by the blocking electrode. Within the electrolyte, the applied field which is attempting to induce migration in one direction is balanced by a chemical potential gradient (caused by the difference in concentration of carrier species across the electrolyte) which works in the opposite sense. The cell is then said

to be polarized, and any residual current is due to electronic carriers.

In addition to ionically blocking electrodes, electronically blocking electrodes, which act as a filter to permit ions but not electrons to pass, have been described.[119] An example is the use of an AgI-coated Ag electrode in the cell Ag|AgI|Ag$_2$S|AgI|Ag. It is perhaps better to describe the AgI as being part of the electrolyte rather than the electrode however. Some electrolytic cell studies, such as those described in sections IIIB and IIIC, are carried out with a unidirectional dc applied voltage, whereas others utilize ac conditions. Under dc conditions a Faradaic current flows if reversible electrodes are used, but with irreversible electrodes the cell becomes polarized. Hence an ac current, often of angular frequency 10^4 Hz (corresponding to an applied frequency of 1592 Hz), is used.

If the ac frequency is varied, then more detailed information can be obtained. The passage of current through a cell is impeded not only by the circuit resistance, which is frequency independent, but also by capacitive and inductive effects, the latter being negligible for liquids and often insignificant for solid-state cells. A capacitance arises whenever charges are separated; an important example is the *double-layer capacitance* at the electrode–electrolyte interface, which is caused by the separation between, say, cations on the electrolyte side of the interface and electrons on the electrode.[118] In liquid studies, this region is of particular interest because of the balance between the orientation caused by the charges and the disordering effect of thermal motion within the electrolyte. In solid electrolytes, the immobile host sublattice restricts the freedom of movement of ions within the mobile sublattice, and convective effects are absent, so that double-layer effects are different. Frequency-dependent impedance spectra (section IIID) can provide insight into interfacial and other capacitive effects. Solid-state capacitors such as Au/Li$_2$TiO$_3$/Au have also been studied;[35] they offer a possible application as a thermal battery because the stored charge ($\sim 10^6$ times the double-layer capacitance) does not leak away at room temperature but can provide currents of up to 100 μA when heated.

Finally, because their use is so widespread as to make specific citations superfluous, the techniques for measuring the total (ionic plus electronic) conductivity, σ_{tot}, will be discussed here, the determination of the separate ionic, σ_i, and electronic, σ_{el}, contributions being discussed later (sections IIIB, IIIC1). σ_{tot} is related to the conductance, G, by

$$\sigma = GL/A$$

where $G = 1/R = I/V$, L is the distance between two parallel electrodes of equal cross-sectional area A, R is resistance, I is current, and V is voltage. The SI unit for G is the siemens, S, formerly Ω^{-1} or mho, and it is conventional to present values of σ in units of S cm^{-1} rather than S m^{-1}. σ is therefore the ratio of current density, I/A, to voltage gradient (i.e., electric field), V/L.

A typical conductivity cell consists of two identical test electrodes in intimate contact with the electrolyte under investigation. In the case of compacted powder materials, the electrodes can be pressed graphite in firm contact with metal strips or caps, evaporated metal

contacts,[120] or low melting point solders. In the two-probe system an ac bridge is connected to the cell and the resistive and capacitive arms of the bridge are balanced. Although G is obtained from the resistance reading alone, this cannot be found unless the capacitance is balanced out. When the impedance of the charge-transfer interface is considerable, the four-probe method, involving separate current and voltage leads, is used.[121] The voltage probes are located on the electrolyte, near the interface. Unlike liquid systems, it is not possible to immerse the probes in the electrolyte without severe mechanical distortion of the system. Consequently these measurements can be affected by surface effects and electrolyte structural anisotropy. On the other hand, four-probe measurements can give the dc conductivity if the impedance spectrum[122] is known.

Another method for the measurement of conductivity which has been applied to β-alumina is the contact-free induced torque method.[123] The electrolyte is placed in a rotating magnetic field, and eddy currents cause the sample to twist through an angle that can be measured with a laser-mirror arrangement. Electrode contact problems are eliminated in this method.

Two important parameters will be encountered below are the transport number of species i, t_i, and the mobility μ_i. t_i is the proportion of the current carried by the ith species and is defined for a system of m species as

$$t_i = \sigma_i / \sum_{j=1}^{m} \sigma_j$$

so that $\sum_{j=1}^{m} t_j = 1$.

It is dimensionless, whereas the mobility, which is related to the number of carriers per unit volume, n, of charge e by

$$\mu_i = \sigma_i / ne$$

has the dimensions of area per unit potential difference per unit time (m^2 V^{-1} s^{-1}).

A. Battery Performance Characteristics

The emphasis here is on technological parameters of an "applied" nature relating to galvanic (predominantly primary) cells.

1. Open Circuit Voltage (ocv)

This is the voltage generated between the anode and cathode compartments of a cell incorporating a solid electrolyte and such ancilliary components (e.g., depolarizers, contact caps, encapsulators, etc.) as are necessary, under conditions where negligible current passes. The electrode compartments contain the active electrode materials that participate in the cell reaction, often together with electronic and/or ionic carriers which facilitate transport to and from the charge-transfer interface. The relationship between the ocv and other parameters has been discussed above and it is further considered in section IVC.

It is usually measured by connecting a high impedance voltmeter to the battery. Sometimes, as in the case of CuI batteries,[77] the ocv is a function of cell lifetime. In high-temperature oxide electrolyte cells the ocv can also change with time because of the effect of electronic currents on the oxygen chemical potentials

at the electrodes,[124] and indeed such ocv measurements can yield the electronic transport number.[125]

2. Discharge Curves

In their most simple form, these are plots of the voltage, V, obtained from a battery as a function of time, t, when a finite constant resistive load is used in place of an infinite load. Under high loads, they usually take the form of a plateau region (V independent of t) followed by a steep descent as the limiting cell reactant approaches depletion. If the cell product is very resistive, as in the case of the LiI system, the potential difference between the two working electrodes is reduced by the increasing IR drop across the electrode;[126] an approximate relationship is

$$V_{actual} = V(t)_{measured} + IR(t)$$

where $I = V_{ocv}/R_L$, and $R(t)$, the internal electrolyte resistance is much less than R_L, the external load. Hence the discharge curve plateau will have a gentle downwards slope.

Several technological parameters can be obtained from discharge curves. It is most unusual for all the chemical reactants to be consumed within the useful lifetime of the cell. The efficiency of the cell can be calculated from an integration of the V–t plot, usually from $t = 0$ to the time at which $V = 0.6V_{ocv}$. This enables the total charge passed, Q, to be found since

$$Q = \int I(t) \, dt = (1/R_L) \int V(t) \, dt$$

Alternatively, Q can be measured by a coulometer. Q/zF gives the amount of cell reactant that has been consumed, M_c, and comparison of this with the amount available, M_a, gives the efficiency, E (=M_e/M_a).

When determining efficiencies, it is usual to use either anode-limiting or cathode-limiting cells so that the electrode from which M_a is calculated is known. Some of the performance parameters commonly used are defined as follows:

$$\text{mass efficiency} = Q_{obtained}/Q_{obtainable}$$

$$\text{energy density} = \frac{1}{M} \int V dQ$$

$$\text{power density} = V^2/(RM)$$

where M is the mass of the system, including electrodes, electrolyte, and ancilliary components.

If a second plateau region is found in a discharge curve, it can be assumed that the initial available reactants have been consumed and a different cell reaction is proceeding.[77] Short plateau regions, corresponding to low efficiencies, can indicate a chemical reaction that consumes some of the active material, or alternatively a surface oxidation or similar reaction that "locks up" some of the electrode material.

3. Three-Electrode Measurements

The problems of using a three-electrode arrangement in solid state systems are nontrivial. In liquid systems, a reference electrode is chosen so as to (a) have a known, constant emf, (b) have a large surface area to minimize the current density, and (c) be capable of being placed in close contact with the electrode being measured so as to minimize the IR drop of the electrolyte (this is often achieved by using a capillary salt bridge).

In solid-state systems these criteria can be approached by (i) splitting the anode or cathode in two and using one half as the reference and one half as the working electrode[39]—this has the disadvantage that the reference electrode does not see exactly the same IR drop as the working electrode, but does have the advantage of being in good mechanical contact with the substrate; (ii) inserting a fine wire, which will act as a reversible electrode, e.g., Ag coated with AgI, between the working and counter electrodes[127]—this has the disadvantage of poor mechanical contact, but the advantage of being positioned close to the working electrode; (iii) using a capillary salt bridge, connected to a conventional reference electrode outside the test cell[127]—the disadvantage here is again with mechanical contacts.

4. Compatibility Tests

A battery will not perform satisfactorily if its constituents react chemically. It can happen, for example, that the electrolyte reacts with the cathode material or with the cell reaction product. This type of problem is particularly severe in room temperature solid electrolyte batteries involving organic halide dopant materials. In a study[58] of AgI/sulfonium iodide electrolytes, used in conjunction with sulfonium polyiodide cathodes and metallic silver anodes, the discharge curves were very unsatisfactory for many electrolyte-cathode combinations. The compatibility of the materials was investigated by following the conductivity as a function of time for electrolyte samples into which cathode material had been incorporated. Incompatible materials showed a drop in conductivity after a few days.

A further example is the stability of Ag_4RbI_5 towards I_2 which has been determined[114,128] by measuring the ocv of cells of the type $Ag|Ag_4RbI_5|Ag_4RbI_5(x_1) + I_2(x_2)|Pt$. The voltage was as expected in the range 0.004 <x_2 < 0.162, but below 0.004 the reaction

$$I_2 + Ag_4RbI_5 = 4AgI + RbI_3$$
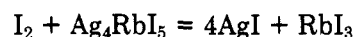
took place. Compatability problems have been reviewed elsewhere.[22]

5. Self-Discharge in Electrode Limited Systems

Self-discharge can be estimated from electronic conductivity data (section IIIB) or measured directly by high-precision microcalorimetry (section IVA). It is also possible to determine this parameter by studying the discharge curves of severely anode- or cathode-limited systems under infinite external load. If the electrolyte is not an electronic insulator, there is an internal short circuit within the cell and the voltage will fall after the cell reactants have been consumed. Practical considerations have recently been reviewed.[32]

B. Electronic Conductivity

Electronic conductivity σ_{el} arises when current is carried by electrons (subscript e), or holes (subscript h). It is useful to be able to consider σ_{el} as a property of the solid electrolyte, but its measurement has to be carried out in conducting mode. Hence the parameter determined is the sum of σ_{el} and the two electrolyte–test

electrode conductivities. Not only is σ_{el} difficult to obtain, but for prediction of device behavior it is not the sole determinand of the electronic conductiviy of the system. In a battery, for example, the system behavior will also be affected by the electrolyte-real electrode interfaces.

Wagner's method has been much used to study σ_{el}, but other techniques are now coming onto prominence.

1. Wagner's Method

This employs an electrolytic cell with one reversible and one blocking electrode.[119,125,129] When a voltage, E, of below the decomposition potential of the electrolyte is applied to the cell, ionic migration will occur until the concentration-induced chemical potential gradient balances the applied field.[13] At the resulting steady state, the cell is polarized and any residual current, I_{el}, flows because of electron and/or hole migration across the electrolyte and the interfaces.

From consideration of the overall cell reaction, which is totally determined by the electrolytic/electronic charge transfer at the working electrode, and the resulting concentration gradients, it can be shown that[130]

$$I_{el} = I_e + I_h =$$
$$\frac{RTA}{zLF}\{\sigma_e[1 - \exp(-EF/RT)] + \sigma_h[\exp(EF/RT) - 1]\}$$

when the electrolytic species is a cation, and

$$I_{el} = I_e + I_h =$$
$$\frac{RTA}{zLF}\{\sigma_h[1 - \exp(-EF/RT)] + \sigma_e[\exp(EF/RT) - 1]\}$$

for mobile anions. A and L are the electrode cross-sectional area and separation.

If $E > 0.3$ V so that $\exp(EF/RT) \gg 1$ and $\exp(-EF/RT \ll 1$, then[131] for mobile cations

$$I_e = \frac{RTA}{zLF}\sigma_e$$

$$I_h = \frac{RTA}{zLF}\sigma_h \exp(EF/RT)$$

and for mobile anions

$$I_e = \frac{RTA}{zLF}\sigma_e \exp(EF/RT)$$

$$I_h = \frac{RTA}{zLF}\sigma_h$$

Thus under steady-state conditions, if one electronic carrier dominates, current should be independent of applied voltage for the cation/electron and anion/hole combinations. For cation/hole and anion/electron combinations, a plot of $\ln I$ as a function of E should have a gradient of F/RT and an intercept of $RTA\sigma_{el}/zLF$.

For many electrolytes, both electrons and holes act as carriers, in which case a plot of $(zLF/RTA)I_{el}$ $[\exp(EF/RT) - 1]^{-1}$ against $\exp(-EF/RT)$ will have σ_e as the gradient and σ_h as the intercept for a mobile cation system and the reverse for a mobile anion system.

As discussed above, these measurements are not directly applicable to battery systems. They are actually the parameters that would apply to an electrolytic cell containing the electrolyte under study and two identical working electrodes. In such a cell, however, as in the working battery, an applied voltage would be carried mainly by ions, and direct measurement of the electronic contribution is difficult.

The Wagner polarization cell therefore differs from the practical system in several important ways: (i) The electrode/electrolyte interfaces are different. (ii) Ions are depleted at one end of the Wagner cell and enriched at the other. In the battery, this would be prevented by charge transfer at the two working electrodes. (iii) In a battery in which the anode reaction involves the production of electrons and the cathode reaction involves their consumption, the galvanic field that drives the ions across the cell clearly opposes the motion of the electrons. A similar argument applies to hole conduction. Hence, Wagner cell measurements overestimate the electronic conductivity that is found in the real system. (iv) The contact resistance may be different, especially in the case of compacted powder systems. It is best to study I as a function of L, the other parameters being kept constant; the dependence will be linear if the contact resistance is negligible.

It has been argued[132] that the transport number of electrons, t_e, is lower in the battery than in the Wagner cell, whereas the reverse applies to t_h. The same author has pointed out that transport numbers in a galvanic cell are of less importance than the Faradaic efficiency, $\eta_{F,i}$. This is defined as

$$\eta_{F,i} = Q_i / \sum_{j=1}^{m} Q_j = Q_i / Q_{tot}$$

and is a function not only of t_i but also of the rate at which charge is drawn from the device. Whether a battery will self-discharge or not depends on the relative Faradaic efficiencies of two competing processes, firstly the combination of internal ionic transport and external electron transport, and secondly the internal electron transport process.[132]

The Wagner technique has been applied to many electrolytes; recent examples include studies of halogenides[32] and β-alumina[133] which have been reviewed elsewhere and also[134] the mixed conductor $AgCrS_2$.

2. Pulse Methods

Electronic carriers can respond more rapidly than ionic carriers to fluctuations in the applied potential. A technique based on this has been suggested[135] in which a dc voltage is applied across an electrolytic cell incorporating two similar working electrodes, e.g., M|MX|M. The current-time characteristics are monitored as a rapid voltage pulse is superimposed. If electronic conductivity is insignificant, then the slow response time of the ions will cause a smooth rise to the new current plateau corresponding to the higher voltage level and a similar smooth decline when the voltage pulse is removed. If on the other hand there is an electronic contribution, the smooth rises and falls will be preceded by abrupt jumps. This method has been recently developed,[136] and transient currents arising from the redistribution of electronic carriers and the motion of ions in CuI have been studied. A polarization cell -Cu|CuI|graphite+ was used which, as in the case of all the cells described in this section, was atypical of the battery application.

C. Direct Current Techniques

In part 1 the measurements of the ionic contribution to conductivity are discussed. Experiments to elucidate the charge-transfer process at the electrode–electrolyte interface are described in part 2.

1. Ionic Transport Number Determinations

The simplest method is to measure the ocv of a system under a chemical potential gradient.[136] Side effects obviously need to be absent. The galvanic cell M|MX|X is used, X being in its standard state.[137] The ratio of the ocv to the expected emf, E, calculated from thermodynamic data (section IVC) is taken as the ionic transport number, t_I. This also yields an estimate of t_{el}, since $ocv/E = t_I = (1 - t_{el})$, and this can be compared with the results from Wagner's method.[138] The agreement is usually poor.

An alternative is Tubandt's method[17,139] which is conceptually very simple, being merely a coulomeric determination in a solid-state system. An electrolytic cell is used, usually assembled from disks comprising an identical cathode and anode and three electrolyte regions, each of which can be separated. After passage of a suitable amount of current, the cathode and its adjacent slab of electrolyte will have increased in mass and the anode plus neighboring electrolyte will have decreased, the mean mass transferred being m. If the current that passes through the cell is integrated with respect to time, the mass transferred if the current were purely ionic, m_q, can be calculated, and t_I obtained from

$$t_I = m/m_q$$

In practice, the disks tend to stick together. Nevertheless, the method is much used and recent applications include halogenides,[32,140] oxides,[124] and lithium nitride halides.[120] Studies have also been carried out on systems involving more than one electrolytic species.

2. Electrode Kinetics

Electrochemical behavior at the electrode–electrolyte interface depends on two processes, charge transfer and diffusion. Detailed description of the charge-transfer process is not appropriate here, but for clarification the major parameters pertaining to the processes are briefly described.

Charge transfer is a redox reaction, which is characterized by a potential difference, E_e, at equilibrium. The excess of the applied potential, E, over E_e is the *overpotential*, E_η. At equilibrium, the rates of the oxidation and reduction reaction are equal, and these are described in terms of an *exchange current density*, I_0. A high value of I_0 means that the activation energy barrier, i.e., the difference in Gibbs energy between the oxidized (or reduced) species and the activated complex, is small and vice versa. Consequently I_0 is an important parameter for practical devices as it is a measure of the intrinsic rate of charge transfer. The Gibbs energies of the oxidized, reduced, and activated species, G_0, G_R, and G_+, are all linear functions of overpotential, and the slope of G_+ against E_η is characterized by the *charge-transfer coefficient*, α. The dependence of current, I, on overpotential is given by the Butler–Volmer equation which, in the *Tafel region* for the case when reduction predominates, simplifies to

$$\ln I = \ln (AI_0) + \alpha z E_\eta F/RT$$

A being area and z being the number of electrons involved in the charge transfer. Provided that charge transfer is not the rate-limiting step, the Tafel plot of $\ln I$ vs. E_η is linear for values of overpotential (corrected for electrolyte IR drop) greater than about 100 mV.

For liquid electrolytes, there are many techniques[118,141,142] which allow the kinetics of charge transfer to be studied under diffusion-controlled conditions. Because of the nature of the solid–solid interface certain techniques, such as those involving the rotating disk or the dropping mercury electrode, are not applicable to solid electrolyte systems.

Electrokinetic studies require a three-electrode system operating under conditions chosen to allow rapid charge transfer, so that measurements are taken under diffusion-limited conditions. Various modes of address, such as potentiostatic, galvanostatic, potentiodynamic, and steady-state ac, are possible, and the information obtained depends on these and also on the nature of the electrode–electrolyte couple.

If electrodes with well-defined cell reactions are used, e.g., Ag electrodes with an AgI electrolyte, essentially zero current flows until the applied voltage equals that for the cell reaction (e.g., $E_{Ag/Ag^+} = 0.69$ V vs. the reversible hydrogen electrode). For such electrodes, a Tafel plot can be obtained by *potentiostatic* address, in which a voltage step is applied between the working and counter electrodes and dI/dt monitored.

For variable stoichiometry electrodes such as the intercalation compound[143] Li_xTiS_2, there is no fixed cell voltage, and consequently when used in a battery, there is a steady decay in voltage during the discharge process ($E = 2.43$ V when $x = 0$ and $E = 1.72$ V when $x = 1$). Potentiostatic voltage steps applied to these systems give current growth/decay curves to/from $I = 0$, dI/dt being proportional to the diffusion of intercalated species. At short times, the time dependent current $I(t)$ varies with $t^{1/2}$ and the diffusion coefficient can be evaluated from the slope.[144] Tafel relationships cannot be applied to such systems, however, as increasing the voltage changes the stoichiometry of the electrode.

Galvanostatic address, in which a constant current is applied and the voltage response measured, can be used with both types of electrode. It has the experimental advantage that, provided the internal resistance remains constant, the IR drop is independent of time.

Potentiodynamic or voltammetry methods involve the monitoring of the current density response to an applied voltage that is varied with time. The sweep is normally linear, a triangular wave voltage being applied to the cell in the anodic (oxidizing) or cathodic (reducing) directions. In cyclic voltammetry, the sweeps are repeated many times, one after the other. Voltammetry is one of the most reliable electrochemical techniques for elucidating the nature of electrode process and for providing insight into complicated reactions. It is applicable to solid-state systems provided that the sweep rate is sufficiently slow for diffusion to remain the rate-determining step.

Direct information on the reversibility and kinetics of solid electrolyte systems has been obtained from voltammograms and Tafel plots for Cu/Cu^+ systems,[127,145] Ag_4RbI_5,[114,115] oxide conductors,[124] and vitreous glasses.[146] Other electrokinetic techniques used

for solid-state studies include *chonoamperometry*, the study of current as a function of time at fixed voltage, which has been used[147] to investigate CuBr–organic bromide solid electrolytes, and *chronopotentiometry* ($V(t)$ at fixed I), which has been applied[148] to high temperature electrolyte materials.

D. Alternating Current Techniques: Impedance Plots and Related Presentations

Conductivity measurements are normally carried out under ac conditions because, as discussed above, polarization effects are minimized. Many electrochemical parameters including conductivity are a function of the applied frequency. This is because the alternating current is out of phase with the applied ac voltage, and this perturbs the various processes within the cell (such as surface, interfacial, and bulk ionic transport, double-layer formation at the electrode–electrolyte interfaces, and charge-transfer reactions at working electrodes) in different ways.

One type of frequency dependence, discussed later, occurs when electromagnetic vibrations, particularly those in the microwave[149-152] and far-IR[153] region, are transmitted through a solid electrolyte. What is discussed here, however, is the dependence of the *impedance*, Z, on the angular frequency, ω, of the small-amplitude-applied ac electric field. Z is a complex quantity involving not only resistance, R, but also capacitance, C, and inductance, L, and the $Z - \omega$ relationship is usually represented in the complex plane, in the form of an impedance plot, admittance plot, permittivity plot, or modulus plot.[12] In principle, the various forms of impedance spectra provide detailed and separate information about many of the processes within the electrochemical cell. This is done by comparing the experimental plots with those that would have been generated by model systems called *equivalent circuits*. These consist of resistances, capacitances, and/or inductances in appropriate series and/or parallel combinations. The weakness of the method is that the choice of equivalent circuit is not unique. For example, resistances and capacitances can be combined on the basis either of a Maxwell model or a Voigt model (which involve quite different series and parallel combinations) to provide the same overall impedance.[154] The appropriate choice can only be made on the basis of assumptions about the relative configurations of, and importance of, the various parts of the cell process that cause the impedance. The different plots emphasize different regions of the frequency spectrum, and therefore the choice of the most appropriate plot depends on which part of the cell process is dominant.

Impedance spectroscopy is a very well established technique, especially for the study of liquid systems.[155-157] Only an outline of its basic principles will be given here, since the fundamentals of the method as applied to solid-state systems have been comprehensively reviewed recently.[122,154,158-165]

The ac voltage and current across a cell have the form

$$V = V_{max} \sin (\omega t)$$

$$I = I_{max} \sin (\omega t - \phi)$$

where ϕ is the phase angle. If ϕ is negative, so that the current leads the voltage, the impedance is composed of a frequency-independent resistance term, R, and a

capacitance term, $-j/\omega C$ or $-1/j\omega C$, where $j = (-1)^{1/2}$. If ϕ is positive, then V leads I and Z is composed of R and an inductance term, $+j\omega L$. In the complex plane representation, real quantities, i.e., those not involving j, are plotted on the x axis and imaginary quantities are plotted on the y axis. The conventional Argand diagram used by electrical engineers displays positive imaginary quantities, i.e., inductances, in its upper part and negative imaginary quantities, i.e., capacitances, in its lower part.[155] Because, until recently, it was not envisaged that inductive processes could take place within cells,[155,164] electrochemists normally invert the y axis so that the data, which are of a predominantly R/C nature, fall mainly in the upper quadrant of the diagram. This convention will be used in the description here.

The R, C, and L components can be combined in series or in parallel. A circuit consisting of a resistance, R_s, in series with a capacitance, C_s, will have an impedance

$$Z = R_s - j/\omega C_s$$

The impedance plot in this case is a vertical straight line intersecting the x axis at R_s; the y coordinate decreases as ω increases. The magnitude of $Z(\omega)$ is the length of a line from the origin to the point on the plot corresponding to the value of ω; this line is inclined at ϕ to the x axis. For a parallel network involving resistance, R_p, and capacitance, C_p, then

$$1/Z = 1/R_p + j\omega C_p = Y$$

where Y is the admittance. The impedance plot is now a semicircle of radius $R_p/2$, which meets the x axis both at R_p (for which $\omega = 0$) and the origin ($\omega = \infty$). Z is again given by the length of the line from the origin to the plot.

Additional complications arise in the equivalent circuit used to model a real cell incorporating a working electrode. Elements must be present that account for the impedances due to the various electrode processes discussed in section III, namely the double-layer capacitance, C_{dl}, and the charge-transfer and the diffusion steps. The charge-transfer contribution can be characterized by a *transfer resistance*, R_t, since the current that flows as a result of the applied voltage is in phase with the potential. R_t is usually proportional to the rate of the electrode reaction. The concentration-dependent diffusion term is a function of frequency, however, because the bulky ions move too slowly to respond in phase with the applied potential at high frequencies.[166] A suitable ansatz (or simplified expression) for the interfacial impedance at a working electrode is

$$Z = [j\omega C_{dl} + 1/(R_t + W)]^{-1} \qquad (1)$$

where W, the *Warburg impedance*, is given by

$$W = \lambda\omega^{-1/2} - j\lambda\omega^{-1/2}$$

the Warburg coefficient, λ, being a function of the concentrations and the diffusion coefficients of the oxidizing and reduced species.

Solid electrolyte systems often involve grain boundaries between polycrystals and/or interparticle boundaries within compacted powders, and elements have to be incorporated in the equivalent circuit to account for these. Inductive effects can also arise, particularly at high frequencies. These can be caused by the meas-

TABLE I. Impedance Studies of Some Solid Electrolytes

material	ref	material	ref
oxygen ion conductors	172	silver conductors	190
β-alumina	133, 173–176	thin AgCl films	85
zirconia-based and related materials	177–179	Ag_4RbI_5	114, 191
pyrochlores	180	α-AgI	192, 193
glasses	146, 181–183	$Ag_{26}I_{18}W_4O_{16}$	112, 194
lisicon and related materials	86, 103, 184, 185	$Ag_7QI_8{}^a$	195
lead chloride	186	$Ag_5pyI_6{}^b$	196
potassium hydrogen fluoride	187	interface properties	114, 197, 198
substituted lithium nitrides	188, 189		

^{a} Q = tetraalkylammonium. ^{b} py = pyridinium.

uring lead impedance[164] and also by rough electrode-electrolyte interfaces.[155] They give rise to appropriate semicircles, vertical lines, and Warburg lines which lie in the lower quadrant of the conventional electrochemical complex diagram. The high- and low-frequency ends are inverted with respect to the capacitance contributions.

The selection of the correct combination of elements to produce an equivalent circuit that corresponds to an experimental plot which may well take the form of a faintly wavy, roughly vertical line requires not only ingenuity but faith. In practice, to select the most likely out of several equivalent circuits, assumptions are made about which processes are physically likely to be working in series and which are in parallel. Also, the separation of bulk and interfacial effects is aided by the fact that they depend in different ways on sample length and area.[12]

Highly convoluted combinations of lines and semicircles in the impedance plot can sometimes be more easily interpreted from an alternative complex plane representation. An admittance plot has conductivity rather than resistance as the real axis and is suited to predominantly parallel networks. It is also possible effectively to interchange the real and imaginary axes by considering the permittivity (or its reciprocal, the modulus) in place of the impedance (or its reciprocal, the admittance). The permittivity, ϵ, is defined as

$$\epsilon = C_p l / A \epsilon_0$$

where l and A are the cell length and area and ϵ_0 is the permittivity of free space ($=8.854 \times 10^{-11}$ F cm^{-1}). In a permittivity plot, the real axis is C_p and the imaginary axis is $Y/j\omega$; in a modulus plot, the real axis is $1/C_s$ and the imaginary contribution is $j\omega Z$. The merits of these alternative representations have been reviewed elsewhere.[12,162,167]

The normal range of the frequency, f ($=\omega/2\pi$), is 100 Hz to 100 kHz, but the regime down to 1 mHz can provide valuable information about the charge-transfer process and assist in separating bulk and interfacial behavior.[159] High-frequency studies can also be carried out.[168]

Experimentally, bridge techniques were much used,[122] but because the determination of a complete plot could take many hours, during which time the cell behavior could change, it is now common to use automated systems.[169]

Many recent impedance studies of solid-state systems have been carried out to elucidate electrokinetic behavior,[127] to explain cell failure, and to provide reliable conductivity values. Two-dimensional nucleation has been investigated[170] and the behavior of powdered and

sintered systems studied.[97,113] Temperature-dependent Warburg coefficients had to be used to explain the behavior of the Pt/Ag_2S interface.[171] Some examples of impedance studies on a selection of materials are given in Table I.

IV. Electrochemical Properties: Indirect Measurements

This section describes how some of the parameters discussed previously can be measured by other techniques.

A. Calorimetric Studies of Self-Discharge

These measurements represent a useful synthesis of the sometimes conflicting approaches of scientist and technologist. As has been mentioned in earlier sections (IIIA5; IIIB), battery cells containing solid electrolytes that truly possess negligible electronic conductivity will not self-discharge. The electronic conductivity measurements relate to test systems rather than to isolated solid electrolytes, however, and it is difficult to be confident that the possibility of electronic conductivity in a given electrolyte has been eliminated. They also do not detect electronic leakage through the cell casing, spacers, and other nonelectrochemical components. Direct self-discharge tests relate better to the practical battery configuration in most respects except the system is not under load.

For many practical battery applications, a misestimate of self-discharge characteristics merely causes the expense of replacing batteries that have failed on the shelf. In the heart-pacemaker battery field, however, such an error could be literally deadly.[199] The technologist's need in this situation is to study self-discharge in the real system, rather than in a model; the scientist's response, in the absence of a direct probe, is to provide an indirect one.[200,201]

One method is to measure the very small heating effects that accompany self-generating processes within the battery, using a microcalorimeter.[202,203] The results of such measurements pertain not only to self-discharge but also to other effects detrimental to battery performance,[202] including corrosion reactions[204] and electrolyte degradation.[205] Differential heat-flow, twin-cell commercial instruments are often used,[206] although alternatives have been described.[204,207] A typical isothermal instrument used to measure internal resistance in LiI pacemaker batteries[204] involves a copper test chamber located within a massive aluminum heat sink, to which it is coupled through a BiTe thermoelectric module. It is thermostated to 37 ± 0.005 °C and is accurate to 5 μW, being sensitive to 1 μW, this being

necessary because the external current drain under normal load is only 27 μA. It is used both as a means of identifying faults in preproduction models immediately after fabrication and as a means of confirming conjectures based on electrical measurements, prior to destructive testing.

LiI cells used in pacemaker applications have design lifetimes exceeding a decade, which is longer than the batteries themselves have been in existence. Consequently, there is considerable interest in a more accurate description of their end-of-life characteristics than can be obtained from accelerated discharge tests. Calorimetric studies have been carried out[208] on cells that differ from the real system only in that they have a depolarizer that is deficient in iodine. This enables the end-of-life internal resistance to be found within a reasonable test time without higher current carrying loads being employed. A complication is that the internal resistance in such a system is determined largely by the depolarizer, rather than by the thin, highly resistive layer of LiI cell reaction product. The effect of ageing on the open circuit voltage of various battery systems has also been studied calorimetrically.[206]

B. Thermoelectric Power (TEP)

Measurement of the TEP or Seebeck coefficient, θ, is a simple alternative means of obtaining the activation energy of the ionic conductivity process. θ is the ratio of the potential gradient, ∇V, developed across a sample to the temperature gradient, ∇T, required for its production. It is related to the activation energy, Q (sometimes called the heat of transport), by

$$\theta = \nabla V / \nabla T = -Q/qT + H \qquad (2)$$

where q is charge, T is temperature, and H (which, like θ, has the dimensions of potential per temperature or alternatively entropy per charge) is a term accounting for electrode contact potentials. If the electrodes contain the mobile ion, then H is normally independent of temperature.[192,209]

In a solid electrolyte to which the so-called free ion model applies, Q is equal to E_a determined from conductivity studies. When correlation effects are present, then Q is less than E_a. The sign of Q given in eq 2 follows the convention that θ is positive if the hot end of the sample is at a positive potential with respect to the cold end. The sign of θ and the sign of the charge of the carrier species are therefore opposite, and it has been claimed that this enables ion and vacancy conduction to be distinguished.[192] In principle, because TEP is a zero current process, it has several advantages over impedance measurements of conductivity.[192] Contact problems are reduced and, provided small temperature gradients are used, the equilibrium distribution of ions is not perturbed by the measurement, thus eliminating contact polarization (the Soret effect). Further, interfacial effects such as interparticle and intergranular resistances and capacitances in polycrystalline materials do not change θ (provided they do not disturb the heat flow).

Although the data can be difficult to interpret quantitatively, the experimental procedure is simple. The sample can be a thin film[209] or a compacted powder,[192] in contact with metal test electrodes. One electrode is in contact with an adjustable temperature

heat sink, and a heater in contact with the other electrode is used to produce a temperature gradient across the sample. This is kept small to minimize the Soret effect and is monitored by a thermocouple with junctions in contact with each electrode. Minicomputer control can be used to change the temperature of the heat sink at which ∇T and ∇V are measured,[192] thus enabling θ to be easily studied as a function of T. It is necessary to measure θ during both heating and cooling in order to confirm that effects due to electrical signal drifts or thermal equilibration difficulties can be neglected.[192,209,210]

The problem of data interpretation arises because it is uncertain whether H is truly independent of temperature. Results for Ag_4RbI_5 in the form of thin films, pressed pellets, and samples solidified from the melt have been critically compared.[209] The lowest value for H was obtained for thin film samples, and it has been claimed that this was because of better experimental control of electrode contacts.[209] Solid-solution films of doped CdS, formed by spray pyrolysis, have also been studied.[211]

Early TEP studies of solid electrolytes have been comprehensively reviewed elsewhere.[14,212] Apart from Ag_4RbI_5, systems that have been recently investigated by this technique include pyridinium pentasilver hexaiodide[192,213] and reinvestigations[192,214,215] of AgI.

C. Thermodynamic Measurements on Cell Reaction

The emphasis in this section is on the determination of cell voltages from thermodynamic measurements carried out under reversible conditions. There are other thermodynamic parameters such as heat capacities,[212] entropies of disorder,[216] and phase transition quantities[144,217-220] which are relevant to the understanding of solid electrolyte behavior, and these are discussed later. The relation between electrokinetic parameters and equilibrium thermodynamic properties such as Gibbs energies[118] has already been considered. Transport properties such as diffusion, conductivity, and thermoelectric effects belong to the provinces of irrevesible statistical mechanics and thermodynamics[221] and are covered elsewhere in this article. The relationship between the standard molar Gibbs energy change for a reaction, $\Delta G^\ominus$, and the corresponding standard electrochemical potential, $E^\ominus$, is

$$\Delta G^\ominus = -zFE^\ominus$$

where z is stoichiometric charge number and F is the Faraday constant. $\Delta G^\ominus$ is a molar quantity whereas $E^\ominus$ is an equivalent quantity. Care must be taken when considering solid electrolyte cells that the data used refer to appropriate standard states. This reservation applies particularly to comparisons of half-cell potentials for solid-state systems, obtained from three electrode measurements, with tabulated electrode potentials. It must also be remembered that the latter are not experimentally accessible quantities in themselves. They are in fact $E^\ominus$ values for cells in which two electrodes are present, one being the electrode under consideration and the other being the standard hydrogen electrode.[222] As in all aspects of thermodynamics, it is essential to have clearly in mind the standard states that relate to the process under consideration and also

the physical state (solid, liquid, or vapor) that is involved. It is possible, for example, when considering room-temperature iodine cathodes, to forget that data pertaining to the vapor need to be converted for the solid state by subtraction of $\Delta_s^g G$ the Gibbs energy of sublimation.

In principle, the decomposition potential of the electrolyte, E_d, can be estimated from the Gibbs energies of formation of the electrolyte and its decomposition products. In practice, because of the effects of uneven potential distribution and IR drop, it is more usual to measure E_d directly. In recent studies[120] of Li_3N the lower limit of E_d was taken as the intersection of the I-V curve with the V axis. An alternative method is to measure the current passing through a graphite|-electrolyte|graphite cell as a function of applied voltage, E_d being taken as the voltage at which the current starts to rise steeply.[223] This procedure is open to question because of the polarizable nature of the graphite electrodes.

The major uses of thermodynamic data in the solid electrolyte field are to estimate the cell voltage to be expected for novel systems and to verify the cell reactions. If a particular cell reaction if assumed, then the electromotive force E, under thermodynamically reversible conditions (i.e., infinite load), is given by the Nernst equation.

$$E = E^{\ominus} - (RT/zF) \ln Z$$

R being the gas constant, T the temperature, and Z the function that defines the equilibrium constant. Under load, if side reactions involving ancillary cell components are absent, the measured voltage E_{meas} is given by

$$E_{meas} = E + IR + E_{\eta}$$

E_{η} being the total overpotential. E is a thermodynamic property whereas the voltage actually obtained from the cell system under infinite load, namely the open circuit voltage, ocv, is a technological parameter. The ocv is only equivalent to the calculated value of E if the correct cell reaction is assumed, the measuring procedure draws no current, and there is no electronic conduction within the electrolyte.

In practice, however, $E^{\ominus}$ can be used to predict the ocv of a room temperature cell to within a few percent. For certain systems on the other hand, large discrepancies are found. An example is the formation of CuI system for which $E^{\ominus}$ from thermodynamic data is 0.72 V, but the measured ocv is in the region of 0.4 V (even after due allowance has been made for the modified activity of the complexed iodine cathode).[77] In this situation it is clear that either there is significant electronic conductivity or the cell reaction taking place is not the one assumed. The presence of an induction period preceding the attainment of the ocv suggests the possibility of a chemical reaction taking place among the initial reactants within the cell to produce the electrochemical cell reactants.

Thermodynamic data can be obtained from cell voltage measurements. However, when a galvanic cell is on open circuit, the electrochemical potential (Fermi level) of the electrons in the two electrodes are different.[224] This means that, unless the electrolyte is truly an electronic insulator, self-discharge and a consequent

departure from reversible conditions will occur. As has been mentioned, this is not normally a problem with liquid electrolytes, but when solid-state systems are used to provide thermodynamic values, it is essential to establish that the concentration of ionic charge carriers greatly exceeds the concentration of electronic charge carriers.

The effect of junction potentials on E values for solid electrolyte systems has been recently discussed,[224] as have the relationships between defect concentration and oxygen partial pressure in high-temperature oxide cells.[122,124,224] In the room temperature electrolyte field, recent studies of modified silver iodide cells have been carried out to determine energies of formation of the complexed-I_2 cathode materials.[225] Other systems that have been examined include $LiAlCl_4$[226] and $Cu_xMo_6S_8$.[227] The thermodynamics of intercalation cathodes such as tungsten bronzes[228] and titanium disulfide[229] have also been investigated. In the latter case, a novel quasi-equilibrium method was used in which a series of potential steps were applied and open-circuit parameters were obtained by monitoring the current decay process. This technique of electrochemical potential spectroscopy[229] not only enables electrokinetic quantities to be evaluated but also permits the study of cell and cathode compressibilities and related thermodynamic response functions. It also provides information about adsorption thermodynamics.

D. Radioactive Tracers, Haven Ratios, and the Nernst-Einstein Equation

For materials for which defect-hopping models are applicable, radiotracer techniques can be used to measure diffusion coefficients which, if certain assumptions hold true, are related to conductivities.[12,230,231] The diffusion coefficient, D ($m^2 s^{-1}$), is related to the flux of diffusing species, J (mol $m^{-2} s^{-1}$), and the concentration gradient dc/dx (mol m^{-3}/m) by Fick's first law.

$$J = -DdC/dx$$

D has a similar temperature dependence to that for conductivity, σ, namely

$$D = D_0 \exp(-E_a'/RT)$$

and if diffusion and conductivity proceed by the same mechanism, the activation energy, E_a', will be approximately equal to E_a in eq 1. The tracer diffusion coefficient, D_t, which can be determined by one of the techniques described below, is equal to the "true" diffusion coefficient, D_T^*, if the process proceeds under equilibrium conditions throughout, and to $\tilde{D}_T$, the "chemical" diffusion coefficient, when it does not.[12] D_T^* can relate to an impurity-controlled, extrinsic diffusion process or to an intrinsic, self-diffusion process. For ionic conductors, in which the number of sites available for migration outweighs the number of defects produced, it is possible to study defect formation and mobility separately. The activation energy, which is in fact a Gibbs energy, is split into its entropy and enthalpy contributions, the former being subsumed into the D_0 term. The enthalpy term remaining in the exponent is divided into two contributions, H_m and H_f, which are respectively the enthalpies of motion and formation of 1 mol of defects, giving[82]

$$D_T^* = D_0' \exp[-(H_m + H_f/2)/RT]$$

This equation holds in the high-temperature, intrinsic region where thermally produced defects predominate. At lower temperatures, in the extrinsic region in which impurities are responsible for defect production, the corresponding relationship is[230]

$$D_T^* = D_0'' \exp(-H_m/RT)$$

so that H_m and H_f can be found from plots of D_T^* against $1/T$ over a suitably extensive temperature range. Because of the assumptions involved, this approach is more applicable to ionic conductors than to solid electrolytes. Isotope effect studies,[230] however, which are closely related to this approach, have found recent application for silver-based solid electrolytes.[232]

The major application of tracer studies to solid electrolytes is to relate conductivity and diffusion processes via the Nernst–Einstein equation and the Haven ratio, thus enabling considerable insight to be gained into the mechanisms of conduction.[12,82,231] A charged species diffusion coefficient, D_q, may be obtained from the Nernst–Einstein equation

$$D_q = RT\sigma/n_c F^2$$

n_c being the concentration of charge carriers and F being the Faraday constant. The Haven ratio, H_R, is the ratio of D_T^* to D_q, and its importance is twofold: it relates the jump frequencies, Γ, and jump distances, r, for the conduction and diffusion processes, and it measures correlations in diffusive motion.

H_R is related to the correlation factor, f, by

$$H_R = D_T^*/D_q = \frac{\Gamma_T (r_T)^2 f}{\Gamma_q (r_q)^2} \qquad (3)$$

The subscripts T and q on Γ and r pertain to tracer and conductivity studies, respectively. When the conduction process proceeds via a low concentration of defects, it is uncorrelated. In contrast, the diffusion process is nonrandom, and this is expressed by the fact that $f \neq 1$. For solid electrolytes, the conduction process also is correlated since the defect and charge carrier concentrations are comparable and f becomes a function of temperature. In this situation, the Haven ratio is no longer given by eq 3 but can be calculated by probability methods[233] or what are sometimes described[234] as Monte Carlo methods.[235]

D_t and, hence, under suitable conditions D_T^* can be determined[231] by serial sectioning or by the exchange technique. In the former, a thin layer of radioactive tracer is deposited on one end of a sample that is then annealed and subsequently sectioned at room temperature (at which D is small so that corrections for the change in concentration profile resulting from the sectioning process are minimized). In the latter, the tracer diffuses from the solid electrolyte into a well-stirred molten salt bath in which it is immersed, and either the residual activity of the solid or the activity of the liquid can be determined. Many studies have been carried out, especially on β-alumina.[133,231]

E. Molecular Dynamics Simulation of Ionic Conductivity

Computer simulations are included in this review although theoretical calculations are not, because simulations are experiments whose outcome, as in the case of physical techniques, is not predictable at the outset.

Although they depart from the real system because they are carried out on a model, they are nonperturbing in the sense used in the introduction, and all the parameters affecting the experiment are directly under the experimenter's control. Hence, unlike seemingly more direct physical measurements, they are not so susceptible to errors caused by unsuspected effects such as contact problems.

The method is described in detail later (section VI.I) together with many of its applications (see also section VII.F). Here, only the use of the technique to provide diffusion and conductivity information is considered. Molecular dynamics (MD), unlike Monte Carlo simulations, is not restricted to equilibrium situations and is well suited to the study of transport processes. It is becoming much used in the study of solid electrolyte properties, an application to which most of a NATO summer school was devoted in 1980.[7]

In outline, the method involves following the motion of a microcanonical ensemble (constant energy collection) of particles that are allowed to collide like balls on a pool table. The potential function under which they interact is specified by the experimentalist, and despite the small size of the systems commonly used (a few hundred particles), periodic boundaries enable the time-dependent behavior of much larger systems to be followed for "real" times in the order of nanoseconds (albeit at the expense of many hours of computing time). It has been used to determine the self-diffusion coefficient of Na^+ in β-alumina,[236] of Ag^+ in AgI, and of Cu^+ in copper iodide.[237] The diffusion coefficients agree well with D_T^* and, in addition, direct information about Γ is obtained. Very thorough studies of F^- diffusion in CaF_2 have been carried out.[238,239] A problem with this material is that the diffusion coefficients at experimentally accessible temperatures are below 10^{-5} cm^2 s^{-1}, which is about the slowest process that can be studied by MD without jettisoning budgetary constraints entirely. The conductivity of $SrCl_2$[240] has also been recently investigated.

F. Hall Effect Measurements

The Hall effect is the production of a voltage when a current passes along a wire situated in a magnetic field. It is much used in the study of metals and semiconductors to give a measure of the density of current carriers. When applied to the study of solid electrolytes in which there is a single mobile species, the wire is replaced by a slab of solid electrolyte cut from a single crystal. The classical equations can be used; the Hall voltage, E_H, is given by

$$E_H = R(IB)/d$$

I being current, B magnetic field, d the thickness of the sample in the direction of the dc magnetic field, and R the Hall coefficient. R is related to the number of charge carriers per unit volume, n, by

$$R = (nez)^{-1}$$

where e is the charge and z the valence. The mobility, μ, is related to the Hall voltage and to the ac applied electric field, V_{st}, by

$$\mu = E_H / V_{st} Bb$$

b being the distance between Hall probes. In practice it is necessary to carry out two measurements under

similar conditions except that in the second, the magnetic field is reversed, thus enabling the magnetoresistance voltage to be eliminated.

Studies of Ag_5pyI_6 suggest[241,242] that the density of charge carriers is unexpectedly small or alternatively that a hopping mechanism is involved, only ions in "mid-hop" contributing to the Hall voltage. Hall effect measurements have also been carried out of the Ag^+ ion mobility in Ag_4RbI_5[16,241,243,244] and AgI.[241] In the presence of light, the Hall signals arise from the passage of photoelectrons rather than ions.[16] The technique can be applied to powdered as well as to single-crystal samples,[97,245] but in all cases, the information on solid electrolytes must be interpreted with caution.

V. Structure Determinations

An understanding of the behavior of any solid material is facilitated by a knowledge of its structure. This is often obtained from a diffraction study, which produces atomic positions that are averaged not only over the time duration of the experiment but also over all the unit cells in the sample. The time averaging causes difficulties with disordered substances because it is difficult to separate the blurring arising from random site occupancy from that due to the thermal vibrations of the atoms about their lattice positions. The space averaging gives rise to problems in the study of defective solids in that the defect positions are not well revealed. As solid electrolytes are usually both defective and disordered, the double averaging greatly limits the completeness of the picture obtained from diffraction studies, and complementary techniques, which are discussed in the next section, are also required.

Too great a reliance on the conventional interpretation of diffraction data can also provide misconceptions about solid electrolyte behavior. It is possible to refine diffraction data for disordered solids by assuming that the materials are in fact ordered but the thermal vibrations are severely anharmonic, an approach that does not easily lead to an understanding of the conduction mechanism.[246] Further, diffraction methods sum all the correlations between the positions of atoms. This is exactly what is required for the estimation of the structure of well-ordered solids since the large amount of information permits the atomic positions to be determined precisely. For solid electrolytes, the rigid ion sublattice can be well characterized, which is useful, but much of the information pertaining to the mobile ion sublattice that is obtained from diffraction experiments is misleading, because the refinement techniques attempt to localize the mobile ion positions.

When an X-ray or neutron beam impinges on a sample, several types of event occur. Much of the beam is transmitted and a further proportion is utilized in the initiation of internal rearrangements within the sample, giving rise to photoelectric and similar effects. Only a small part of the beam is scattered, and of this, only the coherent, elastically scattered portion leads to conveniently observable diffraction effects. Although for most solids, this portion is of paramount importance compared with the remaining components of the scattered beam, for solid electrolytes this is not so.[247]

When considering diffraction, scattering, and related phenomena, it is helpful to make use of the concept of k space, which under appropriate circumstances is also called *momentum*, *reciprocal* or *Fourier* space. For entities such as photons and electrons that exhibit both wavelike and particlelike properties, the wavelength λ may be related to a quantity k called the wave vector, which in one dimension is defined by

$$k = 2\pi/\lambda$$

k may be expressed in three dimensions as $\mathbf{k}$, and the momentum, p (which is related to λ through the de Broglie relationship $\lambda = h/p$), may be restored to three dimensions as $\mathbf{p}$, so that

$$\mathbf{p} = \hbar\mathbf{k}$$

where $\hbar = h/2\pi$, h being Planck's constant. The elements of the vector (i.e., list of elements or components) $\mathbf{k}$ describe a position in $\mathbf{k}$ space related to momentum or reciprocal length, just as the spatial position of the particle can be described as a vector $\mathbf{r}$ in real or $\mathbf{r}$ space.

Both momentum and position are very fundamental properties for particles in a physical system as they relate to the kinetic and potential energy contributions, respectively. Also, the former helps to characterize transport properties and the latter is strongly involved in equilibrium behavior.

Conversion between $\mathbf{r}$ and $\mathbf{k}$ space is achieved by Fourier transformation, with which the chemist is becoming increasingly familiar through spectroscopic and other applications.[248,249] A diffraction pattern exists in $\mathbf{k}$ space, specified for a first-order diffraction by the same Miller indices hkl that describe a set of planes in $\mathbf{r}$ space.

It is unfortunate that atomic structure cannot be probed by an X-ray microscope in the way that microscopic structure can be studied under the optical microscope or the domain structure in thin samples can be investigated by electron microscopy. In microscopy, the scattering of waves by the sample can be thought of as producing an image in $\mathbf{k}$ space that is transformed by a suitable lens back into $\mathbf{r}$ space, in which form it is more readily appreciated. Information on the atomic scale cannot be obtained in this way because the wavelength of visible light is too long and X-rays or neutrons have to be used instead; suitable lenses for the recombination of the image do not exist for these beams. The equivalent of recombination is carried out by using either Fourier methods or a least-squares refinement of the difference between the experimental data and that resulting from trial structures. The latter is at present favored for general usage, but Fourier techniques are more suited to the more complicated scattering found in solid electrolytes.[247] Fourier synthesis plays a similar role in diffraction to that taken by the lens in microscopy.

Before considering X-ray and neutron diffraction methods separately, the relative merits of studying powdered, polycrystalline, and single-crystal forms will be compared. Many solid electrolytes are most easily prepared in powdered form, and a direct study of their structure avoids the possible complications of conversion to a different structure that could result from preparation of a single-crystal form. Because lines rather than spots are produced, the position and intensity data in $\mathbf{k}$ space are much more limited than for a single crystal.

The major use of powder diffraction data is as an aid to material characterization during synthesis,[246] al-

though they have been used to provide structural information. For AgI, single crystals of which do not easily survive the $\beta \rightarrow \alpha$ transition at 145 °C, the original determination of the highly disordered structure was in fact carried out in 1936 on a powdered sample.[250] Comparison of X-ray and neutron diffraction studies carried out on powdered samples of $Ca_xZr_{1-x}O_{2-x}$ have cast light on the behavior of the mobile oxide ion.[246] Despite the lack, therefore, of sufficient information for complete structure determination, powder diffraction studies have a role to play in elucidating solid electrolyte properties.

A. X-ray Diffraction

Consider X-rays as electromagnetic waves of wavelength λ similar in magnitude to the lattice spacing within a crystal. They are scattered by the outer electrons of atoms or ions, and some of the scattering is elastic, i.e., the scattered waves have the same energy and wavelength as the incoming beam. In certain directions relative to the incoming beams and the crystal lattice, the elastically scattered waves are coherent, i.e., in phase, and they reinforce each other. This is diffraction, and information about the lattice structure can be obtained from the positions and intensities of the diffracted beams. If the scattering centers (atoms) are considered to be located in a set of crystal planes whose directional properties are described by the Miller indices hkl, then the distance between the planes, d_{hkl}, is related to the angle θ_{hkl} between the planes and the incoming beam, by the Bragg equation

$$\lambda = 2d_{hkl} \sin \theta_{hkl}$$

where λ is the wavelength. For diffraction, it is also necessary for θ_{hkl} to be the angle between the diffracted beam and the planes and for the incoming and diffracted beams to be in a plane normal to the set of diffracting planes. In crystal chemistry it is conventional to reduce hkl to their lowest rational values and to multiply λ by the order of diffraction, n, which corresponds to the integer number of wavelengths by which the path length of beams, diffracted by adjacent planes, differs. It is customary for crystallographers, on the other hand, to describe higher order diffractions in terms of a single-wavelength path difference between planes spaced at d_{hkl}/n. Thus the second-order diffraction from the (100) set of planes is alternatively described as the first-order diffraction of the set of planes half as far apart, namely the (200) planes.

For a given X-ray wavelength the scattering power of an atom increases with the number of electrons it contains. Because the atomic diameter is not negligible compared with the X-ray wavelength, X-rays scattered on one side of the atom will partially interfere with those scattered from the other side, and so the atomic scattering factor, f, is a function of the wave vector $\mathbf{k}$, here expressed as $(\sin \theta_{hkl})/\lambda$. The atoms are not stationary, but vibrate about their lattice sites; to account for this, f is corrected by the temperature-dependent *Debye–Waller* factor. The scattering power of the unit cell can be expressed in terms of the frequency-independent *structure factor*, F_{hkl}, given by

$$F_{hkl} = \sum_j f_j \exp[2\pi i(hx_j + ky_j + lz_j)] \qquad (4)$$

the summation being carried out over the j atoms, of

TABLE II. X-ray Diffraction Studies

material	ref	material	ref
α-AgI	16, 21, 74	$Na_3Zr_2Si_2PO_{12}$	18, 246
Ag_4RbI_5; Ag_4KI_5	16	$Na_3Sc_2P_3O_{12}$	262
Ag_2S	252	$Na_4Zr_2Si_3O_{12}$	263
Ag_2Se	253	$NaLiSO_4$	254
$AgCrS_2$	134	K_2SO_4	254
Ag_3SI	16, 98	H_2/metals	252
Ag_2SO_4	254	CaF_2, BaF_2, $BaCl_2$	16
Ag_2HgI_4	16	$SrCl_2$, $SrBr_2$	16
$Ag_{26}I_{18}W_4O_{16}$	16	LaF_3	16
$Ag_5pyI_6{}^a$	16	$PbSnF_4$	181
AgI/QI^b	16, 76	Na-β-Al_2O_3	133, 246, 264
other Ag^+ salts	16	$(K,Mg)\beta$-Al_2O_3	265
$Cu_4NH_4Cl_3(I,Cl)_2$	75	$(Fe,K)\beta$-Al_2O_3	266
$CuTeX$	255		
Cu_6PS_5Br	256	Phase Diagram Studies	
$Cu_5py_2Br_7{}^a$	257	AgI/AsO_4	267
$Cu_{2-x}Mo_3S_4$	258	AgI/Cr_2O_7	267
Cu_3VS_4	259	AgI/Mo_2O_7	267
other Cu^+ salts	16	$CuCl/CuI/RbCl$	217
$LiTa_3O_8$	260	$CuCl/TlCl$	268
$Li_4B_7O_{12}Cl$	261	Bi_2O_3/MoO_3	269
other Li^+ salts	252	$B_2O_3/Li_2O/LiX$	181

fractional coordinates x_j, y_j, z_j in the unit cell. The intensity, I, of the diffracted beams is given by

$$I = |FF^*|pL$$

F^* being the complex conjugate of F; p and L account for multiplicity and Lorentz polarization factors.

It is easy to compute structure factors for known structures, but the reverse problem is much more difficult. The X-ray information is averaged in space and time and does not permit the phases of the individual scattering atoms to be determined. Various procedures have been devised to overcome this phase problem so that structure determinations can be carried out.[251]

It is possible to satisfy the Bragg equation in several ways. In the Laué method, mainly used to check the orientation of single crystals, a stationary sample and a polychromatic X-ray beam are normally used, although monochromatic Laué diffraction is discussed later (section VID). Alternatively, many of the hkl planes of the sample can be presented to a monochromatic beam, either simultaneously as in powder diffraction or sequentially as with single-crystal studies. Powder diffraction is particularly useful when studying phase transitions (section VIIB) and when characterizing phase diagrams, examples of which are included in Table II.

From single-crystal studies, the structure of complex materials can be determined. The use of automatic data collection and computer data processing has made this a much less tedious and more rapid process. The structures of many solid electrolytes and mixed conductors have been studied; some recent examples are cited in Table II.

B. Neutron Diffraction

In neutron scattering, much of the beam is not scattered elastically; this reduces the diffracted intensity and complicates the interpretation of the results. This results in neutron diffraction being more limited than X-ray diffraction but in neutron scattering being more rewarding than X-ray scattering. Neutron studies re-

TABLE III. Neutron Diffraction Studies

material	ref	material	ref
α-AgI	270, 271	LiAl	273
β-Ag$_2$S	271	Li$_x$NiPS$_3$	274
Ag$_2$SO$_4$	254	PbF$_2$	275
K$_2$SO$_4$	254	SrCl$_2$	275
LiNaSO$_4$	254	PbSnF$_4$	181
Na$_3$PO$_4$	254	Pb$_{1-x}$Bi$_x$F$_{2+x}$	276
Ag$_3$PO$_4$	254	β-Al$_2$O$_3$	277
Cu$_6$PS$_5$Br	272		

quire expensive equipment, available only at a few places, and the useable neutron flux is several orders of magnitude below that of X-rays. However, the atomic scattering factor b_j is similar for most elements, even hydrogen, in contrast to X-rays for which f_j for heavy elements greatly exceeds that for light elements. Also neutrons are scattered by the nucleus, which is small, rather than by the large electron clouds, and so b_j, unlike f_j, is independent of $(\sin \theta/\lambda)$. Other advantages of neutron diffraction include the relative ease with which variable temperature studies can be carried out and the higher transmission by the sample of neutrons compared with X-rays. f_j varies regularly with atomic number, making it difficult to distinguish neighboring elements by X-ray diffraction; the minor variation of b_j is irregular, so that neutron diffraction is not limited in this way. The phase problem is no less severe for neutrons than for X-rays. The mobility of one of the sublattices in solid electrolytes inevitably makes it very difficult to arrive at a suitable starting model.[246,247] In practice, the usual Fourier transform is quite complex, even for solids of high symmetry, and the disorder complicates the least-squares refinement techniques used for well-behaved structures. A procedure that can be used is the *difference Fourier* method in which a Fourier synthesis is carried out of the difference between the observed structure factor and that calculated from a specific model. The phases are provided by the model structure. Sometimes it is necessary to omit certain features from the model structure factor so that those features are highlighted in the difference map. This so-called *partial Fourier synthesis* helps to overcome the blurring caused by the need to truncate the Fourier series, and thus enables mobile and fixed ions to be displayed together.

Neutron diffraction structural studies have recently been reviewed,[247] and some examples of both single crystal and powder studies are given in Table III.

VI. Sublattice Mobility, Disorder, and Structure

For all solid materials, including solid electrolytes, the structure-determining techniques described above provide valuable insights into the physical and mechanical properties. Solid electrolytes differ from the majority of solid materials in that some of the ions are free to move within a relatively rigid framework or matrix. Consequently, it is also necessary to focus attention on the properties of the mobile sublattice and in particular its relationship to the rigid host lattice.

There are a number of techniques which can be used to study the local host lattice environment around the mobile ions.[278] They help, in varying degrees, to elucidate the pathways traversed by the moving ions on their journey from site to site, the number and nature of the sites, the residence time at the sites, and the

frequency of hops between them. Some techniques are more direct than others in addressing such intimate, atomic scale detail. Because the techniques that highlight the mobile–host interactions most directly, such as EXAFS and molecular dynamics, are perhaps less familiar to chemists than NMR, calorimetry, and so on, the more generally encountered types of study are covered first.

A. Nuclear Magnetic Resonance and Nuclear Quadrupole Resonance

To a chemist accoustomed to the subtle chemical shifts in proton and ^{13}C NMR used for molecular structure determinations, this technique appears in an unfamiliar guise when used for the study of solid electrolytes. Unusual nuclei such as ^{6}Li, ^{7}Li, ^{11}B, ^{19}F, ^{23}Na, ^{51}V, and ^{87}Rb are studied. Attention is concentrated on spin–lattice relaxation times (T_2), spin–lattice relaxation in the rotating frame. (T_{1p}), quadrupole interactions, and motional narrowing behavior. Therefore, although this technique is commonly used by chemists, a brief description of its basic aspects is given.[279,280]

Nuclei often possess spin, I, quantized in units of $^1/_2$. When I is 1 or greater, the nucleus can also have a nuclear quadrupole moment. The nuclear spin can interact with large external magnetic fields, which split the spin states of the nuclei into $(2I + 1)$ separate energy levels. The energy difference between these levels, ΔE, can be modified when $I \gtrsim 1$ by an interaction between the nuclear quadrupole moment and the crystal field gradient, produced by the inhomogeneous charge distribution in the crystal surrounding the nucleus. A further perturbation of ΔE is caused by a magnetic dipole coupling between the spin of the chosen nucleus and other spins in the lattice.[281]

Transitions between the energy levels can be induced by radio-frequency (rf) electromagnetic radiation of Larmor frequency, ν, given by

$$\nu = \Delta E/h = -\gamma H_0/2\pi = \mu H_0/hI$$

where h is Planck's constant, γ is the "gyromagnetic ratio", H_0 is the static magnetic field strength, and μ is the nuclear magnetic moment. A suitable fixed value of the applied field, H_0, can be chosen so that for, e.g., protons, ν is close to 60 or 100 MHz or some other suitable value. Chemical analysis is usually carried out on solutions and examines the *intramolecular* interactions. It utilizes "chemical shifts" of a few parts per million in ν which are caused by the screening effect of the electrons on neighboring protons within the same molecule. These are normally detected by scanning radio frequency at constant applied magnetic field strength.

Although this type of NMR has a role to play in the confirmation of the molecular structure of ligands used in solid electrolytes,[88,282] the main application within the field rests on the time taken for the nucleus to decay from an excited spin state via *intermolecular* interactions. A given nuclear spin state can exchange energy with other spins through magnetic dipole spin–spin coupling and also with its surroundings by means of spin–lattice coupling. In solid electrolytes, the surroundings are not static with respect to the given nucleus because diffusion moves the spins among different environments. NMR is therefore able to give a measure

of the residence time of a given nucleus at a particular site. Thus the hopping frequency can be obtained from studies of various time parameters associated with the exchange of energy between nucleus and surroundings.[280] The results are more precise than hopping frequencies obtained from conductivity measurements where a model must be assumed for the diffusion process since conductivity, unlike NMR, also depends on jump distance.[280]

NMR cannot distinguish local motion among a cluster of neighboring sites from the long-range transport needed for good dc ionic conductivity. It can indicate, however, whether the conductivity is dominated by motion along the surface, through grain boundaries, or via the bulk of the material.[283]

Dynamic effects are characterized by a correlation time[281] or time of stay, τ, given by

$$\tau = \tau_0 \exp(E_a/RT)$$

and a correlation frequency $1/\tau$ which is related to he Larmor frequency line width $\Delta\nu$ by the Heisenberg uncertainty principle, for static spectra.

$$h \leq \delta p \delta x = \delta E \delta t = h \delta \nu \tau$$

Therefore

$$\delta \nu \geq 1/\tau$$

There are consequently two regimes to be distinguished, one where $1/\tau \ll \delta\nu$, in which the static spectrum is seen, and the other in which the resonance line structure collapses into a single peak.[281]

The correlation time is related to the important parameters T_1, the *spin–lattice relaxation time*, and T_2, the *spin–spin relaxation time*, via rather complicated terms involving a number of factors, which may be simplified to give[281]

$$1/T_1 = f(\tau/(1 + \tau^2\nu^2), ...)$$

$$1/T_2 = f(\tau, ...) + f(\tau/(1 + \tau^2\nu^2), ...) \quad (5)$$

Hence, when $1/\tau \gg \nu$, the factor $\tau/(1 + \tau^2\nu^2)$ reduces to τ, whereas when $1/\tau \ll \nu$, it is proportional to $1/\tau$. There is therefore another regime demarcation when $1/\tau \approx \nu$. The $\partial\nu$ and ν crossovers typically occur at 10^5 and 10^8 Hz, respectively,[281] corresponding to a line width of about 1000 ppm. The first term in eq 5 is related to *motional narrowing*. This arises when the jump rate of the nucleus exceeds the frequency width of the rigid lattice NMR line and accompanies the minimum that occurs at the ν crossover. It is caused by a substantial reduction in the dipole and quadrupole interactions that give rise to the broadening of the absorption line in the stable lattice;[12] as the temperature rises, this reduction causes τ to rise.[279]

Other important parameters are the *phase correlation loss* arising from motion in a spatially varying magnetic field and the *spin–lattice relaxation time in the rotating frame*, $T_{1\rho}$. The latter is measured by studying the decay of the NMR signal "locked" in a transverse direction by a second rf pulse;[279,284] it has properties intermediate between T_1 and T_2.

Experimentally, there are two very different NMR procedures which can be used to study solid electrolytes, broad line (continuous wave, CW) and transient

TABLE IV. NMR Studies

material	nucleus used	spin	ref
AgI	^{127}I	$^5/_2$	289
Ag$_4$RbI$_5$	^{87}Rb	$^3/_2$	290
AgI/B$_2$O$_3$ glass	^{11}B	$^3/_2$	291
Cu$_3$VS$_4$ (Sulvanite)	^{51}V	$^7/_2$	279, 292
Li$_3$Al	^{7}Li	$^3/_2$	293
Li$_3$N	^{7}Li	$^3/_2$	294
Li$_3$N	^{6}Li	1	288
Li$_x$NPS$_3$	^{31}P	$^1/_2$	274
LiAlSiO$_4$ (β-eucryptite)	^{7}Li	$^3/_2$	279
LiAlSiO$_4$	^{27}Al	$^5/_2$	295
LiSCN/poly(ethylene oxide)	^{7}Li	$^3/_2$	296
LiX glasses	^{7}Li	$^3/_2$	181
(Li,Na)β-Al$_2$O$_3$	^{7}Li	$^3/_2$	297–300
(Li,Na)β-Al$_2$O$_3$	^{23}Na	$^3/_2$	298
Na-β-Al$_2$O$_3$	^{23}Na	$^3/_2$	133, 281, 301–303
Na$_2$O-enriched Na-β-Al$_2$O$_3$	^{23}Na	$^3/_2$	304
Na-β-Al$_2$O$_3$	^{27}Al	$^5/_2$	305
Na$_3$Zr$_2$Si$_2$PO$_{12}$ (Nasicon)	^{23}Na	$^3/_2$	306
LaF$_3$	^{19}F	$^1/_2$	307
electrochromic WO$_3$	^{1}H	$^1/_2$	308
glasses	^{205}Tl	$^1/_2$	309
	^{7}Li	$^3/_2$	181
	^{19}F	$^1/_2$	181
	^{11}Bi	$^3/_2$	181, 291

(Fourier transform). In both cases a static external magnetic field is used; in the former, the rf field is continuously applied, whereas in the latter, a brief intense rf pulse is employed. In broad-line NMR, the important parameters are the position, width, and shape of the rf absorption peak. Transient NMR gives the phase correlation loss and the parameters T_1 and T_2.

The temperature variation of the line width[279] or its second moment, the mean square width,[285] can be used to study motional narrowing in broad-line NMR. In transient mode the temperature variation of T_2 can be used.[286] Paramagnetic impurities affect T_1 and T_2 because mobile nuclei tend to diffuse to their vicinity,[279,280] and this is likely to be increasingly studied in the future. Both single crystals and powders can be studied, and impurity diffusion has been investigated.[15,287]

Nuclei such as ^{2}D, ^{7}Li, and ^{23}Na possess a nuclear quadrupole moment. For ^{7}Li, dipole and quadrupole interactions are comparable, but in ^{23}Na and ^{2}D, the quadrupole term dominates. In Li$_3$N, the quadrupole interaction gives a ^{7}Li triplet and a ^{6}Li doublet,[288] thus illustrating that the quadrupole–crystal field gradient interaction splits into $2I$ levels.

The nuclear quadrupole resonance (NQR) spectrum is characterized by five parameters,[281] the coupling constant C (which is a function[285] of quadrupole moment, electric field gradient, and nuclear spin), the assymmetry parameter, η, and three angles which give the orientation of local principal axes relative to crystalline axes. The quadrupole coupling gives rise to line broadening and sometimes to a spectrum of resolved resonance lines. There are certain relationships between C, η, and site symmetries; for example, C is zero for a cubic environment and η is zero for an environment of 3-fold or higher symmetry. This helps in determining ionic motion, phase changes, and site occupancy. NQR spectra have been studied for β-alumina by rotating the magnetic field about the crystal C axis to vary the three angular parameters.[281] A few examples of NMR solid electrolyte studies are given in Table IV.

B. Electron Spin Resonance or Electron Paramagnetic Resonance

This technique is similar to NMR in that electron spin states are split by a static magnetic field and transitions between the states can be induced by electromagnetic radiation. The radiation is of microwave rather than radio frequency, however. ESR only occurs for paramagnetic species, i.e., those containing one or more unpaired electrons, such as radicals, di- and trivalent transition-metal cations, and color centers.

Most mobile ions are monovalent, diamagnetic species, which cannot be studied directly by ESR. Instead low concentrations (1000 ppm) of paramagnetic impurities are introduced either into the immobile, host sublattice or as a mobile species, to act as a probe of the local environment. Hence like EXAFS, but unlike X-ray or neutron diffraction, a subset of the overall structure is examined.

The ESR spectrum of the paramagnetic constituents of the sample is modified by internal and external interactions. Certain paramagnetic species such as $^{55}Mn^{2+}$ have a nuclear spin, which interacts with the electron spin to produce hyperfine structure. An additional internal effect is spin–orbital coupling which allows resonance only when the angular momentum changes as a result of a reorientation of the orbital.[310] For P states this only occurs in extremely strong magnetic fields; under normal conditions, the ESR spectrum is orbitally quenched. This quenching is not so severe for D and F states, and does not affect S states. Thus Mn^{2+} which is in an S state by virtue of its half-filled d shell, gives a strong ESR spectrum.

There are several external effects that perturb the energy gap between electron spin states. Interaction with the electrostatic field produced by the ions in the crystal surrounding the probe species causes a fine structure. Analagous to the hyperfine splitting already mentioned is superhyperfine structure in which the nuclear spins involved are on neighboring atoms.[311] Relaxation effects can also take place and are characterized by spin–lattice (T_1) and spin–spin (T_2) times as for NMR. For ESR, however, T_1 is substantially more important, although the 60-GHz frequency needed is larger than ionic hopping frequencies except at high temperatures.[280] It is necessary for the paramagnetic probe species to be in low concentration because of the obscuring effect on the spectrum of strong spin–spin interactions.[15,280,311] In particular, the superhyperfine splitting is lost to ESR, and the rather more sophisticated technique of electron–neutron double resonance (ENDOR) has to be employed.

In practice, two experimental regimes are used, the normal X band at about 10 GHz and also the Q band at about 35 GHz. It is best to study single-crystal samples because of the crystal-field information that can be accessed, but powders and polycrystals can yield limited information. Care must be taken in choosing the probe species in order to minimize undesirable effects arising from cation size and valence. In common with many of the other techniques discussed here, it is nondestructive except insofar as variable-temperature studies may modify the sample, although it must be classified as a perturbing technique because a probe species must be incorporated. Applications to oxides of fluorite structure have recently been reviewed.[311]

β-Alumina has been studied, using Mn^{2+} as a probe;[312] two different sites have been identified at room temperature. Mn^{2+} has also been used in PbF_2, in which the onset of conductivity with rising temperature is gradual, rather than rapid, as in the case of Ag_4RbI_5. In this anion conductor, the hyperfine structure disappears and the lines narrow at 220 °C as the F^- ions become mobile.[313] Above 400 °C, however, the lines broaden again, perhaps due to a change in spin–orbit coupling restrictions,[313] although this has been disputed.[280] X-band studies of Cu^{2+} in sodium gallate[314] show hyperfine splitting which disappears either through Cu^{2+} motion or by fluctuation of oxide ion bridges as a result of Na^+ diffusion.[280,314]

C. Calorimetry

Calorimetry is a generic term, covering the measurement of the temperature rise accompaning many different heating effects. Its use in connection with self-discharge measurements and related battery parameters has been covered in section IVA. In its adiabatic, isothermal, or differential scanning (DSC) forms, it is much used in the study of phase transitions. For solid electrolyte studies on sublattice disorder, calorimetry can be used to provide the temperature dependence of C_p, the heat capacity at constant pressure. From this $C_v(T)$, the heat capacity at constant volume, which can be related to lattice vibrational terms, can be obtained.

The most precise determinations of C_p are by adiabatic calorimetry, in which the sample (usually several grams) contained in a sealed vessel is brought into thermal equilibrium with its surroundings and then subjected to an electrical heating pulse, usually of several minutes' duration. The system is reequilibrated at the new temperature and the process repeated. C_p at a given temperature is obtained by dividing the heat input (appropriately corrected for deviations from adiabatic conditions, etc.) by the temperature rise and then subtracting the heat capacity of the vessel, thermometer, exchange gas, and so on.

Phase transitions and Shottky and other anomalies can be directly detected from the C_p vs. T curve. Also, the residual entropy S°, which is the positional disorder frozen-in at 0 K, can be obtained from

$$S^{\ominus} - S^{\circ} = \int_{T=0}^{T=T} C_p^{\ominus} \, d \, (\ln T)$$

$S^{\ominus} = (H^{\ominus} - G^{\ominus})/T$, $S^{\ominus}$, $H^{\ominus}$, and $G^{\ominus}$ being the standard entropy, enthalpy, and Gibbs energy at T (usually 298.15 K). S° yields the number of energetically equivalent configurations taken up per formula unit at 0 K, W, since

$$S^{\circ} = k \ln W$$

where k is Boltzmann's constant. A similar use can be made of the entropy change $\Delta_\alpha^\beta S$ accompanying a first-order phase change, and thus relative disorder between two phases can be measured.

Many calorimetric studies of disorder have been carried out.[285,315,316] Like X-ray structural studies, the results are time averaged, but with calorimetry both heavy and light atom disorder is equally easy to detect.

It is possible by use of the thermodynamic relation

$$C_p - C_v = TV\alpha^2/\kappa$$

(V being volume, α the coefficient of thermal expansion, and κ the compressibility) to obtain C_v. This is predominantly a function of the long-wavelength, lattice vibrational (or phonon) frequencies. The calorimetrically derived value of C_v can then be compared with that obtained from spectroscopic measurements. This can help to elucidate entropy differences between polymorphs in situations where transitional entropies are not involved.[317] Anomalously high heat capacities, arising from unexpected disorder of a supposedly ordered form, can be detected.

For many solid electrolytes, C_p falls with rising temperature. For Ag_4RbI_5, this behavior has been well characterized,[318,319] and, in addition, it has been shown that (i) the substance has residual entropy of 9.4 J K^{-1} mol^{-1}; (ii) there is a configurational contribution to C_p from 50 K upward; (iii) the configurational entropy of the phase at 300 K is 45.2 J K^{-1} mol^{-1}.

In estimating these properties, a Schottky anomaly was allowed for and the 18 degrees of freedom for Rb$^+$ + 5I$^-$ were treated by the continuum model Debye functions whereas the 12 degrees of freedom pertaining to the 4 Ag$^+$ were taken as independent oscillators using Einstein functions.

The heat capacity of the solid electrolyte form of CuI also falls with rising temperature.[320] The effect is too protracted to be ascribed to the disappearance of short-range order and in fact indicates directly the conversion of vibrational to translational motion, as shown by the loss of some of the phonon contributions.[285] Calorimetric data have been obtained for other silver salts such as $Ag_7I_4AsO_4$[321] and the mixed conductor $AgCrS_2$, although the original measurements[322] have been criticized[134] for the probable presence of unreacted Ag_2S.

Excess specific heat contributions for the mobile cations in substituted β-aluminas have been found to be in good agreement with infrared data.[303] For PbF$_2$, C_v obtained calorimetrically from C_p as described above is considerably lower than the expected value of $9N_Ak$ JK^{-1} mol^{-1} (N_A being Avogadro's constant and k Boltzmann's constant) given by the three degrees of freedom for each of the three atoms in the formula unit.[323]

D. X-ray Scattering

X-ray scattering is essentially restricted to the diffuse part of the coherent, elastically scattered beam. In other words one studies, using conventional single-crystal photographic film or diffractometer techniques, the rather blurred bands lying between the spots corresponding to Bragg peaks. It is simpler but more limited than neutron scattering. The difficulty is to deconvolute the effects of thermal vibrations from those due to the mobile ions. The X-ray/atom interaction lasts for 10^{-18} s, whereas both thermal vibrations and diffusive jumps are of about 10^{-13} s in duration. Inevitably, the data obtained are similar to a set of superimposed snapshots.[48]

One-dimensional conductors such as Hollandite are particularly suitable for investigation because the restriction on possible paths makes it relatively easy to select a suitable model. The difference Fourier procedure described earlier is often used. For K-Hollandite the scattering was found to be caused by the presence

of subdomains, mainly consisting of rods of from two to five K$^+$ ions.[324-326]

Another material to have been studied is β-eucryptite, LiAlSiO$_4$. This has a conductivity sufficiently high to measure; it has been used as an electrolyte in conjunction with a small Li anode and a large cathode in an electrolytic cell. The only part of the cathode to be plated with lithium was that part directly opposite the anode. This shows that the electrolyte is a one-dimensional conductor.[327]

For this material at room temperature, the structure is ordered and diffuse scattering is not seen in monochromatic Laué scattering studies. In this technique, a conventional single-crystal camera is used but neither the sample nor the film are rotated, subsequent exposures being taken at slightly different angles so that the whole k space is eventually covered. The Li$^+$ reflections weaken with increasing temperature and diffuse layers appear.[48]

The technique has been used to show[301,328,329] the presence of an order–disorder transition in stoichiometric Ag-β-Al$_2O_3$ and to study β-Al$_2O_3$ in which some of the Al^{3+} in the spinel blocks has been replaced by Mg^{2+}.[330]

E. Neutron Scattering

Experimentally, neutron scattering is similar to neutron diffraction. Two types of instrument are commonly used,[331] a time-of-flight (TOF) spectrometer which is most efficient for isotropic measurements such as those on powdered samples and a triple axis (TA) spectrometer. The latter is preferred for single-crystal studies.[331]

Neutron scattering is a very powerful technique that provides considerable insight into mobile ion behavior.[149,247,332,333] To see this, let us consider the scattering process in further detail.

The *total* scattering is made up of two parts, *coherent* and *incoherent*, which cannot be separated experimentally. Incoherent scattering arises because different isotopes of a given atomic species have different scattering cross sections and also because the cross section varies according to whether the neutron and nuclear spins are parallel or antiparallel. Hydrogen exists in two states, ortho and para, with different nuclear spins, and its scattering is almost entirely incoherent.

The coherent and incoherent contributions measure quite different things. Coherent scattering depends on a structure factor that is the Fourier transform of an important quantity called the van Hove correlation function, whereas incoherent scattering involves the van Hove *self*-correlation function. The significance is that the correlation function depends on $\langle r_1(0)r_2(t)\rangle$ whereas the self-correlation function depends on $\langle r_1(0)r_1(t)\rangle$. The former term is the product of the initial position of one atom, $r_1(0)$, and the position of some other atom at a later time, $r_2(t)$; the triangular brackets denote an average taken over time and also over all the atoms in the sample. The latter term correlates the initial and subsequent positions of a given atom, again averaged over time and over all atoms in turn.

Consequently it can be seen that coherent scattering gives information about the position of atoms *relative to their neighbors* and incoherent scattering directly maps *diffusive motion*. The study of gas diffusion in,

e.g., metals is often carried out by neutron scattering. Hydrogen is usually used as the diffusing species not only because it is small and consequently has a high diffusion coefficient but also because of its high incoherence. Very recently attempts have been made to utilize this property in solid electrolyte studies on β-Al_2O_3 in which the Na^+ ions have been replaced by NH_4^+ ions.[332] Proton conductors do not yet appear to have been investigated. More general use of incoherent scattering would be desirable, especially if one could "tune in" to Na^+, e.g., in β-Al_2O_3. Unfortunately this is not possible as the ratio of coherent to incoherent scattering cannot be controlled.[332] A subtle procedure, not so far applied to solid electrolytes, is to use two samples containing different isotopic mixtures of mobile particles and therefore exhibiting different ratios, from which the coherent and incoherent contributions can in principle be separated.[149] The incoherent contribution is quasi-elastic because neutrons scattered by mobile particles will have slightly different energies depending on the position of the particles. The width of the quasi-elastic peak is related to the diffusion coefficient.[149,331]

The coherent contribution is made up of three parts, *elastic, diffuse elastic,* and *inelastic.*

Elastic scattering has already been discussed; it gives rise to Bragg peaks for single crystals and Debye scattering for powders.[334] Diffuse elastic scattering is of two types. The mobile sublattice produces wide bands between the Bragg peaks as in X-ray scattering. Also, the distortions of the rigid sublattice caused by the mobile particles cause *Huang* scattering which appears as a diffuse intensity close to the Bragg peaks.[247]

Elastic coherent scattering is characterized by a simple structure factor described above (eq 4). The total scattering is a more complicated process involving time-dependent behavior and is characterized by a *dynamic structure factor* which is a function of momentum and frequency.

The expression governing coherent inelastic neutron scattering is complicated.[247,331] Essentially, it predicts peaks at energies corresponding to the lattice vibrational modes of the sample. In practice, for solid electrolytes these sharp peaks are broadened into bands of Lorentzian shape, the width of which is affected both by anharmonicity and by defect scattering, so that the interpretation of the results is not simple. The importance of the inelastic contribution is that it probes the time-dependent fluctuations in the average structure, whereas the elastic part is restricted to an overall and less informative study of the time-averaged behavior.

For both elastic and inelastic scattering, energy and momentum are conserved. In both cases, momentum is transferred from the incident neutron to the sample so that there is a difference in the initial and final momentum of the neutron. Elastic scattering occurs when the momentum gained by the sample matches up with a particular reciprocal lattice vector. Since the momentum transfer is related to $(\sin\theta)/\lambda$ and the reciprocal lattice vector is the d_{hkl} spacing for a particular set of planes, this is merely an alternative way of expressing the Bragg condition.

For inelastic scattering, the momentum transfer is accompanied by an energy transfer which gives rise to

TABLE V. Neutron Scattering Studies

material	ref	material	ref
α-AgI	336	H_3O-βAl_2O_3	264
β-AgI	337	BaF_2	341, 342
AgBr	338	$SrCl_2$	341, 342
Ag_4RbI_5	339, 340	PbF_2	343-345
Na-βAl_2O_3	247	$TaS_2 \cdot NH_3$	346
Ag-βAl_2O_3	247	$TaS_2 \cdot (NH_3)_{1/3}(H_2O)_{2/3}$	346
NH_4-βAl_2O_3	247		

the creation of phonons, the quanta of lattice vibrational energy, within the sample. (X-ray photons have too high an energy for phonon creation, but the energy of visible and IR photons is suitable. The momentum of the photons of light is much lower than the momentum of the neutrons, however, which has consequences that are discussed in the next section.)

It has been seen that neutron scattering contains several components, each of which provide information about different aspects of solid electrolyte behavior. The difficulty of separating each component from the experimentally measurable total scattering prevents full use from being made of this information. A further difficulty is that the experimental results do not provide enough information for the complete determination of the van Hove functions that describe the mobile ion behavior.[149]

One way of overcoming these limitations is to use a simplifying model that disregards some of the correlation phenomena. An example is the Sköld model which has been successfully applied to α-AgI. This assumes that the quasi-elastic coherent contribution can be estimated from the incoherent scattering together with the diffuse elastic scattering caused by the mobile sublattice.[149] The detailed diffusional behavior of the Ag^+ ion can then be obtained if certain additional assumptions are made. These include the neglect of Bragg peaks and of inelastic scattering contributions, together with the quasi-elastic scattering due to the I^- ions. This means that the coherent part of the quasi-elastic scattering can be taken as the Fourier transform of the Ag^+-Ag^+ pair correlation function.[335] This procedure successfully explained the results[336] obtained from α-AgI at 250 °C using a TOF spectrometer, but it was necessary to postulate two types of motion. Single-crystal studies using a TA spectrometer cannot be carried out on α-AgI until larger crystals can be grown.[337] Studies of other materials have recently been reviewed;[247] a few examples are given in Table V.

F. Light-Scattering, Raman, Brillouin, and Rayleigh Processes

When a beam of monochromatic light, say from a laser of wavelength $\simeq 500$ nm, strikes a sample, most of the incident beam is transmitted, as for X-rays discussed earlier. About one photon in 10^{14} is inelastically or quasi-elastically scattered and detected. The scattering arises from fluctuations in polarizability, caused by local changes in the relative permittivity (dielectric constant) of the medium.[347] For liquids, one can probe density fluctuations and atomic collision processes (because the electron distribution is distorted in the colliding particles). In ordered solids, lattice vibrations, i.e., phonon modes, can be characterized. Solid electrolytes are more complicated because of the disordered nature of the mobile ion sublattice. The scattering

processes incorporate some of the features of both liquids and solids, which complicates the interpretation. As liquid-state dynamics is not sufficiently advanced to provide a treatment of light scattering from solid electrolytes and specialized theories, designed to account for the anharmonic and disordered nature of solid electrolytes, are still at an early stage, the dynamics of ordered solids is normally used as a basis.[347]

In light-scattering experiments on solids, the frequency, ω, and wave vector, $\mathbf{k}$ of the incident and scattered beams are measured. This enables the frequency and momentum of the phonons that are created to be measured, so that a plot of ω as a function of $\mathbf{k}$, the *phonon dispersion curve*, can be constructed. This is very informative for reasons that will now be considered.

Entities such as phonons, photons, and electrons that exhibit both wavelike and particlelike behavior can be visualized as packets of waves. The waves propagate with a certain velocity, the *phase* velocity, v. The wave packet also moves, with a velocity called the *group* velocity, v_g. It the two velocities are the same, then ω is proportional to $\mathbf{k}$. As the frequency rises, the two velocities become different, a process described as dispersion. The velocities are approximately given by the expressions

$$v = \omega/\mathbf{k}; \qquad v_g = d\omega/d\mathbf{k}$$

The energy and thus the information content propagates at v_g, which can therefore be thought of as the velocity of the entity, in this case the phonon.

The phonon dispersion curve shows a periodic behavior of period a. It becomes flat at $\mathbf{k} = \pm\pi/2a$, so that $d\omega/d\mathbf{k}$, and hence v_g, is zero. This marks the end of a region of $\mathbf{k}$ space called the *first Brillouin zone*. A marginally larger $\mathbf{k}$ value takes the curve into the second zone. The group velocity is still zero, but there is a quantum jump in frequency and consequently an abrupt increase to a new phase velocity. As $\mathbf{k}$ is further increased, the curve exhibits a roughly sigmoidal shape, rising to a maximum at the center of the second zone where $\mathbf{k} = \pm\pi/a$; a curve that is its mirror image rises to this same maximum from a horizontal minimum at the opposite edge of the second zone at $\mathbf{k} = \pm3\pi/2a$. Because of the inherent properties of the periodicity, it is permissible to translate this latter curve so that it runs from the first zone boundary, $\mathbf{k} = \pm\pi/2a$, to the zone center, $\mathbf{k} = 0$.

This allows the phonon dispersion curve to be displaced as two branches, a lower *acoustic* branch and an upper *optical* branch. Each branch contains several lattice vibrational modes. The acoustic modes can be either transverse, the vibration direction being normal to the wave vector, or longitudinal, the vibration being in a direction parallel to the wave vector.

In the long-wavelength (low $\mathbf{k}$) limit near the zone center, the optical branch contains lattice vibrations arising from motions within the unit cell that take place in such a way that the center of mass remains stationary and the acoustic branch contains the vibrations pertaining to the movement of the unit cell as a whole. Near the zone center, optical frequencies are much larger than acoustic frequencies, but their values become closer as the zone boundary is approached.

The boundaries lie at about 10^8 cm^{-1}, which corresponds to interatomic spacings. Neutrons have wave vectors of this order, and so the whole of the first Brillouin zone can in principle be probed by neutron scattering experiments. The wave vectors of the visible photons used in light-scattering experiments are much smaller than this, so that in general only the zone center can be explored.[347]

Originally, *Raman scattering* was used to describe optical branch excitations and *Brillouin scattering* to describe acoustic mode studies. Because the type of instrument used varies with frequency regime, it is now found more convenient to refer to studies above 1 cm^{-1} (or 30 GHz or 0.125 meV), carried out with grating spectrometers, as Raman scattering. This enables the term Brillouin scattering to be used for the lower frequency range; a Fabray–Perot interferometer is normally employed.[347] For quasi-elastic scattering, in which the energy transfer to the sample is very small (i.e., less than 10 mJ mol^{-1} or 30 MHz or 10^{-3} cm^{-1}), a photon beating method is used, and the process is called *Rayleigh scattering*.

Theoretical studies of solid electrolytes and other materials are often concerned with calculating phonon dispersion curves,[348] but experimentally it can be more useful to obtain a plot of intensity I against frequency, which in the long-wavelength limit is the lattice vibrational spectrum. I is a complicated function of $\mathbf{k}$, ω, and time; it can be related[349] to the polarizability, which is a function of dipole moment and field. The polarizability tensor (or matrix) expressing this dual dependence can alternatively be written in terms of two other variables, position vector and time, in which form it can be related to the van Hove correlation function $\langle r_1(0)r_2(t)\rangle$ encountered earlier. Consequently, light scattering relates to the positions of atoms relative to their neighbors rather than to the individual movement of individual particles and therefore resembles coherent rather than incoherent neutron scattering.

In solids, a harmonic approximation can be used which makes it possible to express the scattered intensity as the sum of a series of terms, I_1, I_2, etc.[347] I_1 is the first-order scattering in which one phonon is involved, I_2 is the second-order scattering involving two phonons, and so on. Although, as stated above, first-order scattering involves only phonons near the Brillouin zone center, this need not be the case for second-order scattering. The conservation of momentum requires that the sum of the momenta of the two phonons created is equal to the difference in momentum between the incident and scattered beam. If the two phonons have almost equal magnitudes but opposite directions, the second-order scattering condition is still fulfilled, and they can be anywhere within the Brillouin zone. Thus the region near the zone boundary, corresponding to atomic scale behavior, can be explored. The second-order intensity is weak, and the peaks are relatively broad. As in molecular spectra, the first- and second-order scattering processes are subject to symmetry restrictions. For liquids the harmonic approximation is not appropriate. The incident beam still couples with dielectric fluctuations, but these are now caused by density fluctuations and by atomic collisions (which distort the electron distribution in the colliding particles), rather than by lattice vibrations.

For solid electrolytes, the nature of the response in a light-scattering experiment depends on the depth of

the potential energy wells in the mobile ion sublattice. When one of the classes of solid electrolytes mentioned in the introduction, defect-type materials in which the wells are relatively deep, is used as an example, the residence time at a site, about 3 ps, is several times larger than the time of flight between sites, so that a jump diffusion model is appropriate.[347] The ions have time to execute many vibrations about the site, and the frequencies of these are comparable to lattice vibrational modes so that they are accessible to light-scattering experiments. Unfortunately, they are very anharmonic and, in addition, the high proportion of defects destroys much of the translational symmetry. These two factors make it difficult to apply a treatment in terms of well-defined phonons with definite momentum $\mathbf{k}$ and frequency ω.

Despite these reservations certain relevant parameters can be determined.[333,350] If the vibrations of the mobile ions are fairly well decoupled from the rest of the lattice, then a vibrational frequency, which can be taken as the attempt frequency in a hopping model, can be measured.[347,350] The temperature dependence of the frequency and line width of this vibration can give site-occupancy factors and other information.[351] Hopping between sites of different polarizability produces fluctuations detectable by light scattering.[352]

For the class of solid electrolytes containing materials such as α-Ag I, the wells are very shallow and mobile ion diffusion is virtually continuous. Hence a jump diffusion model is not really applicable, and a phonon treatment is even less appropriate.

Diffusional motion produces broad Rayleigh wings, which are high-frequency tails to the quasi-elastic scattering line.[353] For certain purposes it is useful to emphasize the peaks in the high-frequency region 10–200 cm^{-1} at the expense of the Rayleigh wings by measuring *reduced Raman intensity* I_{red}.[349,354] This is related to the Raman intensity I by

$$I_{red} = \omega I/(1 + n) \simeq \omega^2 I$$

where n is the Bose–Einstein factor, $1/[\exp(\hbar\omega/kT) - 1]$, i.e. the number of quanta associated with a particular vibrational mode.[249] In Brillouin scattering, the frequency of the acoustic modes together with knowledge of the wave vector will provide the velocity of sound in the material, from which the elastic constants of the material can be determined.[347,348]

In summary,[23] light-scattering techniques are particularly well suited for probing low-lying acoustic phonons and the Rayleigh scattering (Z-branch behavior) and other optical events near the zone center, whereas the behavior of other regions of $\mathbf{k}$ space is not easy to examine. Neutron scattering is complementary because it gives results pertaining to phonons throughout the Brillouin zone but is at its weakest near the zone center. Many investigations have been considered in detail in a recent review.[347] Some examples of recent studies are summarized in Table VI.

G. IR, Far-IR, and Microwave Studies

The role of conventional infrared spectroscopy in the range 300–3000 cm^{-1} is straightforward. It is used to characterize aspects of the composition and structure of certain solid electrolytes; investigations of the B–O

TABLE VI. Examples of Light Scattering Studies

material	ref	material	ref
AgI	347, 348, 353, 355–360		
		Li glasses	365
Ag$_4$RbI$_5$	347, 358	Ag-β-Al$_2$O$_3$	133, 347
Ag$_4$KI$_5$	361	Na-β-Al$_2$O$_3$	133, 366
Ag$_2$HgI$_4$	362	Rb-β-Al$_2$O$_3$	303
Ag$_{26}$I$_{18}$W$_4$O$_{16}$	363	(Na,Li)β-Al$_2$O$_3$	298, 367, 368
Ag$_3$SI	358	(K,Li)β-Al$_2$O$_3$	367
Ag$_2$S	358	(K,Sn)β-Al$_2$O$_3$	367
Ag$_5$pyI$_6$	358	PbF$_2$	323, 347, 369
CuI	347, 354, 355, 364	CaF$_2$	370, 371
CuBr	347, 364	SrCl$_2$	323, 347, 372, 373

network in Li glasses[365] and of hydration in Li–Na β-Al$_2$O$_3$[299] may be taken as representative examples.

Microwave and far-IR measurements merit more detailed consideration here because from them it is possible to obtain both the *velocity correlation function*, $Z(t)$, which is related to $G(\mathbf{r},t)$, the van Hove correlation function described earlier, and the *complex frequency-dependent conductivity*, $\hat{\sigma}(\omega)$.[149,323,374] $Z(t)$ is in fact the Fourier transform of the spectral density and can be related to the diffusion coefficient.[323]

Just as $\hat{\sigma}(\omega)$ is related to $G(\mathbf{r},t)$ via $Z(t)$, there exists a quantity $\hat{\sigma}_s(\omega)$, related to $G_s(\mathbf{r},t)$ via the velocity autocorrelation function $Z_s(t)$; it represents the part of the conductivity that would be observed if there were no correlations between the motions of different ions. The ratio $\hat{\sigma}(\omega)/\hat{\sigma}_s(\omega)$ is in fact the correlation factor, f, which enters into the expression for the Haven ratio discussed earlier (section IVD).

$\hat{\sigma}(\omega)$ exhibits structure at frequencies that are characteristic of aspects of the motion of the mobile ion, although its measurement and interpretation are not simple. Recent microwave studies[375] on AgI, for example, showed little variation of $\hat{\sigma}(\omega)$ with frequency, in contrast to earlier results[149,150] on which a rather detailed theory of Ag$^+$ motion had been based.

It is to be expected that the conductivity will be dependent on frequency in this spectral region. Conductivity arises from the movement of charge under the influence of an electric field. If the field changes direction very rapidly, then high-mass charge carriers cannot follow suit fast enough, and they cease to contribute to the overall conductivity. Thus for a field that is varying at a frequency corresponding to that of light in the visible region, electrons and holes can respond to the variations and continuously act as charge carriers but ions cannot. In all solid electrolytes, the ionic motion can be regarded to some extent as a hopping process, the hopping frequency being about 100 GHz (3 cm^{-1}). If the applied field varies with a frequency not dissimilar to this, then an ion that starts to jump in a given direction with the help of the field will still be traveling when the field begins to oppose its motion, and therefore its contribution to the overall conductivity will be diminished.[150]

The complex conductivity $\hat{\sigma}(\omega)$ is made up of a real part, $\sigma(\omega)$, and an imaginary part. It can be related[150] to the complex permittivity $\hat{\varepsilon}_r$,

$$\hat{\sigma}(\omega) = j\omega\varepsilon_0\hat{\varepsilon}_r(\omega)$$

where $\hat{\epsilon}_r$ can be expressed as

$$\hat{\epsilon}_r(\omega) = \epsilon'(\omega) - j\epsilon''(\omega)$$

ϵ_0 ($\approx 10^{-11}$ F m^{-1}) is the permittivity of free space. ϵ', or alternatively[376] the product $\epsilon'\epsilon_0$, can be taken as the "dielectric constant". ϵ' and ϵ'' are the real and the imaginary parts, which can be represented as the x and y axes of the same type of complex plane plot as used for the low-frequency impedance studies discussed earlier. ϵ'' is related to the *dielectric loss*, which is the energy dissipated in the form of heat; the dielectric loss mechanism in β-Al$_2$O$_3$ has been discussed.[377] In the high-frequency regime, the permittivity components can be related to spectral parameters by Maxwell's equations, which give[249]

$$\epsilon' = n^2 - k^2$$

$$\epsilon'' = 2nk$$

n being the refractive index and k being the extinction coefficient. In the far-IR region, n and k can be obtained from separate transmission and reflectance measurements using Fourier spectroscopy. A Michelson or a lamellar grating interferometer is employed.[150] For the microwave region, it is possible to obtain $\hat{\sigma}(\omega)$ and $\hat{\epsilon}_r(\omega)$ from measurements on a rectangular wave guide, the side walls of which are composed of the solid electrolyte.[150,378] The solutions of the wave equations within the wave guide and the walls are checked for consistency using the Kramers–Kroenig equations which interrelate $\epsilon'(\omega)$ and $\epsilon''(\omega)$ over the frequency range. More recent studies[375] have used a tunable Fabry–Perot cavity, the characteristics of which are measured in the presence and absence of the sample.

The microwave experiments cover the range below 1 cm^{-1} (2–40 GHz) and the far-IR investigations are in the region 7–300 cm^{-1} (0.2–10 THz); unfortunately it is not yet possible to study the range 40–200 GHz experimentally. This precludes the possibility of fully investigating the velocity correlation functions for the mobile ions,[149] so theoretical attempts have been made[379] to access this region.

In principle, the frequency-dependent conductivity data can give valuable insights into the nature of the ionic motion in solid electrolytes, provided that the results can be interpreted. In some cases, as when peaks coincide with those found from Raman or neutron scattering, this is straightforward.[366] For α-AgI which has been widely studied, as can be seen from Table VII, the choice of a suitable interpretative model is made difficult because the results of earlier and more recent studies are significantly different. There exists a model due to Drude[380,381] which is appropriate for liquids and which could reasonably be expected to be obeyed for solid electrolytes at low frequencies.[375] The earlier results did not follow this model, and a theory[149,150] that separated the effect of the electric field on initiation (the "start effect") and propagation (the "acceleration effect") of ion motion and incorporated "forward correlation effects" had to be devised to explain this. In the light of the later studies[375] the physical insights apparently gained from this theory are open to question. More generally, models based on the phonon concept may not be valid below 30 cm^{-1} (1 THz).[149] Some recent measurements and interpretations of fre-

TABLE VII. Frequency-Dependent Conductivity Studies

material	ref	material	ref
α-AgI	149–151, 375, 382	α-CuI	150, 151
Ag$_4$RbI$_5$	383	β-CuBr	150, 151
Ag$_{26}$I$_{18}$W$_4$O$_{16}$	363	β-Al$_2$O$_3$	151, 303, 366
Ag glasses	146	Hollandite	384, 385

quency-dependent conductivity data for several solid electrolytes are summarized in Table VII.

H. Extended X-ray Absorption Fine Structure

This technique (EXAFS), which has been used by surface and intercalation chemists for some time,[386] has recently been applied to solid electrolytes, a task to which it is particularly suited.[23,334] Whereas X-ray and neutron diffraction experiments provide information about the mobile species, superimposed on structural information about the immobile matrix, EXAFS probes directly[334] the mobile–immobile species interaction to the virtual exclusion of the immobile–immobile terms. This is a considerable simplification which in principle, because the relevant information is highlighted, enables the path taken by the mobile ions to be determined.

In essence, the method exploits a rather subtle aspect of X-ray absorption. When X-rays pass through a solid, the intensities of the incident (I_0) and reflected (I) beams are related by a Beer–Lambert type law

$$I = I_0 \exp(-\rho\mu x)$$

where x is thickness, ρ is density, and μ is a parameter called the mass absorption coefficient. This latter increases approximately with the fourth power of the atomic number and the cube of the X-ray wavelength, λ. The μ–λ relationship is modified by scattering and photoelectric excitation.

The photoelectric effect is when an X-ray photon of sufficient energy penetrates to the inner electron shells of an atom and causes a core electron to be ejected, e.g., from the K (i.e., 1s) shell. Such an event can only take place if the electron can leave the atom. This means that the photon energy, which is inversely proportional to its wavelength, must exceed the binding energy of the electron. The photon is lost to the transmitted beam as a result of this process. Hence superimposed on the essentially cubic plot of X-ray absorbance against energy are sharp "absorption edges", corresponding to the onset of K, L$_I$ (2s), etc. photoexcitations.

The study of absorption edges has been part of standard X-ray work for over 50 years. Close examination of the region immediately on the high-energy side of the K absorption edge, however, reveals a fine structure extending over a region of width about 10% of the absorption edge energy. This is the EXAFS region, and it has only recently been studied. If a range of wavelengths near the absorption edge of a particular species is studied, then the EXAFS is dominated by that species.

These oscillations in absorbance are caused by what happens to the ejected photoelectrons after they leave the atom. Some of them collide with near-neighbor atoms; this causes them to be backscattered toward the parent atom which influences the final energy state in the photoexcitation process and produces the fine

structure. This influence depends on the momentum, and thus on the energy, of the photoelectron, and this in turn depends on both its binding energy and on the energy of the incident X-ray beam. The distance between the excited atom and its neighbor, and to a lesser extent the atomic nature of the backscattering atoms, also affect the interaction. Because backscattering becomes much less important with increasing separation between atoms, nearest-neighbor interactions are emphasized. Further, it has been shown[387] that electrons scattered by more than one neighboring atom make a negligible contribution to the measured EXAFS. Hence it appears that, unlike diffraction studies of solid electrolytes which contain both Bragg peaks from the long-range ordered immobile sublattice and a diffuse pattern from the short-range ordered mobile sublattice, EXAFS can give a relatively uncluttered presentation of the average positions of the mobile ions. Despite its attractions, there are difficulties in EXAFS, both in carrying out the experiments and in deconvoluting the data. Normally the sample is examined in transmission, but a very high intensity beam, such as that obtained from synchroton source, is desirable;[334] this restricts the availability of the technique. Monochromatizing the beam is relatively straightforward, two diffractions from a silicon single crystal being used. I and I_0 are measured with gas proportional counters. It is also possible to study EXAFS via a byproduct of the photoionization. The original ejection of the electron leaves behind a hole in the shell into which a further-out electron can fall. Such an event is accompanied either by the production of an X-ray photon, as in X-ray fluorescence, or by the production of Auger electrons which will be discussed later. These also reflect the backscattering interaction and can be used to yield absorption fine structure information. This enables mobile ion structural information to be obtained in very dilute systems by the use[388] of X-ray fluorescence and on surfaces by the use of X-ray excited Auger spectroscopy.[389]

To obtain sufficient detail from the absorption fine structure, it is necessary to subtract the background from the EXAFS information. This is difficult as either the need to determine an inaccessible reference energy must be adroitly circumvented[334] or the experimental data, which are obtained in **k** space, must be compared with calculations based on theoretically derived parameters.[390] This comparison is carried out more easily in **r** space, where the nearest-neighbor shells are better separated than in **k** space. The use of a "window function" is necessary, however, to make the Fourier transform possible, and this causes blurring of the data. There is a further problem in selecting a window of suitable width for the transformation, as there is a "white line" very near the absorption edge, which interferes with the EXAFS data. It is also very difficult to treat data involving electrons that are not tightly bound, and this effectively restricts EXAFS to the K shell. The nature of EXAFS data makes it eminently suitable for testing models of mobile ion behavior related to site residence times, hopping frequencies, and so on. It has been used to examine the excluded volume model,[334,391] the quasi-lattice gas model,[392] and a hard-sphere fluid model[393] and for charge density and ion flow studies.[394,395] The results of EXAFS studies[396] on AgI, which show that the site residence time is about

three times the flight time, are compatible with conductivity studies in the microwave frequency range.[375] The technique has also been used to show that[397,398] the octahedral as well as the tetrahedral sites in CuI are significantly occupied. It is likely that the range of systems studied will be considerably extended in the next few years.

I. Molecular Dynamics

This is a type of computer simulation,[238,399] carried out under statistical-mechanical rules. The experimentalist can both control and measure parameters on the atomic scale. The behavior of the mobile ions can be closely observed provided that a well-chosen model system is used; the technique gives access to reliable direct information about mobile ion sites, residence times, interconnecting pathways, and hopping frequencies. The energetics of each stage of the process can also be found, and converted into parameters such as activation energies, suitable for direct comparison with the results from more conventional experiments. The reliability of the method depends on the fidelity with which the physical system is represented by the model. It is also possible to study systems the physical counterparts of which have not yet been found; in principle, therefore, novel solid electrolyte systems can be suggested by this technique.

The method originated in a simulation that predated computers. In 1934, Morrell and Hildebrand[399,400] carried out a detailed photographic study of gelatin balls suspended in a liquid gelatin matrix of the same density contained in a transparent box. By measurement of the distance between the balls, they were able to construct a radial distribution function for the system. Comparison of this parameter for different packing densities gave an early insight into the arrangement of neighbors in the liquid and solid states. Other mechanical simulations have also been used.[349] Computer applications were pioneered by Alder[401] who initially studied systems obeying a hard-sphere potential-energy function which contained only a repulsive term. Such systems are at the so-called infinite temperature limit, because their kinetic energy ($^1/_2 kT$ per degree of freedom) so greatly exceeds the potential energy of attraction arising from the presence of an energy well of depth ϵ that the latter contribution can be neglected.

The study of ionic solids required considerable developments of the technique, to enable more realistic potential functions to be handled.[238] Various algorithms (or recipes) had to be devised so that the configurations adopted consecutively by the system could be found. Unless these configurations or atomic arrangements are in the correct time sequence, no meaningful information about transport processes such as diffusion or conductivity can be obtained. Because computational times escalate rapidly with the size of the system, about 1000 atoms or ions is the effective upper limit that can be studied for long enough to provide sensible information about transport processes. Such systems in isolation are dominated by surface effects to a degree that is unrealistic for modeling most physical systems. A "periodic boundary" method, in which the cell containing the model atoms is surrounded by identical cells containing images (ghosts or clones) of the model atoms

that move in unison with them, is therefore used. With this method, the system becomes infinite and surface effects are absent, unless they are deliberately incorporated by sophisticated modifications. In molecular dynamics, the step from one configuration to the next involves the movement of all the atoms. The time step between configurations is under the control of the experimentalist and to be physically realistic is of the order of atomic collision times, namely 10^{-15} s. Hence, to follow a system for a time even as short as 1 ps requires 1000 time steps, which corresponds to many minutes of computer time. Ideally, one would study a system containing a very large number of individual atoms in the model cell for the huge number of time steps necessary to produce results directly comparable to those obtained from fast conventional experiments. The compromise usually employed in the study of solid electrolytes is to study a relatively small model system, say 256 particles, for as long a time as possible, of the order of 20 000 time steps. The limited size makes it difficult to study ionic transport in other than single crystals, although studies on compacted materials are being attempted.[402]

The essence of the method is as follows.[238] The experimentalist sets up "genesis", an appropriate arrangement for the initial configurations of the particles. For α-AgI, for example, the Ag^+ ions might be distributed over some of the tetrahedral sites between the body-centered arrangement of I^- ions. He also ascribes small velocities to each of the particles, often by selecting at random small position displacements corresponding to the configuration adopted one time step previously. The *configurational potential energy* is then calculated, usually by adding up the contribution for each pair of particles as given by the potential function that he has selected. In addition, the forces on each particle, arising from interactions with the neighboring particles, are computed from the derivative of the potential function with respect to distance.

By the use of a suitable algorithm, the particle positions in the next configuration in the time sequence are then obtained. This extrapolation into the future can be carried out by the Verlet algorithm, based on the first three terms in a double-Taylor expansion of positions at time $t + dt$ and $t - dt$. This enables the future positions to be obtained from knowledge of the present and past positions, together with the acceleration terms, given from the forces. A chain of configurations, sequential in time, is therefore set up. The positions of all the particles at all of the time steps is known, so that a wealth of information about the routes followed by moving particles, the vibrational behavior of the host particles staying on their lattice positions, and so on is provided for a system the interatomic properties of which are precisely characterized.

For ionic lattices, there is a particular and rather acute problem. Most potential functions are rather short range in the sense that the potential energy between pairs of particles at large separations is negligible. Ions interact according to the Coulomb potential (the integral of the inverse square force law), and this falls off as $1/r$. With normal potential functions it is adequate to consider just one of the many possible $i-j$ interactions between the ith particle in the model cell and the jth particles in the model and image cells, namely

TABLE VIII. Molecular Dynamics Studies

material	ref	material	ref
α-AgI	237, 271, 405, 406	β-Al$_2$O$_3$	236, 408
α-AgI (two dimensional)	407	CaF$_2$	238, 239, 409, 410
α-CuI	237	SrCl$_2$	239

that involving the shortest $i-j$ distance (the minimum image procedure). With the Coulomb potential, all the $i-j$ interactions have to be included, even those involving images in cells almost infinitely far from the model cell. This is achieved by an Ewald summation, using terms in both real ($\mathbf{r}$) and reciprocal or momentum ($\mathbf{k}$) space. An adroit method due to Singer[403] enables the model cell contribution to be treated in real space and the image contributions to be summed in $\mathbf{k}$ space. This facilitates computation, as in practice only part of the contributions have to be evaluated for all the $i-j$ interactions (of which there are $1/_2n^2$ for an n particle system), and the remainder can be worked out just for each of the n particles. Various other short cuts, such as that devised by Brower,[404] in which the directional nature of the parent-i ↔ image-j interactions is ignored, open up the possibility of applying molecular dynamics to the study of ionic motion in compounds containing several ionic species.

It has been mentioned that many parameters are under the direct control of the experimentalist. This power has been elegantly used by Vashishta and Rahman[237] in their study of the solid electrolytes α-AgI and α-CuI. For AgI, they took maximum advantage of the flexibility open to them and adjusted, among other things, the charges on the ions, in order to mimic the real world behavior. They retained these empirical values in their subsequent study of CuI and were able to reproduce the properties found from conventional experiments. This is a powerful vindication of the method, as α-AgI is body-centered whereas α-CuI is face-centered cubic. It adds credibility to their detailed findings about the routes traversed by the mobile ions, which are not directly obtainable from more conventional studies.

Temperature-dependent properties can be investigated, but with certain algorithms such as that of Verlet, temperature control has to be applied somewhat indirectly. Although molecular dynamics is carried out on a microcanonical ensemble, this does not preclude the adjustment of temperature as it is the total (potential *plus* kinetic) energy that remains constant. The method has been successfully applied to several systems, summarized in Table VIII, and its use is likely to escalate. Its application on the study of phase transitions is discussed in section VIIF.

J. Ion Backscattering

It is possible to study the displacement of ions from high symmetry positions in layer type solid electrolytes with this technique.[303] A beam of high energy ($\sim$1 MeV) He$^+$ ions is channeled along the layers; some of these ions are backscattered from the mobile and host ions. The He$^+$ ions suffer an energy loss that depends on the mass and position of the scattering ions, and if the beam is tilted relative to the channeling direction, the backscattering intensity increases in a manner in-

dicative of the displacement of the scattering ions from high symmetry sites. Ag and K β-Al$_2$O$_3$ have been studied with this technique.[303]

VII. Phase Transitions

As stated in the introduction, a material is a solid electrolyte only when it is in a phase that possesses a structure conducive to ionic mobility. At other temperatures or pressures the conductivity is too low for the term solid electrolyte to be applied. The purpose of this section is to consider in a limited way the nature of phase transitions affecting solid electrolytes and briefly to describe a few techniques pertinent to their determination.

A material that exhibits solid electrolyte behavior in one phase, e.g., α-AgI and α-CuI, may have more than one other solid phase in which the ionic conductivity is low, e.g., β- and γ-AgI and -CuI. Transitions between such phases will not be considered in detail here. The type of transition that occurs at the low-temperature end of the solid electrolyte range is, in certain contexts, referred to as a $\beta \rightarrow \alpha$ or as an insulator–conductor transition. The transition may occur at a unique temperature, or it may be observed to take place over a temperature range spanning several hundred degrees, but by its completion, the conductivity will have changed by several orders of magnitude. Other changes, in crystal structure, thermodynamic parameters, vibrational spectra, and so on, accompany the transition. An example is the ferroelectric transition in Ag$_{26}$I$_{18}$-W$_4$O$_{16}$[363] and the change in dielectric loss in Na$_3$Sc$_2$-P$_3$O$_{12}$.[411] The transition temperature is modified, and otherwise inaccessible solid electrolyte phases may be created by the application of pressure.[412-414] Indeed, it has been suggested[323] that the "metallic" high-pressure phase of ice is in fact a solid electrolyte (or perhaps a mixed conductor).

Theoretical aspects of the phase transition in solid electrolytes have been recently reviewed,[219,285,323,415] and various correlations and models have been discussed.[218,416-418] In certain solid electrolytes in which the phase transition is first order, the phase change is accompanied by an entropy change roughly equal to the entropy of melting of the material;[28,374] added together, these entropy changes are about the same as the entropy of melting in a normal material. This supports the use of the term "sublattice melting" to describe the transition. In AgI the transition occurs sharply at 146 °C; in PbF$_2$ it takes place over several hundred degrees; and the behavior in some other materials is intermediate. Several different classifications have been proposed. O'Keeffe[323] favors a scheme that highlights Faraday's original[29] detection of the PbF$_2$ transition. Mahan[415,419] bases his classification on the temperature dependence of the order parameter ξ, defined as

$$\xi(T) = (n_A - n_B)/(n_A + n_B)$$

n_A and n_B being the fraction of empty and filled sites. Salamon[219] combines the conventional first and second order distinction, based on discontinuities in the first, second, etc., derivatives of free energy with respect to temperature with certain rules advanced by Landau.[420] The most important of these is that the space group of the low-temperature phase must be a crystallographic subgroup of that of the solid electrolyte phase. Boyce

TABLE IX. Phase Transitions in Solid Electrolytes

| class	description	example
M	melting (as O'Keeffe class I)	AgCl, PbCl$_2$
1	first order; disobeys Landau; $\xi \rightarrow 0$ discontinuously and abruptly at transition temperature (O'Keeffe class IIa)	AgI
L	first order; obeys Landau; $\xi \rightarrow 0$ discontinuously and abruptly at transition temperature (O'Keeffe class IIb)	Ag$_2$HgI$_4$
2	second order; obeys Landau; order-disorder or disorder–disorder transition, ξ, decays rapidly but continuously to zero at transition temperature (Mahan class b)	Ag$_4$RbI$_5$ at 209 K
D	diffuse (the Faraday transition) (O'Keeffe class III; Mahan class c; Boyce class II); greater than exponential increase in conductivity	PbF$_2$, Ag$_5$pyI$_6$
E	exponential increase in conductivity; transition may be regarded as absent, or as persisting over an extremely wide temperature range (Boyce class III)	Na – βAl$_2$O$_3$
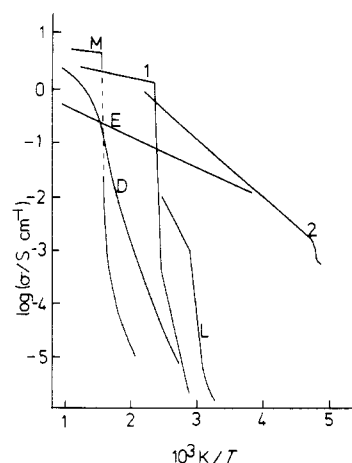
Figure 2. Logarithm of conductivity against reciprocal of temperature for materials exhibiting phase transitions belonging to the different classes described in the text. (M) AgCl; (1) AgI; (L) Ag$_2$HgI$_4$; (2) Ag$_4$RbI$_5$; (D) PbF$_2$; (E) Na-β-Al$_2$O$_3$.

and Huberman[23] include a class for materials such as Na β-Al$_2$O$_3$ for which there is an exponential increase in conductivity. A composite classification that embodies these features was largely suggested by Salamon.[219] The classes may be named as shown in Table IX.

Near a phase transition, it can be convenient to describe properties in terms of critical exponents, which describe the dependence of a given parameter on the quantity $|T - T_c|$, T_c being the critical (or, here, the transition) temperature. For the order parameter, ξ, for example, the ansatz, or approximate expression, is

$$\xi \simeq |T - T_c|^\beta$$

For Ag$_4$RbI$_5$, β has the value 0.35 ± 0.02 below T_c.[219] Other parameters such as the heat capacity are often separated into a "critical" contribution, containing the part strongly affected by the transition, and a "background" contribution, involving the degrees of freedom to which the transition is immaterial.[219]

A. Electrochemical Studies

The shape of the $\ln \sigma$ vs. $1/T$ plot can be used to determine the class of transition, as shown in Figure 2. For transitions of classes 2 and D, the activation energy in the region of the transition is proportional to the "critical" heat capacity, ΔC_p, giving[421,422]

$$d \ln \sigma/dT = \text{const.} \ \Delta C_p/RT_c + \text{const}' \qquad (6)$$

From the simultaneous measurement of σ and ΔC_p described in section VIIC, a linear relationship between $d \ln \sigma/dT$ and $\Delta C_p/RT_c$ was found[421,422] for Ag_4Rb(or K or $NH_4)I_5$, confirming eq 6. For diffuse transitions, there is a small maximum in this plot, lying 15 K below the maximum in C_p itself for Ag_5pyI_6 and a little above the C_p maximum for PbF_2,[219] at a temperature coinciding with that at which anomalies in the optical properties occur. It would appear, therefore, that this plot may provide a particularily appropriate probe for solid electrolyte materials. The experiments must be carried out with great care as solid–solid transitions are affected by mechanical stress. Slightly distorted results were obtained[423] for Ag_4RbI_5 when the sample was clamped between electrodes as opposed to contact being made by flexible wires.

The pressure-dependent ionic conductivity in the vicinity of the transition also provides useful insight. For Ag_4RbI_5, T_c was found[414] to vary with p^2. The results of conductivity studies in the transition region show that σ is dominated by the effects of short-range order; theoretical treatments are not yet sufficiently refined to provide more than a qualitative description.[219]

B. Variable-Temperature X-ray Studies

X-ray structural studies can be performed at temperatures other than 25 °C; thus, the crystal structures of the various phases can be determined. This enables the changes resulting from the transition to be considered. Examples of this type of investigation on halogenide solid electrolytes have recently been reviewed,[16] and other materials recently studied include $AgCrS_2$,[134] Ag_3SBr,[98] Ag_5pyI_6,[424] and Cu_3VS_4.[259]

Many room temperature solid electrolytes are formed by the heavy doping of materials that are solid electrolytes at elevated temperatures but not at 25 °C. In the initial characterization of such electrolytes, it is useful to know whether there are manifestations of the transition of the parent material, as this can point to the presence of unconsumed reactants and also can indicate the degree of structural change. In this context, it suffices to obtain a rapid scan of the powder X-ray pattern as a function of temperature. This can be provided by the Guinier-Lenné camera, in which the powder pattern is produced on a flat photographic plate.[251] As the temperature of the sample is slowly increased, the plate also moves. The lines of the pattern curve slightly because of the effects of thermal expansion; at a transition, discontinuous changes will be seen for materials such as AgI and CuI that undergo substantial structural modification. This technique has been used in the investigation[67] of adducts of CuI and a range of organic sulfonium iodides, some of which are room temperature solid electrolytes.

C. Differential Scanning Calorimetry, Differential Thermal Analysis, and Other Thermal Techniques

Differential scanning calorimetry (DSC) and differential thermal analysis (DTA) are useful techniques for determining phase transitions.[425] In DSC the difference in heat input required to maintain samples of the material under study and in a reference, e.g., alumina, at the same temperature is monitored as a function of T. This technique gives data of lower precision than that obtained from conventional adiabatic calorimetry only because of shortcomings in the normal commercial instrument designs. It is often used, especially for silver systems,[426,427] to complement conductivity and X-ray powder diffraction studies or for comparison with phase transition data from other experimental techniques such as Raman spectroscopy.[359] DTA is a less sophisticated method in which temperature difference between sample and reference is monitored as a function of temperature under conditions of similar heat input. This can be achieved by placing two quartz tubes containing sample and reference, respectively, in a relatively massive metal block that can be heated. One junction of a thermocouple is immersed in the material in each tube to provide a measure of the temperature difference.[425,428] As in the case of DSC, it has been used in studies of silver[61,267,429] and copper[67] systems and for proton conductors.[430] DTA and DSC can also be used to study the phase diagrams of multicomponent solid electrolyte systems.[217] The technique of adiabatic calorimetry, outlined in section VIC, can be used for the precise study of phase transitions.[212,285,303,323,431] These data not only enable transitions to be classified as first order, second order, and so on but also permit order parameters and critical exponents to be obtained.[219,285] Phenomenological models for solid electrolyte behavior in the region of a phase transition can be tested against such experimental parameters. Order parameters of impure AgI,[432] systems containing Frenkel defects,[433] and multiple transition systems[434] have been considered in this way. Comparisons have also been made[435] of the results of calculations based on phenomenological models with excess C_p data, obtained by subtraction of Debye and Einstein terms from the experimental results, as outlined in section VIC. Recently a method for the simultaneous study of C_p and conductivity through a phase transition has been developed[421,422] and applied to the 209 K transition[422] in Ag_4RbI_5 and to similar transitions[421] in Ag_4KI_5 and $Ag_4NH_4I_5$. This involves passing a constant ac current through a thin single crystal slice of a sample, which is being heated at the same time by a light beam, chopped at 1.5 Hz. Temperature oscillations proportional to C_p can be monitored by using a thermocouple and the temperature coefficient of resistance is obtained from the resulting ac voltage modulation, after demodulation from the carrier signal. This technique has been used to find the critical exponent scaling laws in these silver conductors.

The thermopower coefficient has been measured as a function of temperature across the phase transition region for several silver salts[436] including AgI and Ag_5pyI_6.[192] For AgI, the coefficient rises by 20% between 25 °C and the $\beta \rightarrow \alpha$ transition temperature, at which it suddenly falls by 40%. The behavior for the

other solid electrolyte is more complicated. In both cases it has been suggested[219] that not only is the specific heat anomaly mirrored but that a change of the ratio of mobile to available sites immediately before the transition is also shown, in the case of first-order transitions. Second-order transitions are not detected by this method.

D. NMR

The technique has already been described in some detail in section VIA. NQR has been used to study phase transitions for some time;[285] an example is the 20% reduction in resonance frequency, ν, found[437] in N_2 on heating towards $\beta \rightarrow \alpha$ transition at 35.6 K from 4 K. ^{23}Na studies on the λ transition in $NaNO_3$ may be cited as an example[438] of NMR phase transition applications, which have recently been discussed in detail.[285] For solid electrolytes, a recent ^{87}Rb investigation was carried out on Ag_4RbI_5 over a temperature range spanning the 122- and 208-K phase transitions.[290] In an ^{127}I study[289] on AgI an anomalous increase in T_1 was noted just below the $\beta \rightarrow \alpha$ transition, and a similar anomalous increase in relaxation times was found in the ^{63}Cu signal from CuI as the transition was approached, thus providing evidence for sublattice melting.[439] In PbF_2, there is no sharp transition into a solid electrolyte phase, but ^{19}F relaxation rates show anomalous changes as the temperature is increased into the superionic region.[280,440]

E. Acoustic Properties

Measurements of the velocity of sound in particular directions in a crystal can be used to provide certain of the elastic constants, i.e., the ratios of the strain (or dimensional change) to the stress (or component of the pressure tensor). Near transitions, elastic constants with strain components of similar symmetry to the order parameter are "softened" or reduced in value. Consequently, measurements of sound propagation as a function of temperature can provide information about structural processes accompanying the transition.[219] At the transition temperature, peaks are to be expected in the value of the elastic constants or in experimentally related parameters such as the internal friction.

Pulse–echo superposition techniques can be used,[441] the ultrasonic signals being produced by a quartz transducer operating around the 5-MHz range. This method has been used[442] to resolve conflicting reports of a diffuse transition in CdF_2 at about 600 K. Studies have also been carried out on Ag_4RbI_5 in the 110 direction[219,443] involving the c_{44} elastic constant and in the 100 direction[444] involving c_{11}. Anomalies were found for the ultrasonic attenuation near the 208-K transition which have been explained in terms of a Jahn–Teller model.[445] In Ag_2HgI_4 a decrease was found in the velocities of longitudinal, but not of transverse, waves in the region of the 324-K transition.[446] Internal friction studies on Na-β-Al_2O_3 samples grown under different conditions[298] revealed a peak at 140 K for melt-grown samples and at 180 K for flux-grown material. For (Na,Li)β-Al_2O_3, a peak at 220 K in freshly prepared samples was replaced by a peak corresponding to that obtained from Na-β-Al_2O_3 when the mixed alumina had been dehydrated.[298]

TABLE X. Some Recent Studies of Solid Electrolyte Phase Transitions

material	ref	material	ref
AgI	192, 237, 247, 289, 355, 359, 432, 448	CuI	237, 355, 439, 448, 457, 458
Ag_4RbI_5	219, 247, 290, 339 414, 421-423, 443-445 450-452	CuI sulfonium I	67
		Cu_3VS_4	259
Ag_4KI_5	421, 422, 452	$Na_3Sc_2P_3O_{12}$	411
		β-Al_2O_3	298, 328, 366
$Ag_4NH_4I_5$	421, 422, 452		
Ag_3SBr	98	CaF_2	459
		PbF_2	219, 247, 280, 440, 460, 461
Ag_3SI	453		
		$SrCl_2$	247, 373, 459
Ag_2S	218		
$AgCrS_2$	134		
Ag_2HgI_4	446, 454		
$Ag_{26}I_{18}W_4O_{16}$	363, 455		
Ag_5pyI_6	192, 219, 424, 456		

F. Computer Simulation

Molecular dynamics and Metropolis Monte Carlo methods have been widely used for the study of the critical region, the melting process, and certain other phase transitions in solids.[447] The application to the solid electrolyte transition is more limited. CuI has been studied, albeit in a slightly artificial form in which the hexagonal β form existing between 369 and 405 °C was omitted and the transition was considered to occur from the γ to the α phase.[237,448] This meant that the I^- sublattice was of fccub type in both phases and attention could be focused on the behavior in the Cu^+ sublattice. The energy, heat capacity, and diffusion behavior were studied as a function of temperature; agreement with experiment was reasonable. Vashishta and Rahman[448,449] have considered the effect of temperature and density on structures where the rigid ion lattice is either fccub or bccub. By adjusting the conditions, they achieved a range of transformation between the structures: α-AgI (fixed ions bccub; mobile ions, random over tetrahedral sites); α-CuI (fixed ions, fccub; mobile ions, random over tetrahedral sites); γ-AgI (fixed ions, fccub; mobile ions, fixed on tetrahedral sites); NaCl (fixed ions, fccub; mobile ions, fixed on octahedral sites).

The γ-CuI structure is like the α-CuI structure except that every other tetrahedral site is occupied in an ordered way. The $\gamma \rightarrow \alpha$ transition therefore corresponds to a change from 100%:0% to 50%:50% occupancy of the "empty" and "filled" tetrahedral sites, i.e., a change from a zincblende to an averaged fluorite structure. Such studies add to our understanding of the structural features responsible for solid electrolyte behavior.

Interfacial studies are summarized in Table X.

VIII. Interfacial Properties

The techniques covered in previous sections have, in the main, been sufficiently utilized in solid electrolyte studies to demonstrate their capabilities. Surface science is a discipline that has matured in its own right

in the last 15 years, but its application to solid electrolyte interfaces is in its infancy. The increasing interest in this area is shown by a recent major conference,[462] and in this section, a brief overview of aspects of surface science of potential relevance to solid electrolytes will be presented. Certain of the techniques discussed earlier are also useful in this context; these include impedance spectroscopy, electrokinetics, pressure-dependent conductivity studies, and thermopower measurements.

The two main classes of interface that are involved in solid electrolyte systems are (i) intraelectrolyte, including grain boundaries, compacted particle–particle boundaries, and sintered particle junctions; and (ii) electrolyte–electrode interfaces, including both electrolyte–working electrode and electrolyte–test electode interfaces. Further subdivision of this second class has been suggested,[463] to give six classes: (i) metal/cation, e.g., Ag/Ag^+; (ii) metal/anion, e.g., Pb/PbF_2, F^- being the conducting species; (iii) gas-permeable metal electrodes, e.g., ZrO_2/Ag; (iv) intercalation electrodes, which are semiconductors that are nonstoichiometric, so that distortion is minimized when the composition changes, e.g., Na_xTiS_2; (v) doped mixed conductors, e.g., Pt impregnated zirconia; (vi) three-phase interfaces such as that between an AgI-based electrolyte and a cathode comprising solid active material and electron carrier, here iodine and carbon, respectively.

Many interfacial effects observed in solid-state systems are unfamiliar to electrochemists accustomed to liquid-electrolyte behavior;[464] the attainment of equilibrium is more difficult for systems involving solids.[122,136] Many surface-oriented techniques are severely perturbing because of the experimental conditions that are necessary for their execution. A wide variety of techniques exists, each seemingly characterized by an odd acronym. It is not the intention here to duplicate the excellent contemporary coverage of these[465-475] but rather to focus on those that appear to offer immediate reward in the solid-electrolyte interfacial field.

A. Mechanical Properties

The form of an electrolyte affects the paths available for ionic motion. For example, studies of the diffusion coefficient in the Ag_4RbI_5/I_2 system as a function of pressure suggested[114] that one conduction path is through the voids in the compacted solid and that iodine vapor occupies the voids and is adsorbed on the surfaces of the electrolyte particles. Powders, sinters, and thin films are also susceptible to dendrite formation which occurs when the product from a galvanic cell reaction is deposited as long needles penetrating into, or sometimes right across, the electrolyte. In many ceramic electrolytes such as β-alumina conduction takes places through blocks, separated perpendicular to the conduction path by nonionically conducting material. The conducting blocks are misaligned across grain boundaries in polycrystalline samples, and to account for this, a tortuosity factor, defined as the ratio of intergranular resistance in polycrystalline samples to resistance in the direction of the conducting pathway in single-crystal material, has been suggested.[174] Again in block-conducting ceramics formed by compaction or sintering, subtle modifications of the preparative method can result in the selection of grain shape or size

distribution that optimizes conductivity by producing preferred orientations.[174] Conductivity and impedance measurements are affected by the presence of interfaces[136] but thermopower studies are not, unless the heat-conduction properties are changed by their presence.[192,209]

Solid–solid adhesion occurs at interfaces, which modifies the interfacial energy terms.[117] Overriding this is the effect of the bulk stress and strain fields arising from distortion, into which is coupled the effect of the electric field. This coupling, which affects composition as well as configuration, has been considered for liquids[476] but not for solids, although progress is being made.

1. Macro- and Microtopography

Interfaces are not flat, even in the case of the metal plate electrodes commonly used by the liquid electrochemists. All materials with the exception of mica[117] display some surface roughness. This may be sufficiently gross to be visible to the naked eye or under an optical microscope; undulations and irregularities of this magnitude belong to the macrotopography of the surface. At a subtler level, there exist small-scale hills and valleys, caused by mechanical polishing or the electrochemically induced dissolution or formation of material. These are visible under the electron microscope and can be revealed by delicate stylus profilometry (in which the vertical undulations of a hard, sharp stylus are displayed in magnified form on a chart as a function of horizontal distance traversed in a straight line). Neither method is ideal for revealing microtopographical detail; the electron microscope can produce visually misleading contrasts and shadows and the stylus instrument, apart from ploughing a miniature furrow across the surface, is also blind to "ink bottle" pores and similar features in which the body of the pore is wider than its opening on the surface.

Topographical irregularities also exist at the atomic level. *Singular* surfaces of single crystals are flat, low-index planes, i.e., planes with Miller indices such as (100), (110), (111), etc. Vicinal surfaces (so called because they are inclined at small angles to singular surfaces and in that sense are their neighbors) are composed of extensive flat, low index terraces, separated by ledges usually one atom high along which there may well be kinks (the TLK model). The exposed ledge and kink atoms are very labile, essentially because of the larger proportion of neighboring atoms they have lost, and they are the sites for the commencement of catalytic activity. Atomic topography can be studied by low-energy electron diffraction.[467]

Each topographical regime is relevant to solid electrolyte interfacial behavior. The macrotopography dictates the contact area and the path length involved in converting conductance values to conductivities. Values conventionally quoted for conductivities, current densities, and so on are based on superficial (i.e., apparent)[116] dimensions. In tribology[477] (the study of friction, wear, adhesion, and related phenomena) it is not infrequently found that the true area of contact is 1% or less of the apparent area. Unfortunately, the determination of the true area of contact for a multi-interfacial situation such as occurs in a compacted electrolyte is difficult, so that it is likely that topo-

graphical effects will continue to be neglected. The microtopography provides regions of local curvature which can serve as nucleation sites for removal or deposition of material. The degree of curvature also affects the local stress field which will give an as-yet undetermined perturbation to the local electric field. Atomic scale roughness, in combination with microtopographical features, hinders the matching up of conducting blocks, channels, etc., in the many electrolytes in which conductivity is not uniform in three dimensions.

2. Area of Contact

The effect of pressure on the area of contact, and thus on the conductivity, has been mentioned earlier. Electrode–electrolyte contact can be enhanced if the electrode and electrolyte are of different hardness, so that particles of the one become embedded in the other.[114] Also, it is the frequent and sensible practice of the battery technologist to maximize the contact area by incorporating electrolyte material in the electrode compartments.

The change in electrode–electrolyte contact area caused by galvanic reaction can be studied electrokinetically. In cyclic voltammetry on the $Ag|Ag_4RbI_5|Pt$ system using a $Ag|AgI$ reference electrode,[115] the presence of a pronounced peak at small peak current, that diminished on subsequent sweeps, was ascribed to contact loss between the Ag measuring electrode and the electrolyte. Impedance measurements have also been compared with cyclic voltammetry studies to elucidate whether applied pressure merely affects the test-electrode–electrolyte contact area.[115] It was assumed that a few contact points sufficed for electron transfer in the impedance measurements under ac conditions, whereas enhanced contact was needed to carry the high peak currents observed under high pressure. The impedance plot did, however, display features such as increased steepness and a decrease in the imaginary contribution that would be consistent with an enlarged contact area.

3. Elasticity, Plasticity, Stress, and Strain

A material that is elastically distorted resumes its original shape when the constraint is removed; when it is plastically distorted, it does not. The constraint, which can be a pressure or a tension, is referred to as a stress if both the applied force and the area on which it acts are directional in nature. The change in dimensions caused by the stress is called a strain. Both stresses and strains are tensors of the second rank, which merely means that they require a double set of directions, for force and for area, to be properly assigned. The ratio of stress to strain is called a modulus or elastic constant. For a straightforward push or pull, the stress is compressive or tensile, whereas a shear stress produces a sliding motion.

It is clear that interfacial behavior in solid electrolytes is strongly influenced by whether the material is elastically or plastically strained, whether shear stresses are present, and so on. A comprehensive theory has not been developed to relate the mechanical parameters of the electrode and electrolyte materials to the interfacial conductivity. The mechanical cohesion and the propensity to fracture are also dependent on these and other

mechanical properties, as is the degree of strain in thin films.

4. Electron Microscopy

The electron microscope can be used to view thin sections of samples in transmission (TEM) or to scan reflected images of a surface (SEM). The technique of energy dispersive analysis by X-rays (EDAX), in which the X-rays produced by the bombardment of the electron beam are used to "fingerprint" the chemical nature of the surface exposed to the beam, can be combined with EDAX to provide a compositional map of the surface. These techniques are much applied to solid electrolytes, especially β-alumina ceramics.[133,174,478,479] They are experiments of the perturbing class, as the microscope requires high vacuum conditions for its operation ($<10^{-4}$ Pa) which affects any volatile constituents of the sample, and the material requires to be cut or fractured to expose the relevant interface. It is not always necessary to section the material thinly for TEM work as replicas of the surface can be cast and examined.

B. Compositional Properties

The interfacial region can be enriched or depleted in particular constituents relative to the bulk by passage of material from the bulk (segregation) or the surrounding void regions (adsorption). In addition, ionic migration across the interface and adjoining bulk may cause short-range compositional inhomogeneities and consequent local concentration gradients. At the charge-transfer interface, double layer effects,[464,480] caused by the need to balance electron charge on one side of the barrier by ionic charge on the other, make the distribution of chemical species rather complex. The possible rate-determining paths at the charge-transfer interface have been described for oxide fuel cell systems in which the chemistry is somewhat complicated and material transport can be important.[172]

1. Role in Determining Cell Reactions

A knowledge of the species present at the working electrode interface is of particular importance in two instances. The first is when it is suspected that the galvanic cell reaction does not involve the species initially present in the electrodes but rather the products of a chemical reaction that precedes the electrochemical process. This could take the form of a valence change, thus modifying the nature of the metal/ion couple at the electrode, or a complexing reaction that changes the nature of the reactants participating in the cell reaction, and consequently the cell voltage. Such phenomena have been postulated to explain anomalous voltages in CuI systems, and preliminary Auger spectroscopic studies have been carried out.[77] The other situation in which information about the composition adjacent to an electrode would be desirable is when conductivity, electrokinetic, impedance, or battery discharge behavior substantially changes with time, and it is suspected that the cause may be the formation of a resistive layer of cell reaction product. In a study of the current–time dependence of Ag_4RbI_5 following the imposition of voltage pulses, the presence of resistive RbI_3 at the interface was suggested;[114] this would be consistent with

ocv measurements. In many investigations in which Ag electrodes are employed, the conductivity decays with time, suggesting the formation of a surface oxide film.[115,481,482] In contrast, when the behavior of polished and unpolished β-alumina for Na/S batteries was compared, the conductivity of the latter was found to improve with time, which suggests that a resistive film was initially present and was subsequently removed or modified by the molten sodium.[114] It should be noted that in this battery system the electrolyte is solid but the electrodes are not.

2. Electron Spectroscopic Techniques

Electron spectroscopy for chemical analysis (ESCA) is a generic term that embraces techniques in which electrons of characteristic energy are emitted from samples bombarded by electrons, photons, or other particles.[466-473] In X-ray photoelectron spectroscopy, an X-ray beam of well-defined energy (often Al $K\alpha$ at 1486.6 eV) displaces core electrons from the atoms in the sample. The kinetic energy, after correction, is equal to the difference between primary beam and binding energies. Hence if the first two quantities can be measured precisely, the binding energy can be found. It is characteristic of the chemical nature and to some extent the valence state of the species from which it came. UPS in which UV rather than X-ray photons are used and in which valence rather than core electrons are ejected can also be carried out. In both cases, only the outermost few nanometers of the sample is studied and high or ultrahigh (10^{-7} Pa) vacuum conditions apply, which perturbs the surface. In no way are they in situ techniques, and at present they are not available in scanning mode, which means that their compositional information is integrated over an appreciable area.

Auger electron spectroscopy is potentially more useful, as two-dimensional scans can be carried out across the surface and, in combination with SIMS discussed below, a three-dimensional composition profile can be created. The Auger process involves an electron from a further-out shell falling into the hole created by the ejection of the photoelectron from a core shell. The energy available from this transition between electronic energy levels can be used in photon production (X-ray fluorescence, XRF) or, alternatively, it can be donated to yet another electron, the Auger electron, which is then ejected. Its energy depends solely on the binding energies of the three electrons involved in the process. The technique is ideally suited for fingerprinting the nature of adsorbate and other contaminant species. Valence-state information tends to be obscured, but it can be used to distinguish[483] between Cu^+ and Cu^{2+} which is of relevance in clarifying the mechanism involved at Cu/Cu^+ interfaces. It has been applied to the study of fracture surfaces in β-alumina.[484] A related technique, Auger sputter profiling (ASP), has been used to investigate the Si/SiO_2 interface in metal oxide-semiconductor (MOS) devices,[485] and it is to be expected that many additional solid electrolyte applications will soon be forthcoming.

3. Other Techniques

Secondary ion mass spectroscopy (SIMS) involves the identification by time of flight mass spectrometry of positively charged, negatively charged, or neutral species ejected from a solid surface by high-energy noble gas ion bombardment. With careful control of the beam energy, a compositional depth profile can be obtained. In conjunction with AES, it has obvious application to the study of interfaces in solid electrolyte systems provided that the problem of revealing the interface without destroying it can be overcome. The techniques mentioned so far are well-suited to the study of the uppermost few nanometers of the surface. Electron microprobe analysis is capable of providing information about the top micrometer or so of surface. High energy electrons are used to eject core electrons, leaving a hole into which a further-out electron can fall. The transition produces an X-ray of energy equal to the difference in binding energies. Finally, attenuated total reflectance infrared spectroscopy (ATR) can provide limited information about the vibrational modes of surface species, which can aid in their identification.

C. Structural Properties

The structure of the first two or three atomic layers often differs from the bulk lattice structure, and the surface atomic structure can be revealed by low-energy electron diffraction (LEED). A primary beam of electrons of well-controlled energy, and hence wavelength, is aimed at a surface maintained under ultrahigh vacuum conditions. Some of the electrons are elastically diffracted. The beam energy is too low to permit diffracted electrons to pass through the specimen, and it is the back-diffracted electrons that are detected. They are separated from the inelastically scattered electrons by a grid of energy just below that of the primary beam. The position of the diffracted beams can be detected by a fluorescent screen or a Faraday cup. Surface structure can be deduced from the diffraction pattern, but the intensities are difficult to interpret because the real-space lattice causing the diffraction is about three atomic layers in depth. Consequently, it is neither two dimensional nor is it of sufficient depth to be regarded as three dimensional.

It is also possible to study surface irregularities such as asperities by reflective high-energy electron diffraction (RHEED) in which the primary beam of energy about 3 keV is directed at grazing incidence to the surface and the diffracted beams emerge from the other side of the protrusion. High-energy electron diffraction, in which beams penetrate a thin sample, is often carried out in conjunction with TEM. It has been used to study the needle-like crystals of $Na_{0.9}Ti_{1.1}Fe_{0.9}O_4$, a β-alumina type compound,[486] and for certain oxygen conductors.[487]

In surface science, many other structural techniques such as field ion microscopy exist, but the sample configurations required would appear to preclude their use in this field. The application of computer simulation techniques to interfaces is well established,[488] but their use in solid electrolyte interfacial studies is only just beginning.[402]

D. Thin-Film Studies

This is an important field in its own right. For many solid-state battery systems, a thin film is a very suitable form of solid electrolyte because the mass efficiency of the device is enhanced and mechanical integrity may be better than for compacted materials. An enhancement of electrode–electrolyte contact area is also to be

expected, although dendrite penetration can be a problem. In practical LiI systems,[32] the thin-film electrolyte is created in situ by the cell reaction. Other materials such as $Ag_7I_4PO_4$,[489] Ag_4KI_5,[361] and $Ag_4NH_4I_5$[490] are being studied for battery applications. Thin-film fuel cells are also of considerable present interest.[491,492] Novel electrolytes such as the proton conductor $H_{5n-2}UO_2(IO_6)_n \cdot 4H_2O$, $n = 1$ or 2,[430] and $PbSnF_4$[493] can be prepared in thin film, among other forms. A technique that in principle could be used to study thin-film electrolytes is inelastic electron tunneling spectroscopy (IETS).[494] Electrons tunneling through a metal–insulator–metal junction, containing a thin electronically insulating layer between the electrolyte and one of the electrodes, lose some of their energy in exciting vibrations within the electronic insulator.

IX. References

(1) *Top. Appl. Phys.* 1977, 21.
(2) *Top. Current Phys.* 1979, 15.
(3) "Solid Electrolytes, General Principles, Characterization, Materials, Applications"; Hagenmuller, P., Van Gool, W., Eds.; Academic Press: New York, 1978.
(4) "Superionic Conductors"; Mahan, G. D., Roth, W. L., Eds.; Plenum Press: New York, 1976.
(5) "Fast Ion Transport in Solids"; Vashishta, P., Mundy, J. N., and Shenoy, G. K., Eds.; North-Holland: New York, 1979.
(6) "Fast Ion Transport in Solids"; Van Gool, W., Ed.; North-Holland: Amsterdam, 1973.
(7) "Physics of Superionic Conductors and Electrode Materials", Proceedings of the NATO Advanced Studies Institute, Odense, Denmark, Aug 1980; Perram, J., de Leeuw, S., Eds.: Reidel: Dordrecht, in press.
(8) Liang, C. C.; Joshi, A. V.; Hamilton, N. E. *J. Appl. Electrochem.* 1978, 8, 445.
(9) Lazzari, M.; Scrosati, B. *J. Power Sources* 1977, 1, 333.
(10) Holzäpfel, G.; Rickert, H. *Naturwissenschaften* 1977, 64, 53.
(11) Huggins, R. A.; Rabenau, A. *Mater. Res. Bull.* 1978, 13, 1315.
(12) McGeehin, P.; Hooper, A. *J. Mater. Sci.* 1977, 12, 1.
(13) Rickert, H. *Angew. Chem., Int. Ed. Engl.* 1978, 17, 37.
(14) Shahi, K. *Phys. Stat. Solid.* 1977, 41, 11.
(15) Whittingham, M. S. *Electrochim. Acta* 1975, 20, 575.
(16) Geller, S., ref 1, p 41.
(17) McKechnie, J. S.; Turner, L. D. S.; Vincent, C. A.; Lazzari, M.; Scrosati, B. *J. Chem. Educ.* 1978, 55, 418.
(18) Goodenough, J. B.; Hong, H. Y.-P.; Kafalas, J. A. *Mater. Res. Bull.* 1976, 11, 203.
(19) Owens, B. B. In "Advances in Electrochemistry and Electrochemical Engineering"; Tobias, C. W., Ed.; Wiley: New York, 1971; p 1.
(20) Armstrong, R. D.; Bulmer, R. S.; Dickinson, T. *J. Solid State Chem.* 1973, 8, 219.
(21) Funke, K. *Prog. Solid State Chem.* 1976, 11, 345.
(22) Liang, C. C. *Appl. Solid State Science* 1974, 4, 95.
(23) Boyce, J. B.; Huberman, B. A. *Phys. Rep.* 1979, 51, 189.
(24) Hong, H. Y.-P. *Solid State Chem.* 1977, 163, 179.
(25) Farrington, G. C.; Briant, J. L. *Science (Washingon, D.C.)* 1979, 204, 1371.
(26) Geller, S., ref 1, p 1.
(27) Salamon, M. B., ref 2, p 1.
(28) O'Keeffe, M.; Hyde, B. G. *Philos. Mag.* 1976, 33, 219.
(29) Faraday, M. "Experimental Researches in Electricity"; Taylor and Francis: London, 1839.
(30) Warburg, E. *Ann. Phys.* 1884, 21, 622.
(31) Nernst, W. *Z. Elektrochem.* 1899, 6, 41.
(32) Owens, B. B.; Oxley, J. E.; Sammells, A. F., ref 1, p 67.
(33) Voinov, A., ref 3, p 527.
(34) Yushina, L. D.; Karpachev, S. V.; Terekhov, W. I., ref 5, p 121.
(35) Aceves, J. M.; West, A. R. *J. Appl. Electrochem.* 1980, 10, 379.
(36) Gauthier, M.; Belanger, A.; Meas, Y.; Kleitz, M., ref 3, p 497.
(37) Kleitz, M.; Pelloux, A.; Gauthier, M., ref 5, p 69.
(38) Takahashi, T.; Tanese, S.; Yamamoto, O. *J. Appl. Electrochem.* 1980, 10, 415.
(39) Green, M.; Kang, K. S. *Thin Solid Films*, 1977, 40, L19.

(40) Anthony, A. M., ref 3, p 519.
(41) Whittingham, M. S. *J. Solid State Chem.* 1979, 29, 303.
(42) Hagenmuller, P.; Van Gool, W., ref 3, p 535.
(43) Birk, J. R., ref 4, p 1.
(44) Martin, T. L.; Bones, R. J.; Dell, R. M., ref 4, p 15.
(45) Kane, J. S., ref 5, p 7.
(46) Catlow, R., ref 7.
(47) Steele, B. C. H., ref 7.
(48) Schultz, H., ref 7.
(49) Schultz, H.; Thiemann, K. H. *Acta Crystallogr., Sect. A.* 1979, A35, 309.
(50) Schultz, H.; Zucker, U., ref 5, p 495.
(51) Huggins, R. A. In "Mass Transport Phenomena in Ceramics"; Cooper, A. R., Heuer, A. H., Eds.; Plenum: New York, 1975; p 155.
(52) Rubinstein, I.; Gileadi, E. *J. Electroanal. Chem.* 1980, 108, 191.
(53) Owens, B. B.; Argue, G. R. *Science (Washington, D.C.)* 1967, 157, 308.
(54) Bradley, J. N.; Greene, P. D. *Trans. Faraday Soc.* 1967, 63, 424.
(55) Owens, B. B.; Christie, J. H.; Tiedman, G. T. *J. Electrochem. Soc.* 1971, 118, 1144.
(56) Owens, B. B. *J. Electrochem. Soc.* 1970, 117, 1536.
(57) Beradelli, M. L.; Biondi, C.; De Rossi, M.; Fonseca, G.; Giamini, M. *J. Electochem. Soc.* 1972, 119, 114.
(58) Linford, R. G.; Pollock, J. M.; Randell, C. F. *Nature (London)* 1975, 256, 398.
(59) Linford, R. G.; Pollock, J. M.; Randell, C. F. *Nature (London)* 1976, 259, 658.
(60) Linford, R. G.; Pollock, J. M.; Randell, C. F. *British Patent* 1474246, 1977.
(61) Takahashi, T.; Wakabashi, N.; Miyazaki, T.; Yamamoto, O. *Nippon Kagaku Kaishi* 1975, 2, 265.
(62) Owens, B. B.; Christie, J. H.; Tiedman, T. *Proc. 147th Electrochem. Soc.* 1974, No. 20.
(63) Takahashi, T.; Wakabayashi, N.; Yamamoto, O. *J. Appl. Electrochem.* 1977, 7, 253.
(64) Takahashi, T.; Yamamoto, O.; Ikeda, S. *J. Electrochem. Soc.* 1973, 120, 1431.
(65) Takahashi, T.; Wakabayashi, T.; Yamamoto, O. *J. Electrochem. Soc.* 1976, 123, 129.
(66) Dahm, R. H.; Hackwood, S.; Linford, R. G.; Pollock, J. M. *Nature (London)* 1978, 272, 522.
(67) Andrews, K.; Hackwood, S.; Linford, R. G. *J. Power Sources* 1979, 4, 165.
(68) Coetzer, J.; Kruger, C. J.; Thackeray, M. M. *Acta Crystallogr., Sect. B* 1976, B32, 1248.
(69) Geller, S.; Lind, M. D. *J. Chem. Phys.* 1970, 52, 5854.
(70) Thackeray, M. M.; Coetzer, J. *S. African J. Chem.* 1977, 30, 118.
(71) Thackeray, M. M.; Coetzer, J. *S. African J. Chem.* 1977, 30, 117.
(72) Geller, S.; Owens, B. B. *J. Chem. Phys. Solids* 1972, 33, 1241.
(73) Geller, S.; Starskad, P. M. *Phys. Rev. Lett.* 1974, 33, 1484.
(74) Geller, S. *Acc. Chem. Res.* 1978, 11, 87.
(75) Geller, S.; Akridge, J. R.; Wilber, S. A. *J. Electrochem. Soc.* 1980, 127, 251.
(76) Thackeray, M. M.; Coetzer, J., ref 5, p 577.
(77) Hackwood, S.; Linford, R. G. *Chem. Ind. (London)* 1980, 523.
(78) Rao, B. M. L.; Silbernagel, B. G. U.S. Patent 4190706, 1980.
(79) Wapenaar, K. D. *J. Phys., Proc. 3rd Europhys. Conf. Lattice Defects*, 1979.
(80) Wapenaar, K. E. D.; Schoonman, J. *J. Electrochem. Soc.* 1979, 126, 667.
(81) Hildebrand, J. H. *Proc. Natl. Acad. Sci. U.S.A.* 1969, 64, 1331.
(82) Lidiard, A. B. In "Handbuch der Physik"; Flugge, S., Ed.; Springer-Verlag: Berlin, 1957; Vol. 20, 246.
(83) Armstrong, R. D.; Bulmer, R. S.; Dickinson, T., ref 6, p 269.
(84) Heyne, L. *Electrochim. Acta* 1970, 15, 1251.
(85) Buck, R. P.; Mathis, D. E.; Rhodes, R. K. *J. Electroanal. Chem.* 1977, 80, 245.
(86) Hong, H. Y.-P.; Kafalas, J. A.; Bayard, M. *Mater. Res. Bull.* 1978, 13, 757.
(87) Geller, S.; Chan, L. Y. Y.; Ruse, G. F. *Mater. Res. Bull.* 1978, 13, 339.
(88) Linford, R. G.; Pollock, J. M.; Randell, C. F. in "Power Sources 6"; Collins, D. A., Ed.; Academic Press: London, 1977, p 511.
(89) Teicher, M.; Weil, R. *Phys. Rev. B* 1978, 18, 7134.
(90) Tell, B.; Wagner, S.; Kasper, H. M. *J. Electrochem. Soc.* 1977, 124, 536.
(91) Takahashi, T.; Iwahara, H.; Ishikawa, T. *J. Electrochem. Soc.* 1977, 124, 280.
(92) Takahashi, T. *Pure Appl. Chem.* 1978, 50, 1091.
(93) Scholtens, B. B.; Brouwer, A.; Broers, G. H. J. *J. Appl. Electrochem.* 1978, 8, 165.
(94) Scrosati, B.; Ricci, A.; Lazzari, M. *J. Appl. Electrochem.* 1976, 6, 237.

(95) Thackeray, M. M.; Coetzer, J. *Electrochim. Acta* **1979**, *24*, 495.
(96) Browall, K. W.; Kasper, J. S. *J. Solid State Chem.* **1975**, *15*, 54.
(97) Euler, K. J.; Kirchhof, R.; Metzendorf, H. *Mater. Chem.* **1979**, *4*, 611.
(98) Chiodelli, G.; Magistris, A.; Schiraldi, A. *Z. Phys. Chem. (Wiesbaden)* **1979**, *118*, 177.
(99) Matsui, T.; Wagner, J. *J. Electrochem. Soc.* **1977**, *124*, 941.
(100) Lazzari, M.; Pace, R. C.; Scrosati, B. *Electrochim. Acta* **1975**, *20*, 331.
(101) Sammels, A. F.; Gougoutas, J. Z.; Owens, B. B. *J. Electrochem. Soc.* **1975**, *122*, 1291.
(102) Shibata, S.; Hoshino, H.; Shimoji, M. *J. Chem. Soc., Faraday Trans. 1* **1974**, *70*, 1409.
(103) Raistrick, I. D.; Ho, C.; Huggins, R. A. *J. Electrochem. Soc.* **1976**, *123*, 1469.
(104) Nagel, L. E.; O'Keeffe, M., O'Keeffe, 6, p 165.
(105) Schoonman, J.; Bonne, R. *J. Electrochem. Soc.* **1977**, *124*, 28.
(106) Schoonman, J.; Dirksen, G. J.; Blaise, G. *J. Solid State Chem.* **1973**, *7*, 245.
(107) Boyce, J. B.; Mikkelsen, J. C., ref 4, p 413.
(108) Hwang, T. Y.; Lowe, I. J.; Lau, K. F.; Vaughan, R. W., ref 4, p 413.
(109) Shahi, K.; Chandra, S. *J. Phys. C* **1975**, *8*, 2255.
(110) Scrosati, B.; Germano, G.; Pistola, G. *J. Electrochem. Soc.* **1971**, *118*, 86.
(111) Shahi, K.; Chandra, S. *Phys. Stat. Solid.* **1975**, *28*, 653.
(112) Armstrong, R. D.; Dickinson, T.; Taylor, K. *J. Electroanal. Chem.* **1977**, *78*, 45.
(113) Armstrong, R. D.; Dickinson, T.; Taylor, K. *J. Electroanal. Chem.* **1974**, *53*, 389.
(114) Armstrong, R. D.; Dickinson, T., ref 4, p 65.
(115) Eichinger, G. E. *J. Appl. Electrochem.* **1980**, *10*, 239.
(116) Linford, R. G. *Chem. Rev.* **1978**, *78*, 81.
(117) Linford, R. G. In "Solid State Surface Science II"; Green, M., Ed.; Dekker: New York, 1973; p 1.
(118) Albery, J. "Electrode Kinetics"; Clarendon Press: Oxford, 1975; p 64.
(119) Hebb, M. *J. Chem. Phys.* **1952**, *20*, 1109.
(120) Hartwig, P.; Weppner, W.; Wichelaus, W., ref 5, p 487.
(121) Raistrick, I. D.; Huggins, R. A. *J. Electrochem. Soc.* **1976**, *123*, B224.
(122) Bottelberghs, P. H., ref 3, p 145.
(123) Strom, U.; Taylor, P. C. *J. Appl. Phys.* **1979**, *50*, 5761.
(124) Worrell, W. L., ref 1, p 143.
(125) Heyne, L., ref 1, p 169.
(126) Owens, B. B.; Skarstad, P. M., ref 5, p 61.
(127) Armstrong, R. D.; Dickinson, T.; Taylor, K. *J. Electroanal. Chem.* **1974**, *57*, 157.
(128) Armstrong, R. D.; Dickinson, T.; Willis, P. M. *J. Electroanal. Chem.* **1975**, *59*, 281.
(129) Wagner, C. *Z. Elektrochem.* **1956**, *60*, 4.
(130) Raleigh, D. O. In "Progress in Solid State Chemistry"; Reiss, H., Ed.; North-Holland: Amsterdam, 1963, p 3.
(131) Wagner, J. B., ref 6, p 489.
(132) Kennedy, J. H. *J. Electrochem. Soc.* **1977**, *124*, 865.
(133) Kennedy, J. H., ref 1, p 105.
(134) Hibma, T. *Solid State Commun.* **1980**, *33*, 445.
(135) Yakoto, I. *J. Phys. Soc. Jpn.* **1953**, *8*, 595.
(136) Wada, T.; Wagner, J. B., ref 5, p 581.
(137) Wagner, J. B. In "Electrode Processes in Solid State Ionics"; Cleitz, M.; Dupuy, J., Eds.; Reidel: Dordrecht, 1975; p 185.
(138) Bazan, J. C.; Dayen, E. A. *Z. Phys. Chem.* **1977**, *105*, 63.
(139) Tubandt, C. *Hanb. Exp. Physi.* **1932**, *12*, 383.
(140) Heyne, L. *Electrochim. Acta* **1970**, *15*, 1251.
(141) Sawyer, D. T.; Roberts, J. L. "Experimental Electrochemistry for Chemists"; Wiley: New York, 1979.
(142) Bockris, J. O'M.; Reddy, A. K. N. "Modern Electrochemistry": Macdonald: London 1970.
(143) Thompson, A. H., ref 5, p 47.
(144) Huggins, R. A., ref 5, p 53.
(145) Hackwood, S.; Latham, R. J.; Linford, R. G. To be published.
(146) Lazzari, M.; Vincent, C. A.; Scrosati, B., ref 5, p 713.
(147) Armstrong, R. D.; Dickinson, T.; Taylor, K. *J. Electroanal. Chem.* **1975**, *64*, 155.
(148) Vallet, C. E.; Braunstein, J. *J. Electrochem. Soc.* **1977**, *124*, 77.
(149) Funke, K., ref 3, p 77.
(150) Funke, K., ref 4, p 183.
(151) Pietronero, L.; Straessler, S.; Zeller, H. R., ref 5, p 165.
(152) Funke, K.; Hackenberg, T. *Ber. Bunsenges. Phys. Chem.* **1972**, *76*, 885.
(153) Bruesch, P.; Pietronero, L.; Zeller, H. R.; Straessler, S. *Electrochim. Acta* **1977**, *22*, 717.
(154) McDonald, J. R., ref 4, p 81.
(155) Hampson, N. A.; Karunath, S. A.; Leck, R. *J. Appl. Electrochem.* **1980**, *10*, 3.
(156) DeBruin, H. J.; Badwal, S. P. S. *Phys. Stat. Solid.* **1978**, *49*, K181.

(157) Patterson, J. W. *ACS Symp. Ser.* **1979**, *No. 89*, 97.
(158) Britz, D. *Anal. Chem.* **1980**, *52*, 1166.
(159) Boukamp, B. A.; Raistrick, I. D.; Huggins, R. A., ref 5, p 177.
(160) Armstrong, R. D.; Mason, R. *J. Electroanal. Chem.* **1973**, *41*, 231.
(161) McDonald, J. R.; Garber, J. A. *J. Electrochem. Soc.* **1977**, *124*, 1022.
(162) Jonscher, A. K. *J. Mater. Sci.* **1978**, *13*, 553.
(163) Shlesing, M. *Bull. Am. Phys. Soc.* **1980**, *25*, 434.
(164) Grant, R. J.; Ingram, M. D.; West, A. R. *J. Electroanal. Chem.* **1977**, *80*, 239.
(165) McDonald, J. R.; Jacobs, P. W. M. *J. Phys. Chem. Solids* **1976**, *37*, 1117.
(166) Dawson, J. L.; John, D. G. *J. Electroanal. Chem.* **1980**, *110*, 37.
(167) Hodge, I. M.; Ingram, M. D.; West, A. R. *J. Electroanal. Chem.* **1976**, *74*, 125.
(168) Kanazawa, K.; Schoenes, J. *Rev. Sci. Instum.* **1975**, *47*, 160.
(169) Dickinson, T.; Whitfield, R. *Electrochim. Acta* **1977**, *22*, 385.
(170) Armstrong, R. D.; Metcalfe, A. A.; Thirsk, H. R. *Extended Abst., 28th Meeting Int. Soc. Electrochem.* **1977**, *No. 4*, 23.
(171) Yushina, L. D.; Tarasov, A. Ya.; Karpachov, S. V. *Sov. Electrochem. (Engl. Transl.)* **1977**, *13*, 1373.
(172) Dell, R. M.; Hooper, A., ref 3, p 291.
(173) Grant, R. J.; Hodge, I. M.; Ingram, M. D.; West, A. R. *J. Am. Ceram. Soc.* **1977**, *60*, 226.
(174) Powers, R. W.; Mitoff, S. P., ref 3, p 123.
(175) Powers, R. W., ref 4, p 351.
(176) Jaszczynski, K.; Dabkowski, J.; Minc, S. *Pol. J. Chem.* **1980**, *54*, 129.
(177) Trichet, L.; Rouxel, J. *Mater. Res. Bull.* **1977**, *12*, 345.
(178) Avignant, D.; Mansouri, I.; Sabatier, R.; Cousseins, J. C. *App. Chim.* **1979**, *8*, 585.
(179) Matsui, N. *Surf. Sci.* **1979**, *86*, 353.
(180) Grins, J.; Nygren, M.; Wallin, T., ref 5, p 423.
(181) Hagenmuller, P.; Levasseur, A.; Lucat, C.; Reau, J. M.; Villeneuve, G., ref 5, p 637.
(182) Ravaine, D.; Souquet, J. L., ref 3, p 277.
(183) Glass, A. M.; Nassau, K. *J. Appl. Phys.* **1980**, *51*, 3756.
(184) Bayard, M. L., ref 5, p 479.
(185) Hu, Y.-V.; Raistrick, I. D.; Huggins, R. A. *Mater. Res. Bull.* **1976**, *11*, 1227.
(186) Bonne, R. W.; Schoonman, J. *J. Electroanal. Chem.* **1978**, *89*, 289.
(187) Bruinik, J.; Broers, G. H. J. *J. Phys. Chem. Solids* **1972**, *33*, 1713.
(188) Hartwig, P.; Weppner, W.; Wichelhaus, W., ref 5, p 487.
(189) Boukamp, B. A.; Huggins, R. A. *Mater. Res. Bull.* **1978**, *13*, 23.
(190) Ukshe, E. A.; Bukin, N. G. *Electrokhimiya* **1980**, *16*, 313.
(191) Armstrong, R. D.; Metcalfe, A. A. *J. Electroanal. Chem.* **1978**, *88*, 187.
(192) Coleman, L. B., ref 5, p 601.
(193) Bukun, N. G.; Dermanchuk, E. P.; Ukshe, E. A. *Sov. Electrochem. (Engl. Transl.)* **1977**, *13*, 1081.
(194) Yushina, L. D.; Karpachov, S. V.; Tarasov, A. Ya. *Sov. Electrochem. (Engl. Transl.)* **1977**, *12*, 1649.
(195) Mikhailova, A. M.; Shilo, V. I.; Bukun, N. G.; Ukshe, E. A. *Sov. Electrochem. (Engl. Transl.)* **1978**, *14*, 408.
(196) Zekunde, A. A.; Bukun, N. G., *Electrokhimiya* **1980**, *16*, 114.
(197) Yamanka, S. *J. Inorg. Nucl. Chem.* **1980**, *42*, 717.
(198) Hooper, A. *J. Electroanal. Chem.* **1980**, *109*, 161.
(199) *NBS Spec. Publ.* **1979**, *No. 400-50*.
(200) Brennen, K. R.; Fester, K. E.; Owens, B. B.; Untereker, D. F. *J. Power Sources* **1980**, *5*, 25.
(201) Hurzeler, P.; Morse, D.; Leach, C.; Sands, M. J.; Pennock, R.; Zinberg, A. *Pace* **1980**, *3*, 555.
(202) Untereker, D. F.; Owens, B. B., ref 199, p 17.
(203) Owens, B. B.; Untereker, D. F. In "Power Sources 7"; Collins, D. A., Ed.; Academic Press: London, 1979; p 647.
(204) Holmes, W. S., ref 199, p 6.
(205) Owens, B. B.; Untereker, D. F.; Skarskad, P. M., ref 5, p 105.
(206) Hansen, L. D.; Hart, R. M., ref 199, p 10.
(207) Prosen, E. J.; Colbert, J. C., ref 199, p 23.
(208) Schneider, A. A.; Kraus, F. E., ref 199, p 27.
(209) Cowen, J. A.; Foiles, C. L.; Edmunds, D. L., ref 5, p 593.
(210) Coleman, L. B.; LeDuc, H. G. *Bull. Am. Phys. Soc.* **1979**, *24*, 397.
(211) Fergelson, R. S.; N'Diaye, A.; Yin, S.-Y.; Bube, R. H. *J. Appl. Phys.* **1977**, *48*, 3162.
(212) Kasper, J. S., ref 3, p 217.
(213) Takahashi, T., ref 5, p 521.
(214) Ihle, D. *Phys. Stat. Solid.* **1979**, *91*, K49.
(215) Polishchuk, A. F.; Loichenko, V. Ya.; Glagoleva, N. A. *Sov. Electrochem. (Engl. Transl.)* **1978**, *14*, 892.
(216) Tanaka, T.; Sharma, N. *Bull. Am. Phys. Soc.* **1980**, *25*, 434.
(217) Takahashi, T.; Yamamoto, O.; Yamada, S.; Hayashi, S. *J. Electrochem. Soc.* **1979**, *126*, 1654.
(218) Schmalzried, H. *Ber. Bunsenges. Phys. Chem.* **1980**, *84*, 120.
(219) Salamon, M. B., ref 2, p 175.

(220) Weppner, W.; Lichuan, C.; Piekarcz, W. Z. Naturforsch. A 1980, A35, 381.
(221) Hicter, P.; Desre, P. J. Chim. Phys. Phys.-Chim. Biol. 1980, 77, 59.
(222) McGlashan, M. "Physicochemical Quantities and Units"; R.I.C.: London, Monograph for Teachers No. 15, 1971.
(223) Takahashi, T.; Yamamoto, O. J. Appl. Electrochem. 1977, 7, 37.
(224) Steele, B. C. H.; Shaw, R. W., ref 3, p 483.
(225) McKechnie, J. S.; Turner, L. D. S.; Vincent, C. A. J. Chem. Thermodyn. 1979, 11, 1189.
(226) Weppner, W.; Huggins, R. A. Solid State Ionics 1980, 1, 1.
(227) Dudley, G. J.; Cheung, K. Y.; Steele, B. C. H.; J. Solid State Chem. 1980, 32, 267.
(228) Dickens, P. G. Solid State Chem. 1977, 16, 165.
(229) Thompson, A. H. J. Electrochem. Soc. 1979, 126, 608.
(230) Pollock, J. M. Q. Rev. Chem. Soc. 1970, 24, 601.
(231) Mundy, J. N., ref 5, p 159.
(232) Arzigian, J. S.; Lazarus, D. Bull. Am. Phys. Soc. 1980, 25, 413.
(233) Sato, H.; Kikuchi, R., ref 4, p 135.
(234) Adams, D. J., ref 7.
(235) Murch, G. E.; Thorn, R. J. Philos. Mag. 1977, 35, 1441.
(236) De Leeuw, S. W.; Perram, J. W., ref 5, p 345.
(237) Vashishta, P.; Rahman, A., ref 5, p 527.
(238) Rahman, A., ref 5, p 643.
(239) Dixon, M.; Gillan, M. J. J. Phys. C 1978, 11, L165.
(240) Dixon, M.; Gillan, M. J., ref 5, p 701.
(241) Newman, D. S. Electrochim. Acta 1979, 24, 789.
(242) Newman, D. S.; Frank, C.; Matlack, R. W.; Twining, S.; Krishnan, V. Electrochim. Acta 1977, 22, 811.
(243) Knotek, M. L.; Seager, C. H. Solid State Commun. 1977, 21, 625.
(244) Kaneda, T.; Mizuki, E. Phys. Rev. Lett. 1972, 29, 937.
(245) Braun, H. Appl. Phys. 1978, 17, 193.
(246) Roth, W. L., ref 3, p 45.
(247) Shapiro, S. M.; Reidinger, F., ref 2, p 45.
(248) Moore, W. J. "Physical Chemistry"; Prentice-Hall: Englewood Cliffs, NJ, 1972.
(249) Dekker, A. J. "Solid State Physics"; Macmillan: London, 1975.
(250) Strock, L. W. Z. Phys. Chem. 1936, B31, 132.
(251) Dent-Glasser, L. S. "Crystallography and its Applications"; Van Nostrand-Reinhold: New York, 1977.
(252) Huggins, R. A., ref 3, p 27.
(253) Sakuma, T.; Iida, K. J. Phys. Soc. Jpn. 1977, 43, 539.
(254) Newsham, J. M.; Cheetham, A. K.; Tolfield, B. C., ref 5, p 435.
(255) Alpen, U. V.; Fenner, J.; Morcoll, J.; Rabenau, A., ref 4, p 424.
(256) Kuhs, W. F.; Nitscha, R.; Scheunemann, K. Acta Crystallogr., Sect. B 1978, B34, 64.
(257) Chan, L.; Geller, S. J. Solid State Chem. 1978, 25, 85.
(258) Yvon, K. Acta Crystallogr., Sect. B 1977, B33, 3066.
(259) Arribart, K.; Gouyet, J. F.; Saporal, B., ref 5, p 569.
(260) Nord, A. G.; Thomas, J. D. Acta Chem. Scand. A 1978, 32, 539.
(261) Jeitschko, W.; Bither, T. A.; Bierstedt, P. E. Acta Crystallogr., Sect. B 1977, B33, 2767.
(262) Hong, H. Y.-P., ref 5, p 431.
(263) Tranqui, D.; Cupponi, J. J.; Joubert, J. C.; Shannon, R. D.; Johnson, C. K., ref 5, p 439.
(264) Roth, W. L.; Anne, M.; Tranqui, D.; Heidemann, A., ref 5, p 267.
(265) Collin, G.; Comès, R.; Boilot, J. P.; Colomban, Ph. Solid State Ionics 1980, 1, 59.
(266) Biolot, J. P.; Colomban, Ph.; Comès, R. Solid State Ionics 1980, 1, 69.
(267) Lazzari, M.; Scrosati, B.; Vincent, C. A. Electrochim. Acta 1977, 22, 51.
(268) Takahashi, T.; Yamamoto, O.; Sawai, A. J. Appl. Electrochem. 1978, 8, 161.
(269) Takahashi, T.; Esaka, T.; Iwahara, H. J. Appl. Electrochem. 1977, 7, 31.
(270) Wright, A. F.; Fender, B. E. F. J. Phys. C 1977, 10, 2261.
(271) Cava, R. J.; Reidinger, F.; Wuensch, B. J., ref 5, p 217.
(272) Kuhs, W. F.; Heger, G., ref 5, p 233.
(273) Brun, T., ref 7.
(274) Chabre, Y.; Segransan, P.; Berthier, C.; Ouvrard, G., ref 5, p 221.
(275) Dickens, M. H.; Hayes, W.; Smith, C.; Hutchings, M. T., ref 5, p 225.
(276) Lucat, C.; Portier, J.; Reau, J. M.; Hagenmuller, P.; Soubeyro, J. L. J. Solid State Chem. 1980, 32, 279.
(277) Tolfield, B. C.; Newsham, J. M., ref 5, p 389.
(278) Van Gool, W., ref 3, p 24.
(279) Whittingham, M. S.; Silbernagel, B. G., ref 3, p 93.
(280) Richards, P. M., ref 2, p 141.
(281) Story, H. S.; Bailey, W. C.; Chung, I.; Roth, W. L., ref 4, p 317.
(282) Randell, C. F., Ph.D. Thesis, CNAA, Leicester Polytechnic, 1979.
(283) Tabbey, M. P.; Hendrick, J. R. J. Non-Cryst. Growth 1980, 38, 51.
(284) Look, D. C.; Lowe, I. J. J. Chem. Phys. 1966, 44, 2995.
(285) Parsonage, N. G.; Staveley, L. A. K. "Disorder in Crystals"; Clarendon Press: Oxford, 1978.
(286) Berthier, C., ref 5, p 171.
(287) Richtering, H.; Becker, K. D.; Hamann, H. J. Phys., Colloq. (Orsay, Fr.) 1976, 7, 373.
(288) Brinkmann, D.; Mali, M.; Roos, J., ref 5, p 483.
(289) Brinkmann, D.; Freudenreich, W. Solid State Commun. 1977, 25, 625.
(290) Brinkmann, D.; Freudenreich, W.; Looser, H.; Mali, M.; Roos, J., ref 5, p 605.
(291) Avogado, A.; Manzini, S.; Villa, M., ref 5, p 723.
(292) Arribart, H.; Rosso, M.; Sapoval, B.; Levy, C., ref 5, p 573.
(293) Tokuhiro, T.; Marshall, S. A.; Susman, S. Bull. Am. Phys. Soc. 1980, 25, 414.
(294) Brinkmann, D.; Freudenreich, W.; Roos, J. Solid State Commun. 1978, 28, 233.
(295) Follstaedt, D. M.; Richards, P. M. Phys. Rev. Lett. 1976, 37, 1571.
(296) Armand, M. B.; Chabagno, J. M.; Duclot, M. J., ref 5, p 131.
(297) Dubin, R. R.; Casabella, P. A., ref 5, p 367.
(298) Walstedt, R. E.; Berg, R. S.; Remeika, J. P.; Cooper, A. S.; Presscott, B. E., ref 5 p 355.
(299) Dubin, R. R.; Kasper, J. S.; Bates, J. B.; Kaneda, T., ref 5, p 361.
(300) Highe, A.; Vaughan, R. W., ref 5, p 375.
(301) Collongues, R.; Thery, J.; Boilet, J. P., ref 3, p 253.
(302) Bailey, W. C.; Story, H. S.; Ochadlick, A. R.; Farrington, G. C., ref 5, p 281.
(303) Allen, S. J.; Feldman, L. C.; McWhan, D. B.; Remeika, J. P.; Walstedt, R. E., ref 4, p 279.
(304) Brinkmann, D.; Mali, M.; Roos, J.; Story, H. S.; Dubin, R. R., ref 5, p 285.
(305) Bjorkstam, J. L.; Manzini, S.; Villa, M., ref 5, p 293.
(306) Hayes, C. E.; Ailron, D. C., ref 5, p 297.
(307) Chadwick, A. V.; Hope, D. S.; Jaroszkiewicz, G.; Strange, J. H., ref 5, p 683.
(308) Dickens, P. G.; Murphy, D. J.; Halstead, T. K. J. Solid State Chem. 1973, 6, 370.
(309) Panek, L. W.; Exarhos, G. J.; Bray, P. J.; Risen, W. M. J. Non-Cryst. Solids 1977, 24, 51.
(310) Whiffen, D. H. Q. Rev. Chem. Soc. 1958, 12, 250.
(311) Baquet, G.; Dugas, J., ref 3, p 109.
(312) Antoine, J.; Vivien, D.; Livage, J.; Thery, J.; Collongues, R. Mater. Res. Bull. 1975, 10, 865.
(313) Evora, C.; Jaccarino, V. Phys. Rev. Lett. 1977, 39, 1554.
(314) Title, R. S.; Chandrashekhar, G. V. Solid State Commun. 1976, 20, 405.
(315) Waterfield, C. G.; Linford, R. G.; Goalby, B. B.; Bates, T. R.; Elyard, C. A.; Staveley, L. A. K. Trans. Faraday Soc. 1968, 64, 868.
(316) Cooke, M. D.; Linford, R. G.; Staveley, L. A. K.; Worswick, R. D. J. Chem. Soc., Faraday Trans. 1 1978, 74, 2363.
(317) Linford, R. G.; Staveley, L. A. K. J. Chem. Thermodyn. 1969, 1, 1.
(318) Johnston, W. V.; Wiedersich, H.; Lindberg, G. W. J. Chem. Phys. 1969, 51, 3739.
(319) Silva-Moriera, A. F. Phys. Rev. Lett. 1977, 39, 1154.
(320) Nolting, J.; Rein, D.; Troe, J. Nachr. Ges. Wiss. Göttingen, Math.-Phys. Kl. 1969, 2, 31.
(321) Finlayson, D. M.; Leiper, G. A.; Vincent, C. A. Solid State Commun. 1980, 36, 261.
(322) Murphy, D. W.; Chen, M. S.; Tell, B. J. Electrochem. Soc. 1977, 124, 1268.
(323) O'Keeffe, M., ref 4, p 101.
(324) Beyeler, H. U. Phys. Rev. Lett. 1976, 37, 1557.
(325) Geisel, T., ref 5, p 541.
(326) Geisel, T. Solid State Commun. 1979, 32, 739.
(327) Alpen, U. V.; Schönherr, E.; Schulz, H.; Talat, G. H. Electrochim. Acta 1977, 22, 805.
(328) Boilot, J. P.; Colomban, Ph.; Collin, G.; Comès, R., ref 5, p 243.
(329) Boilot, J. P.; Collin, G.; Comès, R.; Théry, J.; Collongues, R.; Guinier, A., ref 4, p 243.
(330) Collin, G.; Colomban, Ph.; Boilot, J. P.; Comès, R., ref 5, p 309.
(331) Shapiro, S. M., ref 4, p 261.
(332) Kjems, J. K., ref 7.
(333) "Proceedings of the International Conference on Lattice Dynamics"; Balkanski, M., Ed.; Flammarion Press: Paris, 1978.
(334) Boyce, J. B.; Hayes, T. M., ref 2, p 5.
(335) Funke, K., ref 4, p 183.
(336) Eckold, G.; Funke, K.; Kalus, J.; Lechner, R. E. Phys. Lett. 1975, 55A, 125; J. Phys. Chem. Solids 1976, 37, 1097.
(337) Bührer, W.; Nicklow, R. M.; Brüesch, P. Phys. Rev. B. 1978, 17, 3362.
(338) Dorner, B.; Windscheif, J.; von der Osten, W., ref 333, p 535.

(339) Shapiro, S. M.; Semmingsen, D.; Salamon, M. B., ref 333, p 538.
(340) Shapiro, S. M.; Salamon, M. B., ref. 5, p 237.
(341) Hayes, W.; Stoneham, A. M. In "Crystals with the Fluorite Structure"; Hayes, W., Ed.: Oxford University Press: Oxford, U.K., 1974; Chapter 2.
(342) Dickens, M. H.; Hayes, W.; Smith, C.; Hutchings, M. T.; Kjems, J. K., ref 5, p 229.
(343) Dickens, M. H.; Hutchings, M. T., ref 333, p 540.
(344) Dickens, M. H.; Hutchings, M. T. *J. Phys. C* 1978, *11*, 461.
(345) Dickens, M. H.; Hutchings, M. T., "Neutron Inelastic Scattering": IAEA: Vienna, 1978, p 285.
(346) Rickel, C.; Scholke, R.; Tomkinson, J. *Z. Naturforsch. A* 1980, *35*, 590.
(347) Delaney, M. J.; Ushioda, S., ref 2, p 111.
(348) Beyeler, H. U.; Brüesch, P.; Pietronero, L.; Schneider, W. R.; Sträessler, S.; Zeller, H. R., ref 2, p 77.
(349) Geisel, T., ref 2, p 201.
(350) Chase, L. L., ref 4, p 299.
(351) Allen, S. J.; Remeika, J. P. *Phys. Rev. Lett.* 1974, *33*, 1478.
(352) Klein, M. V. In "Proceedings of the Third International Conference on Light Scattering in Solids"; Balkanski, M.; Leite, R. C. C.; Porto, S. P. J. Eds.; Flammarion Press: Parie, 1976, p 503.
(353) Geisel, T., ref 333, p 549.
(354) Burns, G.; Alben, R., ref 5, p 617.
(355) Burns, G., ref 333, p 551.
(356) Delaney, M. J.; Ushioda, S., ref 333, p 529.
(357) Winterling, G.; Senn, W.; Grinsditch, M.; Katiyar, R., ref 333, p 553.
(358) Brüesch, P.; Beyeler, H. U.; Bührer, W., ref 333, p 527.
(359) Fontana, A.; Mariotto, G.; Fontana, M. P. *Phys. Rev. B* 1980, *21*, 1102.
(360) Mariotto, G.; Fontana, A.; Cazzanel, E.; Fontana, M. P., *Phys. Stat. Solid. B* 1980, *101*, 341.
(361) Harihara, K. *J. Phys. D* 1979, *12*, 1909.
(362) Nitzan, A.; Ratner, M. A.; Shriver, D. F. *J. Chem. Phys.* 1980, *72*, 3320.
(363) Scott, J. F.; Hubbal, F.; Zvirgzdi, J. A. *J. Chem. Phys.* 1980, *72*, 2760.
(364) Nemanich, R. J.; Martin, R. M.; Mikkelsen, J. C., ref 5, p 547.
(365) Irion, M.; Couzas, M.; Levasseau, A.; Reau, J. M.; Brethous, J. C. *J. Solid State Chem.* 1980, *31*, 285.
(366) Colomban, P.; Lucazeau, G. *J. Chem. Phys.* 1980, *72*, 1213.
(367) Kaneda, T.; Bates, J. B.; Wang, J. C.; Engstrom, H., ref 5, p 371.
(368) Bates, J. B.; Frech, R.; Engstrom, H.; Wang, J. C.; Kaneda, T. *Solid State Ionics* 1980, *1*, 15.
(369) Harley, R. T.; Hayes, W.; Rushworth, A. J.; Ryan, J. F. *J. Phys. C* 1975, *8*, L530.
(370) Kleppmann, W. G.; Elliott, R. J., ref 333, p 544.
(371) Elliott, R. J.; Hayes, W.; Kleppmann, W. G.; Rushworth, A. J.; Ryan, J. F. *Proc. R. Soc. London, Ser. A* 1978, *360*, 317.
(372) Shand, M.; Hansen, R. C.; Derrington, C. E.; O'Keeffe, M. *Solid State Commun.* 1976, *18*, 769.
(373) Hayes, W.; Rushworth, A. J.; Ryan, J. F., ref 333, p 519.
(374) Sato, H., ref 1, p 3.
(375) Gebhardt, K. F.; Soper, P. D.; Mersk, J.; Balle, T. J.; Flygare, W. H. *J. Chem. Phys.* 1980, *72*, 272.
(376) Tennent, R. M. "Science Data Book for the Open University"; Oliver and Boyd: Edinburgh, 1971.
(377) Ingram, M. A. *J. Am. Ceram. Soc.* 1980, *63*, 248.
(378) Funke, K. M. "High Frequency Dielectric Measurement"; Chamberlain, J.; Chantry, G. W., Eds.; IPC Science and Technology Press: Guildford, 1973; p 47.
(379) Fulde, P.; Pietronero, L.; Schneider, W. R.; Sträessler, S. *Phys. Rev. Lett.* 1975, *26*, 1776.
(380) Drude, P. *Ann. Phys.* 1900, *1*, 566.
(381) Richards, P. M., ref 5, p 349.
(382) Shvets, V. T. *Fiz. Tverd. T.* 1980, *22*, 1971.
(383) Funke, K., ref 5, p 609.
(384) Khanna, S. K.; Gruner, G.; Orbach, R. *Bull. Am. Phys. Soc.* 1980, *25*, 414.
(385) Beyeler, H. U.; Bernasconi, J.; Sträessler, S., ref 5, p 503.
(386) Thomas, J. M. *Chem. Brit.* 1977, *13*, 175.
(387) Lee, P. A.; Pendry, J. B. *Phys. Rev. B* 1975, *11*, 2795.
(388) Jaclevic, J.; Kirby, J. A.; Klein, M. P.; Robertson, A. S.; Brown, G. S.; Eisenberger, P. *Solid State Commun.* 1977, *23*, 679.
(389) Lee, P. A. *Phys. Rev. B* 1976, *13*, 5261.
(390) Lee, P. A.; Beni, G. *Phys. Rev. B* 1977, *15*, 2862.
(391) Boyce, J. B.; Hayes, T. M., ref 5, p 535.
(392) Ishii, T. *Solid State Commun.* 1980, *33*, 249.
(393) Hammaberg, J.; Plische, M. *Solid State Commun.* 1980, *33*, 245.
(394) Boyce, J. B.; Hayes, T. M.; Mikkelsen, J. C. *Bull. Am. Phys. Soc.* 1980, *25*, 434.
(395) Hayes, T. M.; Boyce, J. B. *J. Phys. C.* 1980, *13*, L225.
(396) Boyce, J. B.; Hayes, T. M.; Stutius, W.; Mikkelsen, J. C. *Phys. Rev. B* 1977, *38*, 1362.

(397) Boyce, J. B.; Hayes, T. M.; Mikkelsen, J. C.; Stutius, W. *Solid State* Commun. 1980, *33*, 183.
(398) Fox, R.; Gurman, S. J. *J. Phys. C.* 1980, *13*, L249.
(399) Rahman, A. In "Correlation Functions and Quasi-particle Interactions in Condensed Matter"; Halley, J. W., Ed.; Plenum: New York, 1977; p 417.
(400) Morrell, W. E.; Hildebrand, J. H. *Science (Washington, D.C.)* 1934, *80*, 125; *J. Chem. Phys.* 1936, *4*, 3.
(401) Alder, B. J.; Wainwright, T. E. *J. Chem. Phys.* 1959, *31*, 459; *Sci. Am.* 1959, *201*, 113.
(402) Cotterill, R. M. J.; Couchman, P. R.; Linford, R. G., unpublished results.
(403) Jacucci, G.; McDonald, I. R.; Singer, K. *Phys. Lett. A* 1974, *50A*, 2.
(404) Rahman, A., ref 7.
(405) Vashishta, P.; Rahman, A. *Phys. Rev. Lett.* 1978, *40*, 1337.
(406) Schommers, W. *Phys. Rev. B* 1978, *17*, 2057.
(407) Schommers, W., ref 5, p 625.
(408) de Leeuw, S., ref 7.
(409) Rahman, A. *J. Chem. Phys.* 1976, *65*, 4845.
(410) Rahman, A.; Jaccucci, G. *J. Chem. Phys.* 1978, *69*, 4117.
(411) Delbecq, C. K.; Marshall, S. A.; Susman, S. *Solid State Ionics* 1980, *1*, 145.
(412) Kharkats, Y. I. *Sov. Electrochem. (Engl. Transl.)* 1979, *15*, 500.
(413) Fujimoto, S.; Yasuda, N.; Kameyama, S. *J. Phys. D.* 1980, *13*, L95.
(414) Allen, P. C.; Lazarus, D. *Phys. Rev. B* 1978, *17*, 1913.
(415) Mahan, G. D., ref 4, p 115.
(416) Hiwatari, Y. *Phys. Lett. A.* 1980, *75*, 426.
(417) Marsh, N. H.; Richards, D. D.; Tosi, M. P. *Solid State Commun.* 1980, *33*, 903.
(418) Huberman, B. A., ref 4, p 151.
(419) Pardee, W. J.; Mahan, G. D. *J. Solid State Chem.* 1975, *15*, 310.
(420) Landau, L. D.; Lifschitz, E. "Statistical Physics", 2nd Ed.; Pergamon: Oxford, U.K., 1968.
(421) Vargas, R. A.; Salamon, M. B.; Flynn, C. P. *Phys. Rev. B* 1978, *17B*, 269.
(422) Vargas, R. A.; Salamon, M. B.; Flynn, C. P. *Phys. Rev. Lett.* 1976, *37*, 1550.
(423) Borovkov, V. S.; Ivanov-Shitz, A. K. *Electrochim. Acta* 1977, *22*, 713.
(424) Geller, S.; Hibma, T. *J. Solid State Chem.* 1977, *21*, 225.
(425) Todor, D. N. "Thermal Analysis of Minerals"; Abacus Press: Tunbridge Wells, 1976.
(426) Razzini, G.; Lazzari, M.; Scrosati, B. *Electrochim. Acta* 1978, *23*, 805.
(427) Bonino, F.; Lazzari, M.; Lonardi, A.; Rivelta, B. *J. Solid State Chem.* 1977, *20*, 315.
(428) Seyler, R. J.; Kalbfleisch, E. *Int. Lab.* 1978, March, 40.
(429) Chiodelli, G.; Magistris, A.; Schiraldi, A. *Electrochim. Acta* 1978, *23*, 585.
(430) Shilton, M. G.; Howe, A. T., ref 5, p 727.
(431) Miyake, S.; Hoshino, S.; Takenaka, T. *J. Phys. Soc. Jpn.* 1952, *7*, 19.
(432) Gurevich, Ya. Yu.; Ivanov-Shits, A. K. *Sov. Electrochem. (Engl. Transl.)* 1977, *13*, 1366.
(433) Welch, D. O.; Dienes, G. J. *J. Phys. Chem. Solids* 1977, *38*, 311.
(434) Kharkats, Yu. I. *Phys. Stat. Solid.* 1978, *85*, 371.
(435) O'Reilly, M. B. *Phys. Stat. Solid.* 1978, *48*, 489.
(436) Ivanovshi, A. K. *Fiz. Tverd. T.* 1980, *22*, 40.
(437) De Reggi, A. S.; Canepa, P. C.; Scott, T. A. *J. Magn. Reson.* 1969, *1*, 144.
(438) Andrew, E. R.; Eades, R. G.; Hennel, J. W.; Hughes, D. G. *Proc. Phys. Soc.* 1962, *79*, 954.
(439) Boyce, J. B.; Huberman, B. A. *Solid State Commun.* 1977, *21*, 31.
(440) Boyce, J. B.; Mikkelsen, J. C. *Solid State Commun.* 1977, *21*, 955.
(441) Pederson, D. O.; Brewer, J. A. *Phys. Rev. B* 1977, *16*, 4546.
(442) Pederson, D. O.; Brewer, J. A., ref 5, p 695.
(443) Graham, L. J.; Chang, R. *J. Appl. Phys.* 1975, *46*, 2433.
(444) Nagao, M.; Kaneda, T. *Phys. Rev. B* 1975, *11*, 2711.
(445) Leung, K. M.; Huber, D. L. *Phys. Rev. Lett.* 1979, *42*, 452.
(446) Benguigui, L.; Weil, R. *Phys. Rev. B* 1977, *16*, 2569.
(447) Gubbins, K. E.; Reed, T. M. "Applied Statistical Mechanics"; McGraw-Hill: New York, 1973.
(448) Vashishta, P., ref 7.
(449) Rahman, A., ref 7.
(450) Geller, S., ref 4, p 171.
(451) Geller, S. *Phys. Rev. B* 1976, *14*, 4345.
(452) Lederman, F. L.; Salamon, M. B.; Persl, H. *Solid State Commun.* 1976, *19*, 147.
(453) Hoshino, S.; Sakuma, T.; Fujii, Y. *J. Phys. Jpn.* 1979, *47*, 1252.
(454) Girvin, S. M.; Mahan, G. D. *Solid State Commun.* 1977, *23*, 629.

(455) Geller, S.; Wilber, S. A.; Ruse, G. P.; Akridge, J. R.; Tuorkovic, A. *Phys. Rev. B* **1980**, *21*, 2506.
(456) Hibma, J. *Phys. Rev. B* **1977**, *15*, 5797.
(457) Boyce, J. B.; Huberman, B. A. *Solid State Commun.* **1977**, *21*, 31.
(458) Burns, G.; Dacol, F. M.; Shafer, M. W. *Solid State Commun.* **1977**, *24*, 753.
(459) Dworkin, A. S.; Bredig, M. A. *J. Phys. Chem.* **1968**, *72*, 1277.
(460) Derrington, C. E.; Navrotsky, A.; O'Keeffe, M. *Solid State Commun.* **1976**, *18*, 47.
(461) Boyce, J. B.; Mikkelsen, J. C.; O'Keeffe, M. *Solid State Commun.* **1977**, *21*, 955.
(462) "Proceedings at the Snowmass, Colorado, Conference, 1979": *Surf. Sci.* **1980**, *201*.
(463) Bergmann, E.; Tannenberger, M., ref 3, p 173.
(464) Parsons, R. *J. Electrochem. Soc.* **1980**, *127*, 176C.
(465) Baker, A. D.; Brisk, M. A.; Liotta, D. C. *Anal. Chem.* **1980**, *52*, 161R.
(466) Morrison, S. R. "The Chemical Physics of Surfaces"; Plenum Press: New York, 1977.
(467) Somorjai, G. A. "Principles of Surface Chemistry"; Prentice-Hall: Engelwood Cliffs, NJ, 1979.
(468) Blakely, J. M. "Introduction to the Properties of Crystal Surfaces"; Pergamon: Oxford, 1973.
(469) Prutton, M. "Surface Physics"; Clarendon Press: Oxford, 1975.
(470) "Topics in Surface Chemistry"; Kay, E., Bagus, P. S., Eds.; Plenum: New York, 1978.
(471) "Chemistry and Physics of Solid Surfaces"; Vanselow, R., Tong, S. Y., Eds.; CRC Press: Cleveland, OH, 1977.
(472) "Handbook of Surfaces and Interfaces"; Dobrzynski, L., Ed.; Garland STPM: New York, 1978; Vol. 1, 2.
(473) "Methods of Surface Analysis"; Czanderna, A. W., Ed.; Elsevier: Amsterdam, 1975.
(474) Seah, M. P. *J. Vac. Sci. Technol.* **1980**, *17*, 16.
(475) Werner, H. W. *Mater. Sci. Eng.* **1980**, *42*, 1.
(476) Rodriguez, R.; Antoniewicz, P. R. *Chem. Phys. Lett.* **1979**, *66*, 400.
(477) Bowden, F. P.; Tabor, D. "The Friction and Lubrication of Solids, Part 2"; Clarendon Press: Oxford, 1964.
(478) Weiner, S. A. *Adv. Chem. Ser.* **1976**, *No. 163*, 205.
(479) Eyring, L. *Adv. Chem. Ser.* **1976**, *No. 163*, 240.
(480) Mogililevskii, B. M.; Lyalin, O. O. *Elektron. Obrab. Mater.* **1979**, *5*, 60; *Chem. Abstr.* **1980**, *92*, 50680s.
(481) Mikhailova, A. M.; Ukshe, E. A. *Electrokhimiya* **1979**, *15*, 1242.
(482) Borovkov, V. S.; Khachata, N. A. *Sov. Electrochem. (Engl. Transl.)* **1979**, *15*, 599.
(483) Benndorf, C.; Caus, H.; Egert, B.; Seidel, H.; Thieme, F. *J. Electron Spectrosc. Related Phenom.* **1980**, *19*, 77.
(484) Stoddart, C. T. H.; Hondros, E. D. *T. J. Br. Ceram.* **1974**, *73*, 61.
(485) Helms, C. R.; Spicer, W. E.; Johnson, N. M. *Solid State Commun.* **1978**, *25*, 673.
(486) Kuwamoto, H.; Sato, H.; Hirotsu, Y.; Liedl, G. L., ref. 5, p 273.
(487) Allpress, J. G.; Russell, H. J. *J. Solid State Chem.* **1975**, *15*, 68.
(488) Linford, R. G.; Osgood, C. *Surf. Sci.* **1972**, *34*, 482.
(489) Chandra, S.; Agrawal, R. C.; Pandey, R. K. *Phys. Stat. Solid.* **1980**, *57*, 299.
(490) Chandra, S.; Sharma, J. N.; Mohabey, V. K.; Agrawal, R. C. *J. Phys. D.* **1980**, *13*, 495.
(491) Croset, M.; Schnell, J. P.; Velasco, G.; Siejka, J. *Brookhaven Nat. Lab. Report* **1978**, 50756, 139; *Chem. Abstr.* **1980**, *92*, 25494b.
(492) Rohr, F. J., ref 3, p 431.
(493) Couturier, G.; Danto, Y.; Pistre, J.; Salardenne, J.; Lucat, C.; Reau, J. M.; Portier, J.; Vilminot, S., ref 5, p 687.
(494) Bowles, A. J.; Linford, R. G.; Matthews, J. M. F.; Oxley, D. P.; Tunnicliffe, D. *Chem. Ind. (London)* **1981**, 24.